TECHNICAL REPORT STANDARD TITLE PAGE

1. Report No.	2. Government Accession No.	3. Recipient's Catalog No.
FHWA/TX-82/18+303-1F		

4. Title and Subtitle	5. Report Date
THE EFFECT OF TRANSVERSE STRAND EXTENSIONS ON THE BEHAVIOR OF PRECAST PRESTRESSED PANEL BRIDGES	June 1982
	6. Performing Organization Code
7. Author(s)	8. Performing Organization Report No.
L. A. Bieschke and R. E. Klingner	Research Report 303-1F
9. Performing Organization Name and Address	10. Work Unit No.
Center for Transportation Research The University of Texas at Austin Austin, Texas 78712-1075	11. Contract or Grant No. Research Study 3-5-80-303
	13. Type of Report and Period Covered
12. Sponsoring Agency Name and Address Texas State Department of Highways and Public Transportation; Transportation Planning Division P. O. Box 5051 Austin, Texas 78763	Final
	14. Sponsoring Agency Code

15. Supplementary Notes

Study conducted in cooperation with the U. S. Department of Transportation, Federal Highway Administration. Research Study Title: "Behavior of Prestressed Panel, Cast-in-Place Concrete Bridge Decks"

16. Abstract

A series of static and dynamic loading tests was conducted on a full-scale bridge specimen constructed using prestressed precast panels placed on top of prestressed precast girders and covered with a cast-in-place bridge deck. The north half had panels with transverse prestressing strands extending beyond the panel edges, and the south half had smooth-sided panels.

The major objective was to determine if the absence of strand extensions would cause significant deterioration in performance under fatigue and static loading. The bridge was subjected to four static tests (three at levels high enough to cause girder cracking) and two fatigue tests. In addition, ten concentrated load tests were made. All loadings were applied equally to each half of the bridge.

Four major conclusions are apparent from this study:

(1) The overall and local behavior of bridges without extensions is as satisfactory as that of bridges with extensions;

(2) In some cases, prestressed girders can be cracked flexurally and subjected to extensive fatigue cycling without strand fracture;

(3) Bridge deck capacity under concentrated loads should be investigated using yield-line models as well as punching shear models, particularly in overhang areas; and

(4) Construction details were not observed to affect overall performance. However, they can have significant effects on local behavior.

17. Key Words	18. Distribution Statement
bridges, precast, prestressed, panel, transverse strand extensions, static, dynamic, loading	No restrictions. This document is available to the public through the National Technical Information Service, Springfield, Virginia 22161.

19. Security Classif. (of this report)	20. Security Classif. (of this page)	21. No. of Pages	22. Price
Unclassified	Unclassified	116	

Form DOT F 1700.7 (8-69)

THE EFFECT OF TRANSVERSE STRAND EXTENSIONS ON THE BEHAVIOR OF PRECAST PRESTRESSED PANEL BRIDGES

by

L. A. Bieschke and R. E. Klingner

Research Report No. 303-1F

Research Project 3-5-80-303

"Behavior of Prestressed Panel, Cast-in-Place Concrete Bridge Decks"

Conducted for

Texas
State Department of Highways and Public Transportation

In Cooperation with the
U.S. Department of Transportation
Federal Highway Administration

by

CENTER FOR TRANSPORTATION RESEARCH
BUREAU OF ENGINEERING RESEARCH
THE UNVERSITY OF TEXAS AT AUSTIN

June 1982

The contents of this report reflect the views of the authors, who are responsible for the facts and the accuracy of the data presented herein. The contents do not necessarily reflect the official views or policies of the Federal Highway Administration. This report does not constitute a standard, specification, or regulation.

There was no invention or discovery conceived or first actually reduced to practice in the course of or under this contract, including any art, method, process, machine, manufacture, design or composition of matter, or any new and useful improvement thereof, or any variety of plant which is or may be patentable under the patent laws of the United States of America or any foreign country.

PREFACE

This report summarizes an investigation on a full-scale bridge specimen, constructed using prestressed precast panels placed on top of prestressed precast girders, and covered with a cast-in-place bridge deck. The north half of the bridge specimen was made with panels having transverse prestressing strands extending beyond the panel edges, and the south half, with smooth-sided panels. Local and overall behavior of the bridge was studied under static and fatigue loading.

The work was sponsored by the Texas State Department of Highways and Public Transportation and the Federal Highway Administration and administered by the Center for Transportation Research at The University of Texas at Austin. Close liaison with the State Department of Highways and Public Transportation has been maintained through Contact Representative Mr. H. D. Butler and Engineer for Bridge Design Mr. Robert L. Reed. Mr. Charles Duncan was the contact representative for the Federal Highway Administration.

The project was conducted in the Phil M. Ferguson Structural Engineering Laboratory located at the Balcones Research Center of The University of Texas at Austin. The authors appreciate the assistance of the Laboratory's technical and secretarial staff.

S U M M A R Y

A series of static and dynamic loading tests was conducted on a full-scale bridge specimen, constructed using prestressed precast panels placed on top of prestressed precast girders, and covered with a cast-in-place bridge deck. The north half of the bridge specimen was made with panels having transverse prestressing strands extending beyond the panel edges, and the south half, with smooth-sided panels.

The major objective of this study was to determine if the absence of strand extensions would cause significant deterioration in the bridge's performance under fatigue and static loading. The bridge was subjected to four static tests (three of these at levels high enough to cause girder cracking), and two fatigue tests (to a total of 11.5 million cycles). Additionally, ten concentrated load tests were made on the bridge deck. All loadings were applied equally to each half of the bridge.

Four major conclusions are apparent from this study:

(1) The overall and local behavior of bridges without transverse prestressing strand extensions is just as satisfactory as that of bridges with the extensions;

(2) In some cases, prestressed girders can be cracked flexurally and subjected to extensive fatigue cycling without strand fracture;

(3) Bridge deck capacity under concentrated loads should be investigated using yield-line models as well as punching shear models, particularly in overhang areas; and

(4) Construction details were not observed to affect the overall performance of the bridge investigated in this study. However, as discussed herein, they can sometimes have significant effects on local behavior.

IMPLEMENTATION

The results of this study support the use, in bridge construction, of precast prestressed panels without strand extensions, rather than the present system involving prestressed panels with strand extensions.

Additionally, results of this study suggest that flexurally cracked prestressed girders can be subjected to fatigue cycling without failing due to strand fracture. Bridge deck capacity under concentrated loads should be investigated using yield-line models as well as punching shear models. Construction details were observed to affect local behavior, and should be monitored both during panel fabrication and placement.

C O N T E N T S

TABLES

F I G U R E S

CHAPTER 1

INTRODUCTION

1.1 Background

One of the newer types of composite bridge construction includes the use of precast prestressed concrete panels which span between longitudinal girders and act as formwork and base for the cast-in-place deck (Fig. 1.1). Some research on this type of bridge has been completed [1,2,3,4,5] and is discussed in Section 1.3. Based on this research, bridges of this type are in common use today.

The panels used in the above-mentioned bridges typically have 3 in. prestressing strand extensions projecting from the transverse ends of the panels, as shown in Fig. 1.2A. It has been suggested that these 3-in. strand extensions be eliminated from the sides of the panels to allow for a continuous-bed process of manufacture (Fig. 1.2B). Since no previous research existed on the performance of these smooth-sided panels in this type of bridge construction, this present study was undertaken.

1.2 Scope and Objectives

This study was primarily experimental, consisting of a series of tests conducted on a full-scale bridge specimen. The north half of the bridge specimen was made with panels having protruding transverse strands, and the south half with smooth-sided panels. In all other ways this full-scale bridge specimen was similar to those currently being built by the Texas State Department of Highways and Public Transportation. The bridge specimen, shown in Fig. 1.1, is fully described in Chapter 3.

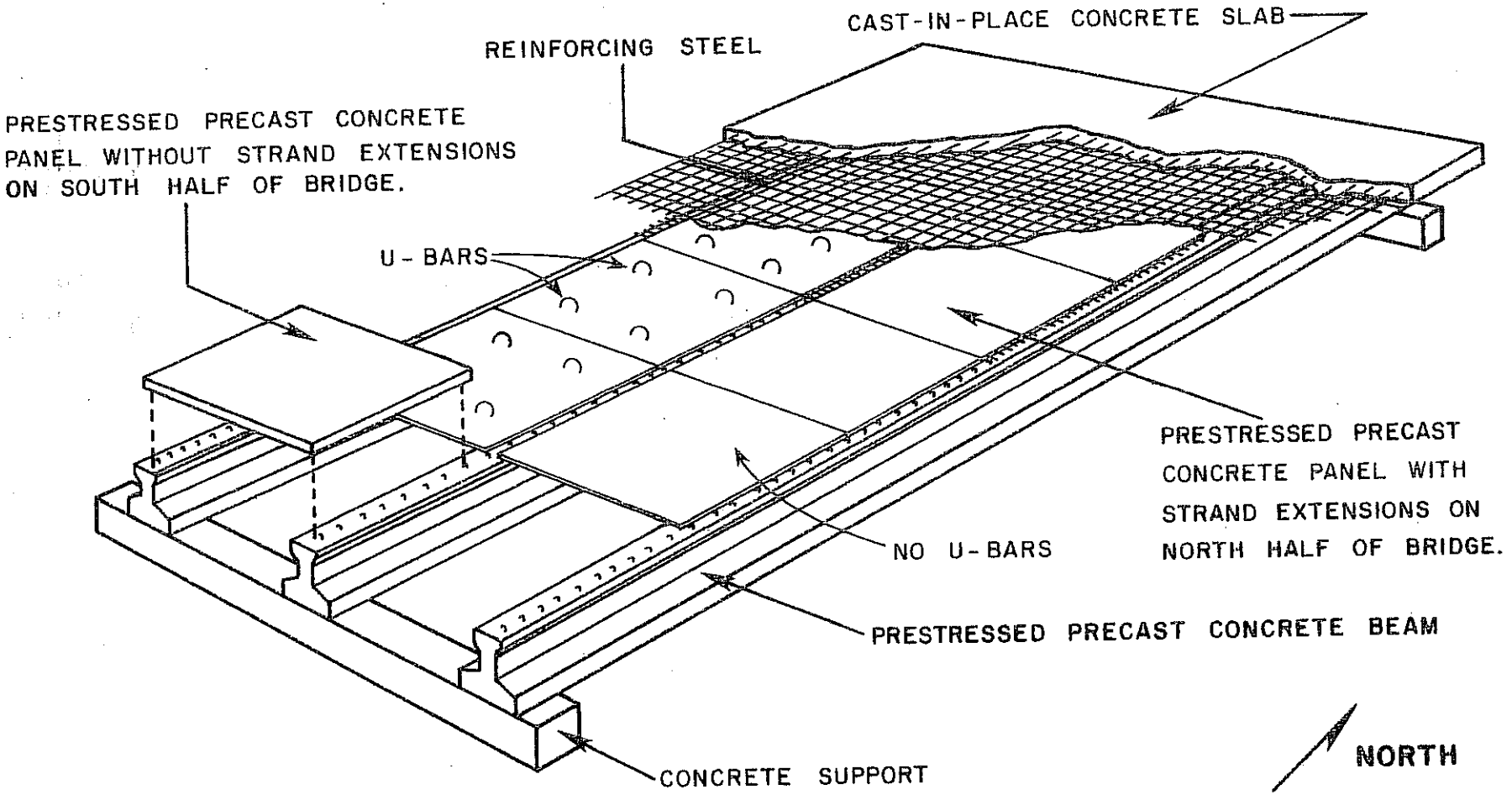

FIGURE 1.1 - CUT-AWAY VIEW OF FULL-SCALE BRIDGE SPECIMEN

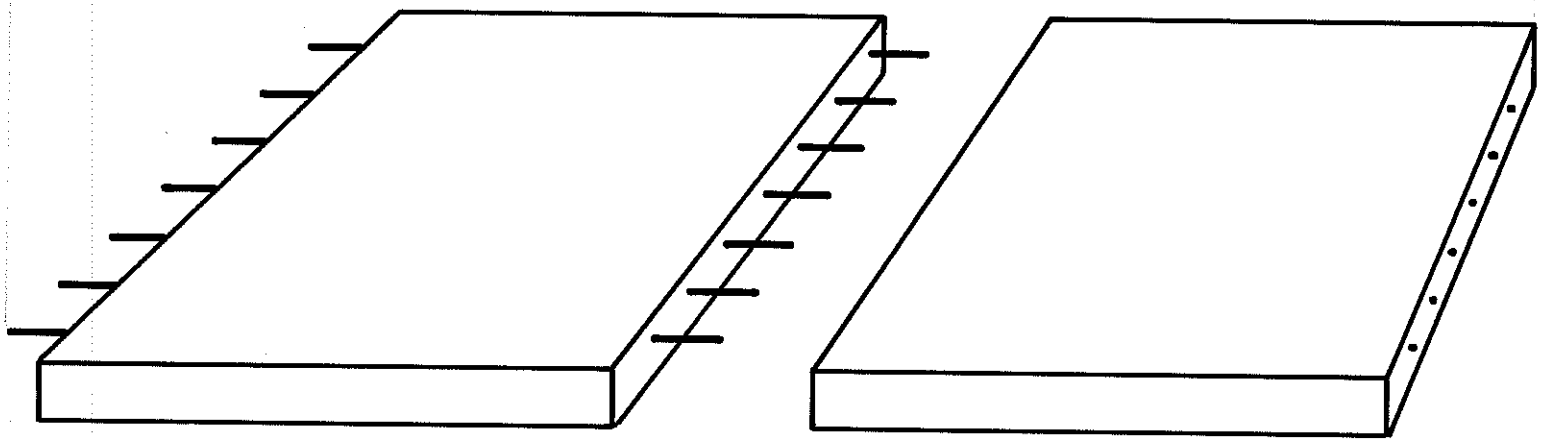

A. PANELS WITH 3" STRAND EXTENSIONS

B. PANELS WITH STRANDS CUT OFF AT THE EDGE OF THE PANELS

FIGURE 1.2 - PRECAST PANELS

The bridge specimen was subjected to static flexural and fatigue flexural loadings (both before and after significant flexural cracking had occurred in the girders), and, also, to concentrated slab loads. Tests and testing apparatus are discussed in Chapters 2 and 4, respectively. The response of both ends of the bridge to flexural and shear loadings was examined for overall load-deflection behavior and also local behavior (surface cracking and panel separation, slip, and rotation). The instrumentation used to study this behavior is described in Chapter 5.

The primary objective of this study was to determine if the absence of strand extensions would significantly decrease the bridge's performance under fatigue and static loading conditions. The evaluation was based primarily on a comparison between the observed local behavior at each end of the bridge. Other objectives were: (2) to evaluate the static and fatigue response of the bridge, particularly the girders, both before and after significant flexural cracking had occurred; (3) to evaluate the response of the deck to concentrated loads; and (4) to evaluate the effectiveness of practical construction details not studied previously. The results of this study are presented and discussed in Chapter 6. An overall summary of the entire investigation is presented in Chapter 7.

1.3 Previous Related Studies

Previous studies have concentrated on various aspects of precast panel composite bridge construction and performance. Kluge and Sawyer [1] examined precast panel bridge deck composite action, and concluded that prestressed precast panels could be used as a composite part of the bridge deck. Barnoff, et al. [2], performed full-scale tests on a precast panel composite bridge. These tests covered many aspects, including verification of design assumptions, fabrication and construction, and service and overload conditions. Furr, et al. [3,4], reported on the feasibility of using precast panel composite bridges. Included in those reports were tests on a full-scale bridge

very similar to the north half of the bridge specimen used in the present study. Barker [5] reviewed all of this research and its applications to the design, fabrication, and erection of precast panel composite bridges. In general, all of the studies looked favorably toward the use of precast panel composite bridges.

Rabbat, et al. [6], conducted fatigue tests on full-scale prestressed girders with slabs. Some of these studies indicated potential problems with the failure of prestressing strands in precast girders subjected to bottom fiber tensile stresses of $6\sqrt{f'_c}$ under fatigue loading, particularly if flexural cracking had occurred. This conclusion will be reviewed later in this report.

CHAPTER 2

DESCRIPTION OF TESTS

2.1 Flexural Tests

A complete history of the flexural-type loading applied to the bridge is shown in Fig. 2.1. Descriptions of the various tests shown in that figure are presented below.

2.1.1 Static Test No. 1. The intent of this test was to find the initial overall and local behavior of both ends of the completed bridge specimen prior to any fatigue loading. The specimen was loaded statically, and girder deflections were measured at various points along the span. Local behavior was also assessed using instrumentation at panel joints. To permit comparison of the performance of each end of the bridge, two such sets of loads were applied, as shown in Fig. 2.2. Each set of two loading points was arranged to simulate dual wheel loads distributed from an axle of an AASHTO standard HS truck [7]. Both sets of loads were applied in unison, increasing monotonically to 48 kips on each axle. As with all other tests depicted in Fig. 2.1, the load shown on the vertical axis is the load applied to one-half of the bridge, comprising two of the four points shown in Fig. 2.2. In concrete terms, this would represent the load applied by one axle of an AASHTO standard HS truck [7].

2.1.2 Fatigue Test Series No. 1. The fatigue loading arrangement was the same as in Static Test No. 1. Loads were applied in phase to the top of the deck. After an initial series of 1.5 million cycles at relatively small load levels, it was decided to apply a load level that could produce tensile cracking at the bottom of the center girder. A maximum tensile strength of $6\sqrt{f'_c}$ was

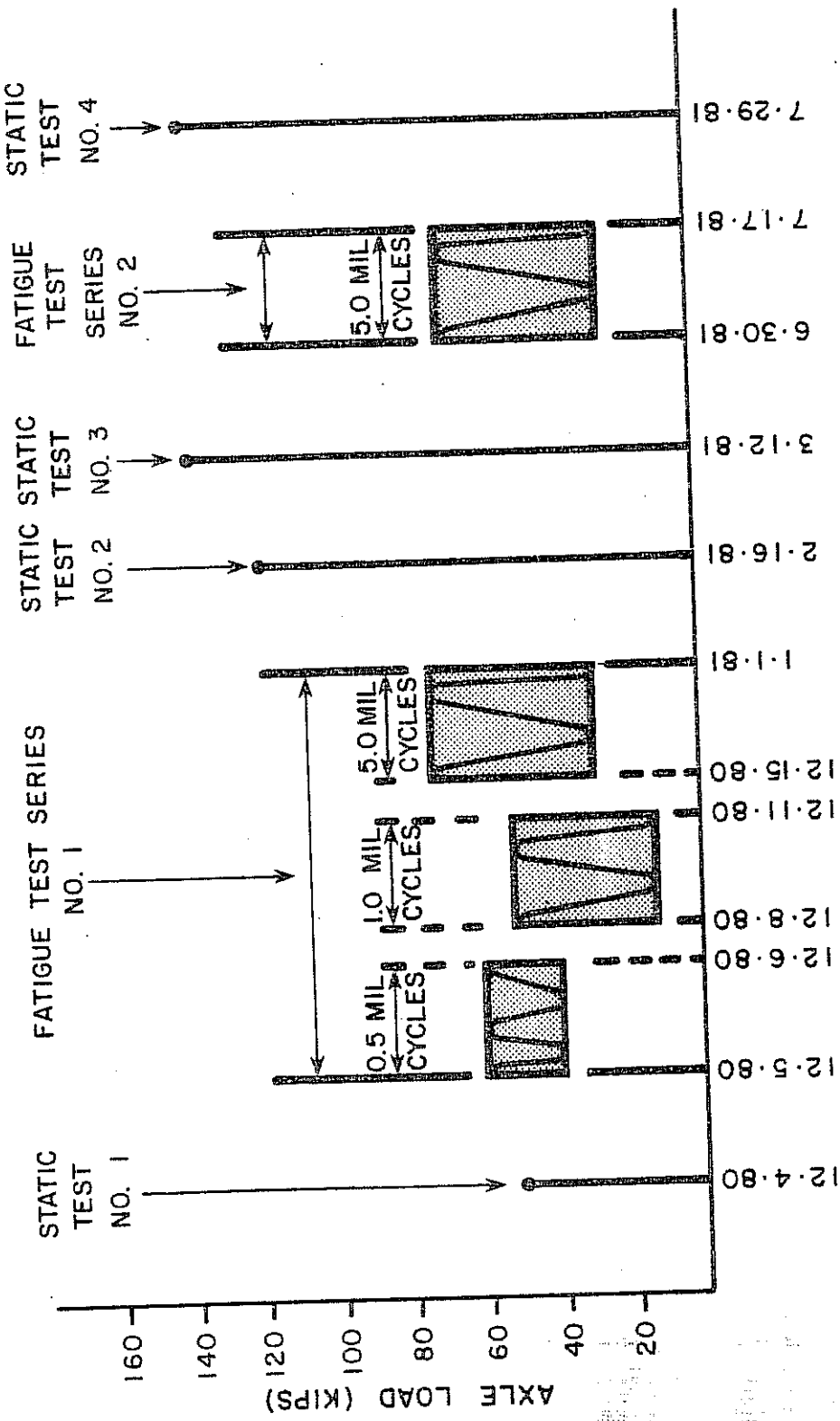

FIGURE 2.1 - BRIDGE FLEXURAL LOADING HISTORY

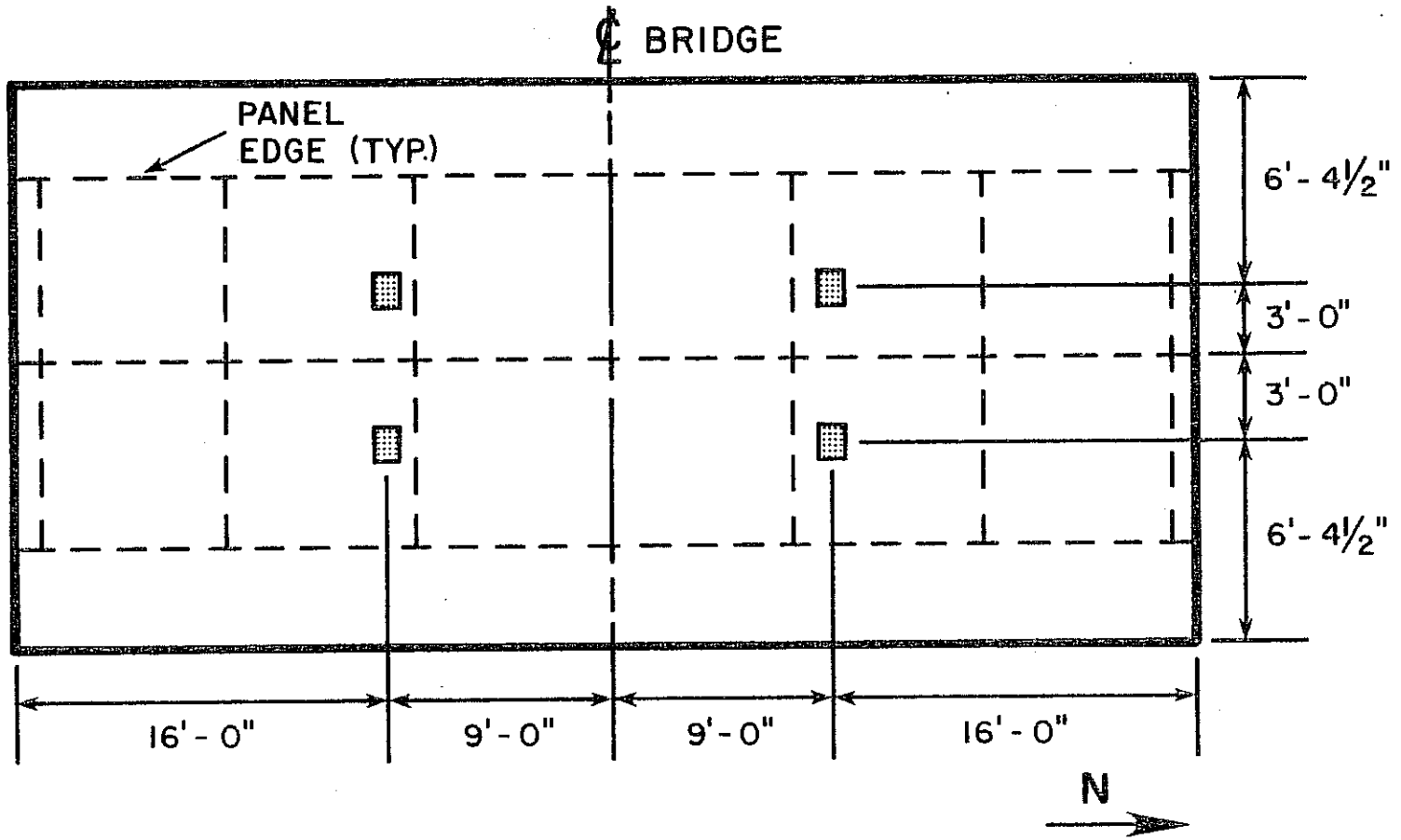

FIGURE 2.2 - FLEXURAL TEST LOADING POINTS

conservatively assumed. As explained subsequently, a load level was selected which would produce a maximum calculated tensile stress of $6\sqrt{f'_c}$ at the bottom of the center girder, assuming uncracked conditions. The analytical background for deriving this load level and range, considering dynamic effects, can be found in Appendix A. This secondary phase of fatigue loading was applied for 5 million cycles. Loading was stopped several times to monitor the progressive cracking of the bridge deck.

2.1.3 Static Test No. 2. In this test the specimen was loaded monotonically until girder flexural cracking occurred. The same four-point loading arrangement was used. Because of constraints on the capacity of the loading apparatus, this test was stopped at the time initial cracking occurred on the center girder. Overall load-deflection behavior, and also local panel behavior were recorded for comparisons with analytical predictions based on current state-of-the-art analysis techniques.

2.1.4 Static Test No. 3. After revising the loading apparatus to increase its capacity, the specimen was again loaded monotonically with the same four-point loading arrangement. The axle load was increased until all girders displayed significant flexural cracking. Overall load-deflection behavior, local panel behavior, and panel and girder cracking were recorded.

2.1.5 Fatigue Test Series No. 2. The intent of this test was to study the fatigue response of the bridge after significant girder flexural cracking had occurred. Axle loads were applied in the same manner as in Fatigue Test Series No. 1. Five million additional cycles were applied, at load levels adjusted slightly from those in Fatigue Test Series No. 1, to compensate for the reduced stiffness of the bridge due to the flexural cracking. Local cracking effects were monitored as before.

2.1.6 Static Test No. 4. The specimen was loaded the same as in the previous static tests in order to observe any change in either the overall load-deflection behavior or the local panel behavior due to Fatigue Test Series No. 2.

2.2 Concentrated Load Tests

Concentrated point loads were applied at various points on the bridge deck (Fig. 2.3). The intent of these tests was to determine if any difference in behavior or failure mode existed between the various points when subjected to the same type of concentrated load.

CHAPTER 3

FULL-SCALE BRIDGE SPECIMEN

As shown schematically in Fig. 1.1, this type of bridge is constructed by first erecting precast pretensioned girders, then placing prestressed panels between the girders, and finally pouring a deck of cast-in-place concrete over the panels. The material characteristics of each type of component are given below, and the construction process will be briefly discussed.

3.1 Components

3.1.1 Precast Pretensioned Girders. Three Texas Highway Dept. Type B girders [8,9], supplied by the Texas State Department of Highways and Public Transportation, were used in the bridge specimen. Each girder (Fig. 3.1) was identical in composition and made for a 50-ft span. The top surface of each girder was rough except along each longitudinal edge, where a 1-in. wide by 1/2 in.-thick pressed fiberboard strip was attached. For material properties, see Table 3.1. All girders were simply supported on top of neoprene pads, and rested on anchor blocks on the laboratory floor.

3.1.2 Precast Pretensioned Panels. Two types of panels [10], both 4 in. thick, were used in the bridge specimen. Both types of panels were supplied by Texas State Department of Highways and Public Transportation. The first type of panel had pretensioning strand extensions projecting 3 in. from each transverse panel edge, identified as "A" panels in Fig. 3.2. Due most likely to manufacturing errors, these panels were not exactly rectangular in shape, making positioning of them difficult. The second type of panel had no pretensioning strand extensions projecting beyond the transverse panel

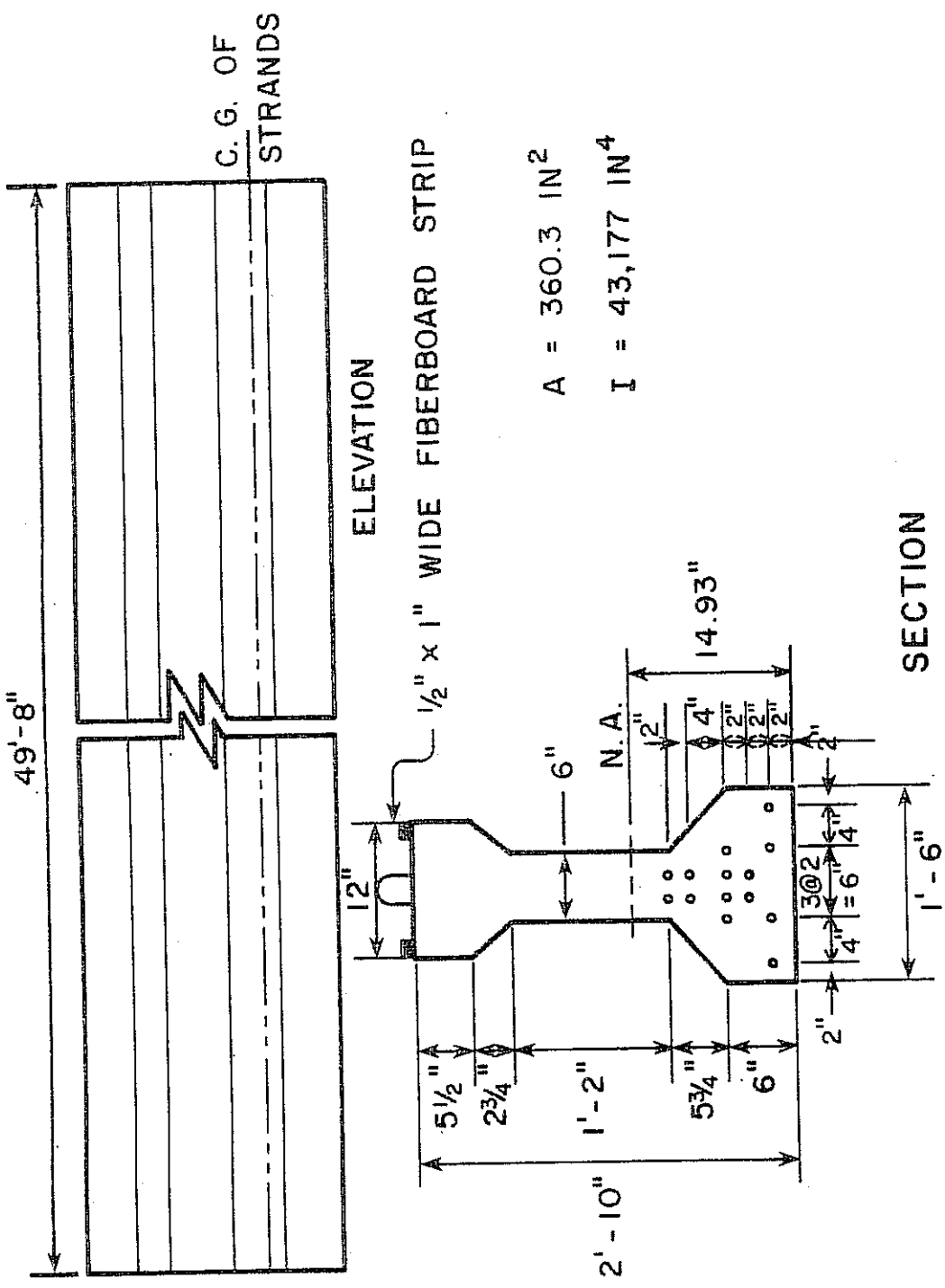

FIGURE 3.1 - TYPE B GIRDER

TABLE 3.1 TYPE B BEAM PROPERTIES

	Cast Date	Slump (in.)	f_c (psi)		
			7-day	14-day	28-day
CONCRETE	6-17-80	3.75	6160	7297	8147

	No. of Strands	Size	Type	Grade	Prestress Force per Strand (kips)
STEEL	14	1/2" dia.	7-wire strand	270 (stress relieved)	28.9

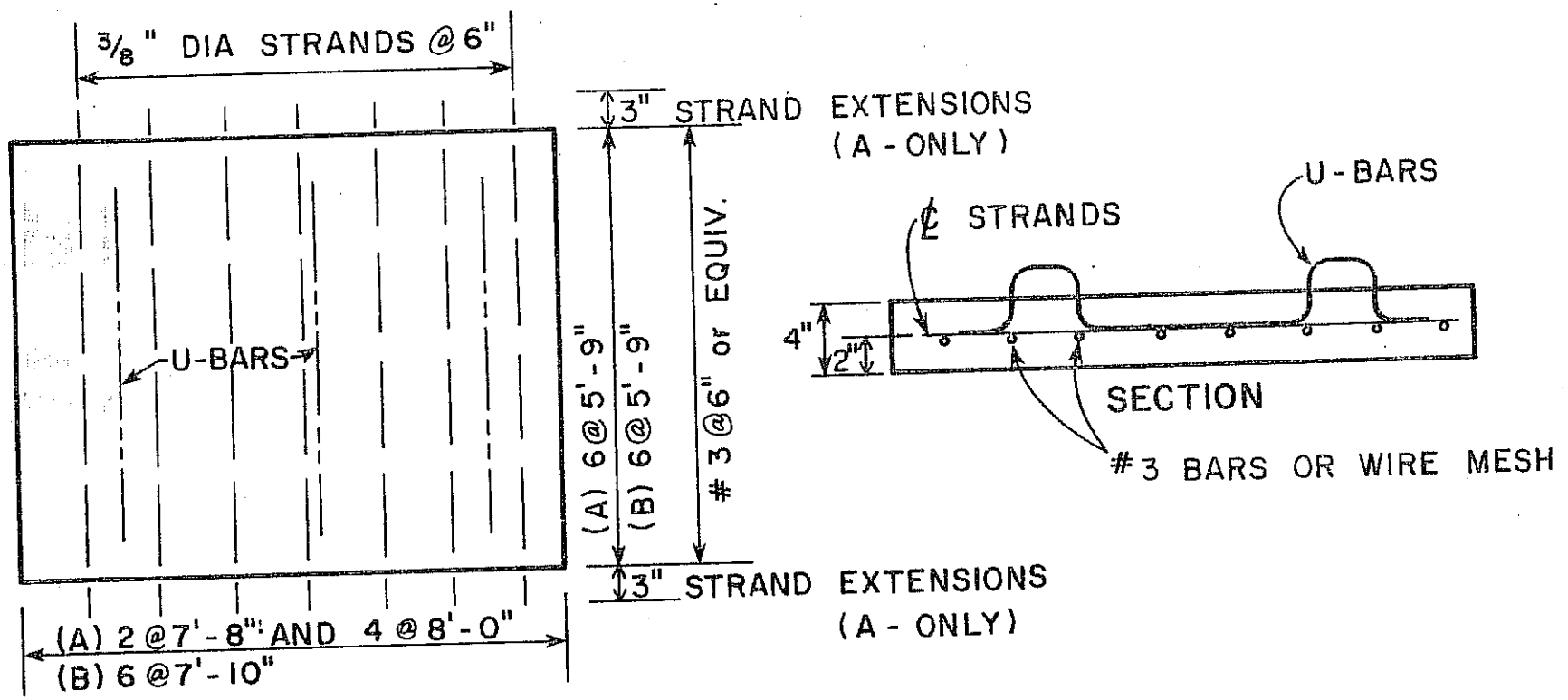

(A) - PANELS WITH STRAND EXTENSIONS
(B) - PANELS WITHOUT STRAND EXTENSIONS

FIGURE 3.2 - PRECAST PANELS

edges, identified as "B" panels in Fig. 3.2. These panels were much more rectangular in shape. Material properties are indicated in Table 3.2. The panels only extended between the girders; cantilever overhangs were constructed entirely of cast-in-place concrete.

3.1.3 Cast-in-Place Deck. The deck above the precast panels in the center area of the bridge, and also the cantilevered deck overhangs on each side of the bridge were cast-in-place concrete reinforced with a steel grid. Table 3.3 shows the material properties for the cast-in-place deck. Deck thickness averaged 7.75 in. ±0.25 in.

Texas SDHPT Class "C" concrete [11] was to be used on the deck. This class of concrete requires 6 sacks of cement per cubic yard of concrete. Because the concrete would be pumped, permission was obtained to modify this requirement to 5.5 sacks of cement per cubic yard of concrete. Additionally, 4 in. is designated as the maximum slump for Texas SDHPT placed "slab" concrete [11]. Because of the mix modifications, the average slump for placed concrete turned out to be 4-1/2 in. (Table 3.3). This average would have been even higher if the slump for the north half of the bridge had been taken in the middle of the north half pumping operation. Instead, it was taken at the beginning when the fresh pumping system was absorbing moisture, thus lowering the concrete slump as placed. Even though these two concrete requirements (cement content and slump) were not met, the 3600 psi strength requirement was clearly exceeded. See Table 3.4 for the concrete mix design.

3.2 Construction

These three components were combined to form a composite bridge, as shown in Fig. 3.3 [12]. The bridge was constructed with methods similar to those now being used in Texas for bridges of the same design. However, several differences do exist and require further explanation.

TABLE 3.2 PANEL PROPERTIES

CONCRETE*	Cast Date	Slump (in.)	f_c (psi) 7-day	14-day	28-day
	8-15-80	3.8	6686	6938	8035
STEEL	No. of Strands	Size	Type	Grade	Prestress Force Per Strand (kips)
	16	3/8" dia.	7-wire strand	270 (stress-relieved)	16.1

*Panels with 3" strand extensions. Properties for extruded panels unavailable.

TABLE 3.3 CAST-IN-PLACE DECK PROPERTIES

	Location	Cast Date	Slump (in.)	f_c (psi) 7-day	28-day	113-day
Concrete	North	9-17-80	3.5	3156	3997	4580
	South	9-17-80	5.5	3784	4840	5276

	Size	Length (ft)	Grade (ksi)	Tested Yield Stress (ksi)
Steel	#4	20	60	63
	#4	50	60	65
	#5	20	60	55

TABLE 3.4 CONCRETE MIX DESIGN

Design Strength:	3600 psi
W/C:	0.53
Type I Cement:	533 lbs
1" Aggregate:	1735 lbs
Fine Aggregate:	1475 lbs
Added Water:	283 lbs

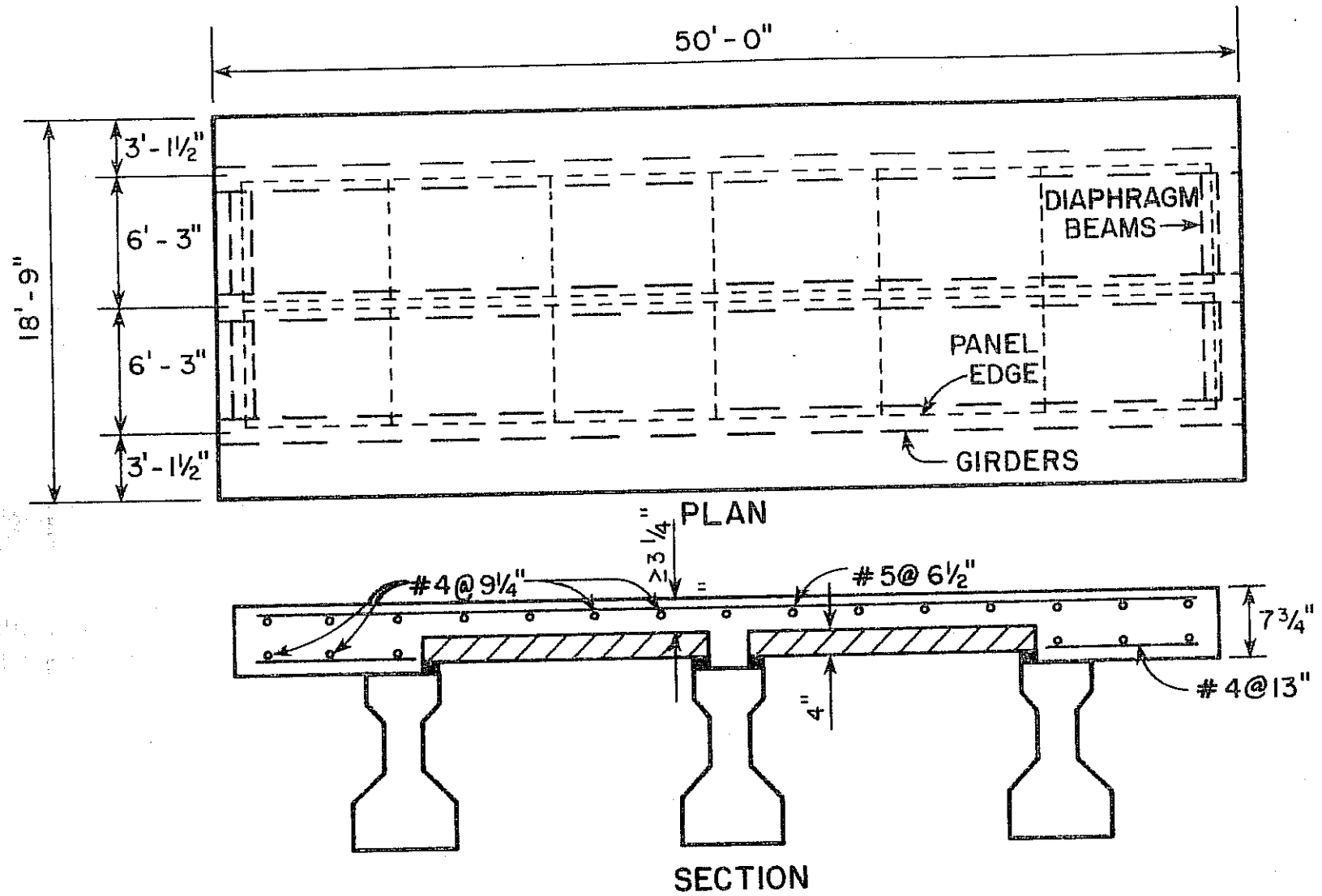

FIGURE 3.3 - COMPOSITE BRIDGE

As noted previously, the north half of the bridge was made with panels having strands projecting beyond the panel edges, while the south half was made with panels having no projecting strands. Panel placement on the north half of the bridge was difficult because of the nonrectangular shape of the panels. Some areas did not even extend past the fiberboard pads (Fig. 3.4.A), while other areas extended at least the recommended 1-1/2 in. beyond the fiberboard pads (Fig. 3.4.B). This problem did not exist on the south half of the bridge, where the rectangular panels without projecting strands had been uniformly manufactured.

This bridge construction normally includes so-called "U-bars" (Fig. 3.2), which are intended to enhance shear transfer between the panels and the cast-in-place deck. While these were left in place on the precast panels on the west side of the bridge, they were removed from all panels on the east side. This was done to permit evaluation of the effect of these bars on composite action.

For drainage purposes, actual field bridge decks will usually slope down from the centerline of the bridge to each overhang. However, since drainage was not a parameter in this test, no slope was necessary, and the deck was cast flat.

The bridge deck was cast on September 17, 1980, using an unshored construction technique. The area of the laboratory where the bridge was located was not directly accessible by concrete trucks. Considering the hot weather at the time of casting, it was decided that placement by overhead crane would take too long. Therefore, the pumping method was selected for placement of the concrete deck. No admixtures were used in the concrete mix. However, as stated previously in Section 3.1.3, the mix was modified to permit pumping.

The bridge deck was broom-finished and covered after casting. After seven days of moist-curing, the plastic covering and formwork were removed.

CHAPTER 4

TESTING APPARATUS

4.1 Flexural Tests

4.1.1 Static Test No. 1. The basic test setup for the first static test is shown in Fig. 4.1. In general, the same arrangement, with minor alterations, was used for all flexural tests (static and fatigue).

Each of the two loading frames consisted of structural steel shapes bolted together. These frames were braced, positioned transversely across the bridge and connected longitudinally by two coupled wide flange beams which supported two hydraulic rams, one at each end. Steel cable "X"-bracing provided additional frame stability. Each ram applied the axle load to the bridge deck through a spreader beam resting on two 1/2-in. × 12-in. × 20-in. long steel plates, grouted to the deck with hydrostone. These plates represented the loading due to an AASHTO standard HS truck axle with a width of 6 ft [7].

Riehle single-action rams with a 160-kip static capacity (120-kip fatigue capacity) were used to load the specimen. The hydraulic source was a Riehle/Los Fatigue Pulsator, used in a static application.

4.1.2 Fatigue Test Series No. 1. The same loading frame and equipment used in Static Test No. 1 were used for this test.

4.1.3 Static Test No. 2. The basic loading system for this test remained the same. However, the rams were changed to Miller 480-kip capacity, double-action rams. The hydraulic source for these rams was an Enerpac Hydraulic Power Unit Console. Additionally, an Edison Hydaulic Pressure Control Unit was used to maintain load levels.

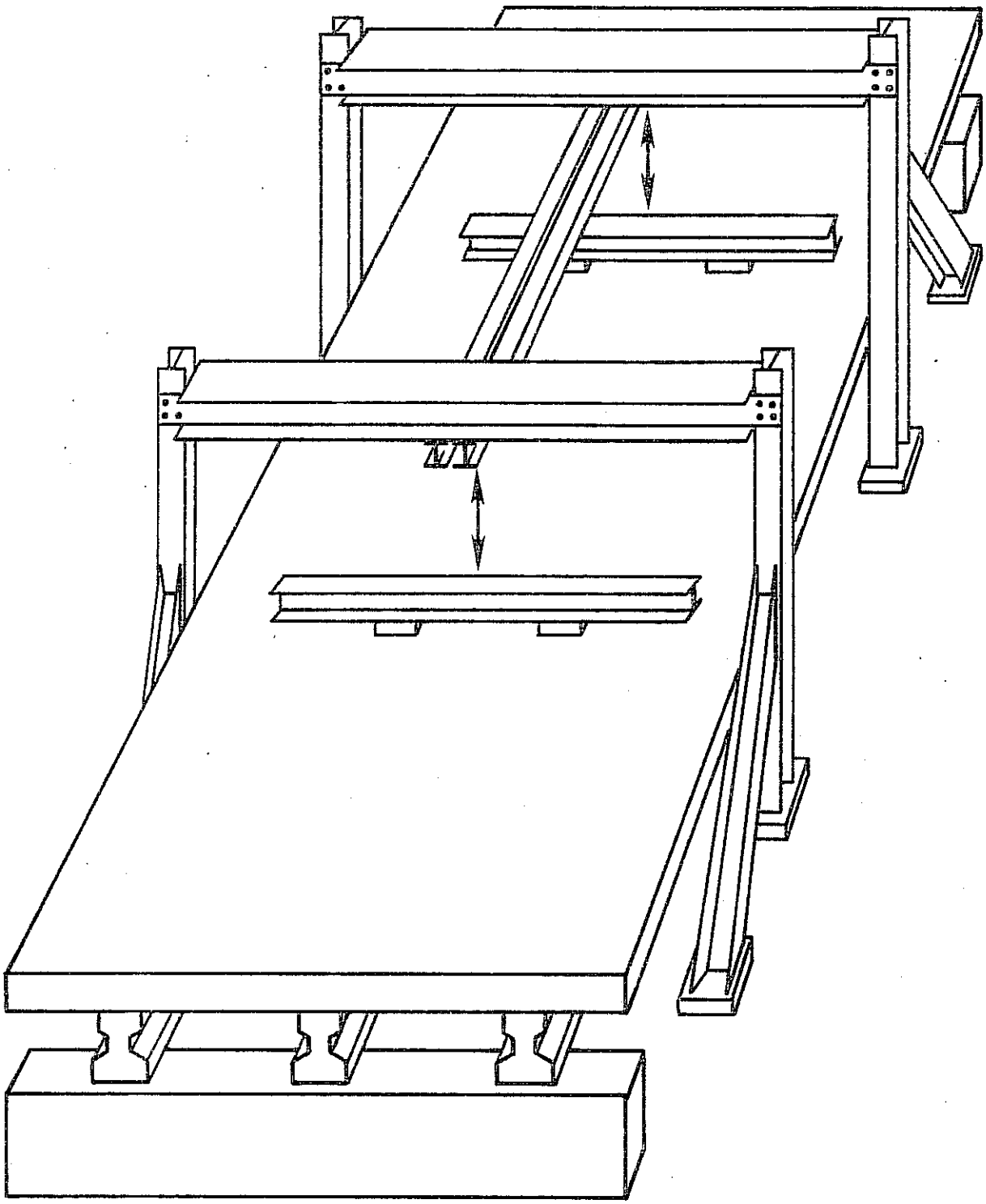

FIGURE 4.1 - FLEXURAL TEST SET-UP

4.1.4 Static Test No. 3. Additional bracing was added to the loading frame of Static Test No. 2 to provide the system with enough capacity to cause extensive flexural cracking in all of the girders. The same rams and hydraulic source previously used in Static Test No. 2 were reused. No load maintainer was used in this test.

4.1.5 Fatigue Test Series No. 2. The same loading frame from State Test No. 3 was used for this test. Two Miller 200-kip capacity, double-action rams were used with the Riehle/Los Fatigue Pulsator to provide the loading.

4.1.6 Static Test No. 4. The same loading frame and equipment used in Fatigue Test Series No. 2 were used for this test.

4.2 Concentrated Load Tests

The basic test setup for all concentrated load tests is shown in Fig. 4.2.

The loading frame was similar to one-half of the loading frame that was used for the flexural tests. The main difference was that this frame used two coupled wide flange beams for its transverse member. These beams were lowered from their previous elevation to allow the ram to bear directly on a plate placed on the bridge deck. For the first concentrated load test, a 1-in. × 12-in. × 12-in. long steel plate was used. For all other punching shear tests, a 1-in. × 8-in. × 20-in. long steel plate was used, with a 3/4-in. × 8-in. × 20-in. long neoprene pad placed between the plate and the bridge deck.

The ram used was a Miller 480-kip capacity, double-action ram, and the hydraulic source for this test was the Enerpac Hydraulic Power Unit Console. Both the ram and source had been previously used in Static Tests No. 2 and No. 3.

CHAPTER 5

INSTRUMENTATION

5.1 Overall Behavior

5.1.1 Load Measurement. Axle load was monitored in several different ways during the tests.

Initially, a strain-gage load cell was used with a Pegasus peak-reading digital voltmeter to check against the pressure gage readings supplied by the fatigue pulsator. After verifying that both instruments were reading within 1 percent of each other for both static and fatigue loading conditions, the load cell and the Pegasus Signal Generator were removed from the system. For Static Test No. 1, the pulsator pressure gages alone were used for measuring the static loads.

For Fatigue Test Series No. 1, the pulsator pressure gage readings were combined with another procedure to monitor the fatigue loading. The bridge was first loaded statically to the desired peak load for the test. Dial gages, which were located under the girders at midspan, were then zeroed to the deflection created by this load. The cyclic load was then adjusted to produce the same peak deflections. As verified in Appendix A, this procedure accounts for dynamic load amplification. This same procedure was used for monitoring the load during Fatigue Test Series No. 2.

For Static Tests Nos. 2, 3, and 4, and for all concentrated load tests, axle loads were measured using the hydraulic source pressure gages and also an independent pressure transducer.

5.1.2 Deflection Measurement. Dial gages were used to measure deflections of the bridge specimen.

For Static Test No. 1, the dial gages were placed at nine locations (Fig. 5.1). Four of these locations corresponded to the supports of the bridge specimen, permitting monitoring of deflections under the neoprene support pads.

During Static Test No. 1, data were taken to examine the relation between girder deflections due to rigid-body movement on the neoprene pads, and the deflections due to deformations of the bridge itself. For loads within the limits of linear elastic behavior, it was then possible to compute the support deflection corresponding to any given total girder deflection, and support deflections were no longer recorded.

5.2 Local Behavior

5.2.1 Measurement of Relative Displacements. Clip gages (Fig. 5.2) were used to measure relative concrete movements at or near panel joints. Included in these types of movements were longitudinal slip between the panels and girders, and also rotations and separations across panel joints. Appendix B describes how clip gages work and how slip, rotations, and separations were calculated.

Clip gages were placed symmetrically on both halves of the bridge in the vicinity of the loading points (Fig. 5.3). These gages were placed both above and below the bridge deck and were connected through switch and balance units to Budd Digital Strain Indicator boxes, from which readings were recorded.

These gages were only used during the static tests. While attempts were made to analyze clip gage data recorded during the initial fatigue tests, the large amount of scatter made trends difficult to evaluate.

5.2.2 Crack Measurement. Cracks on the bridge deck were color-marked at various stages throughout Fatigue Test Series No. 1, and also at the end of Fatigue Test Series No. 2. Cracks were

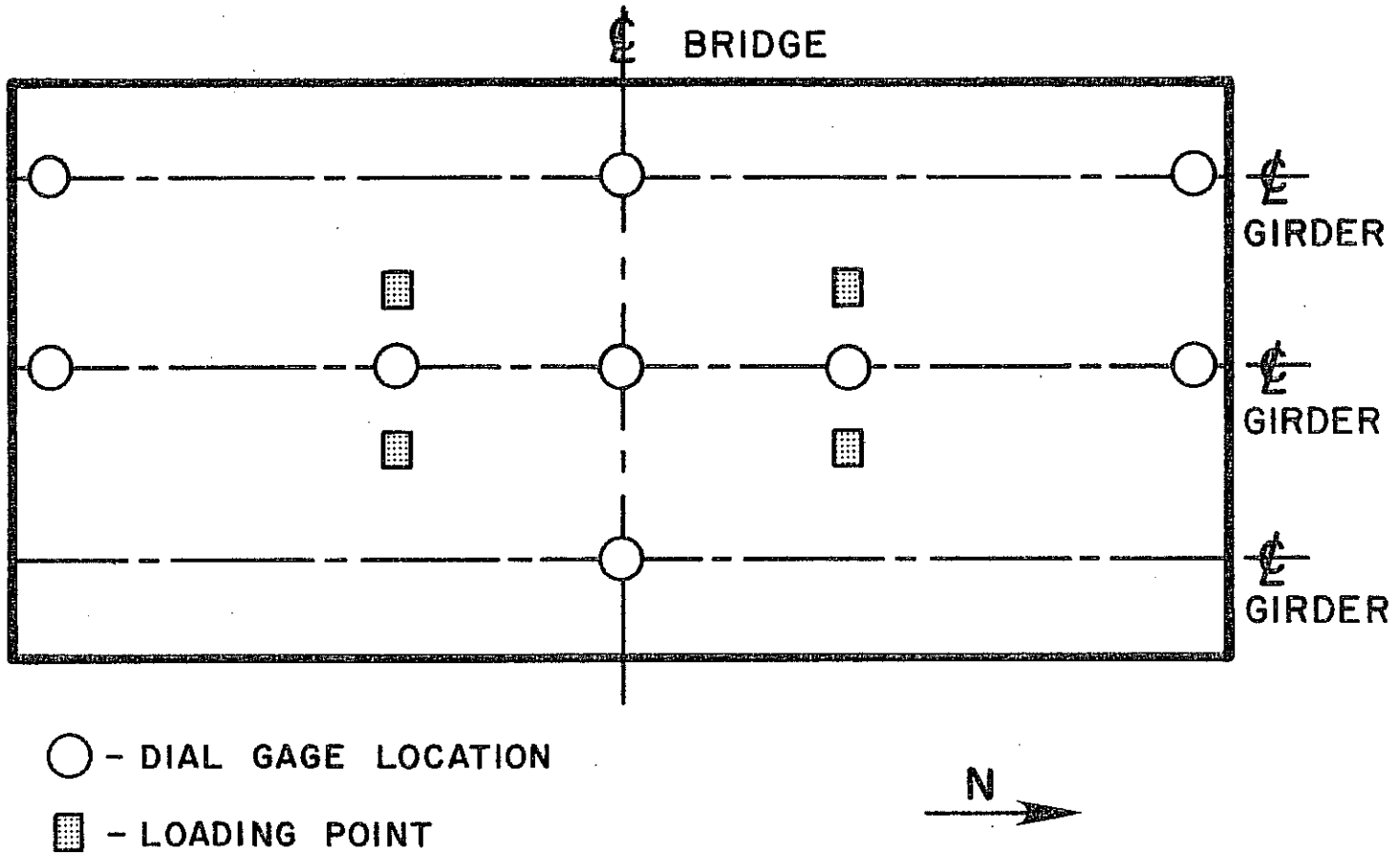

FIGURE 5.1 - LOCATION OF DEFLECTION DIAL GAGES

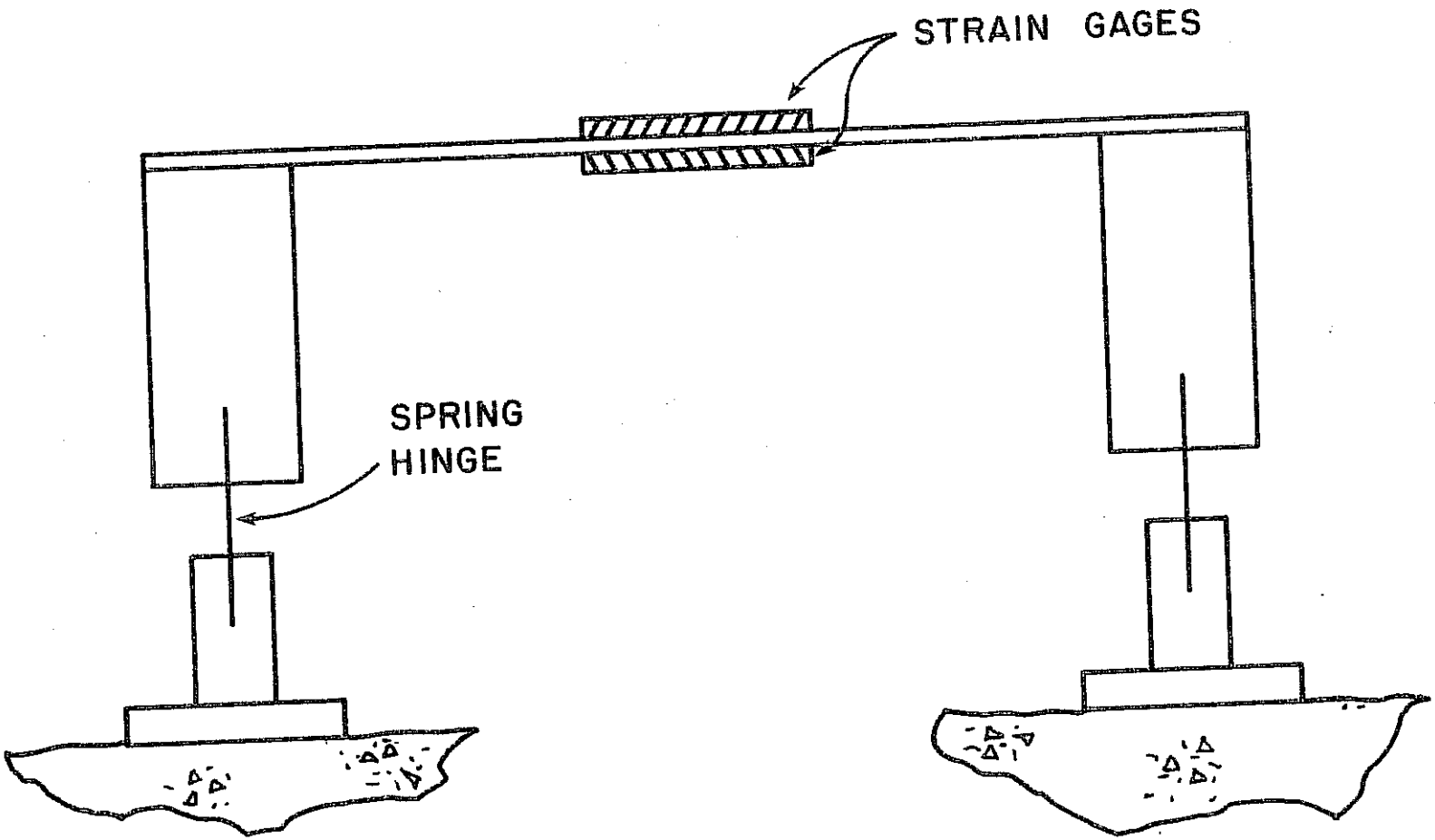

FIGURE 5.2 - CLIP GAGE

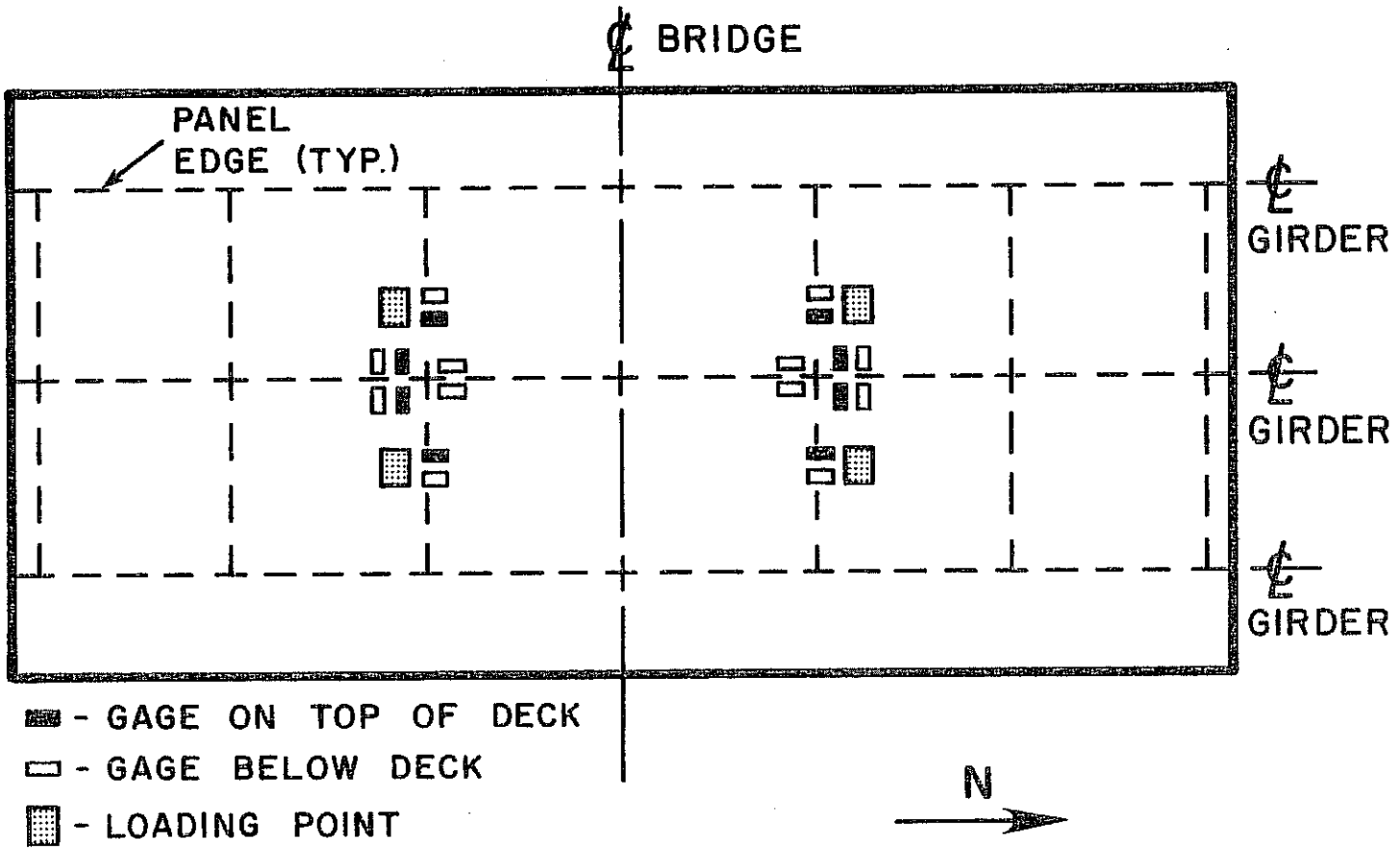

FIGURE 5.3 - CLIP GAGE LOCATIONS

color-marked on the girders during various stages of Static Test No. 3. Crack widths were measured at the various stages using a pocket comparator.

CHAPTER 6

TEST RESULTS

6.1 Introduction

In this chapter the results from the tests described in Chapter 2 will be presented and discussed. The overall load-deflection behavior of the bridge will be compared from load state to load state, and the actual results will be compared to analytical results calculated by established computer programs.

The extent of local composite action of the bridge at panel edges will be examined in several ways. First, results showing the concentrated angle changes between the panels and the center girder will be presented (Fig. 6.1a). Second, the separation of the panels across their longitudinal joint with the center girder will be discussed (Fig. 6.1b). Third, results showing the longitudinal slip between the panels and the center girder will be presented (Fig. 6.1c). Last, the physical cracking pattern on the bridge deck will be discussed. These results will be evaluated using two criteria. First, the results from the north half of the bridge (having panels with strand extensions) will be compared to the results from the south half of the bridge (having panels without strand extensions). The second criterion will be to examine the magnitudes of the movements measured. This will give an indication as to how well the panel/girder joint behaves as a continuous connection (the larger the movements, the less the continuity). In addition to measurements of continuity at longitudinal panel edges, some data were also obtained at transverse joints. Although these were not specifically within the scope of this investigation, they will also be presented and discussed briefly.

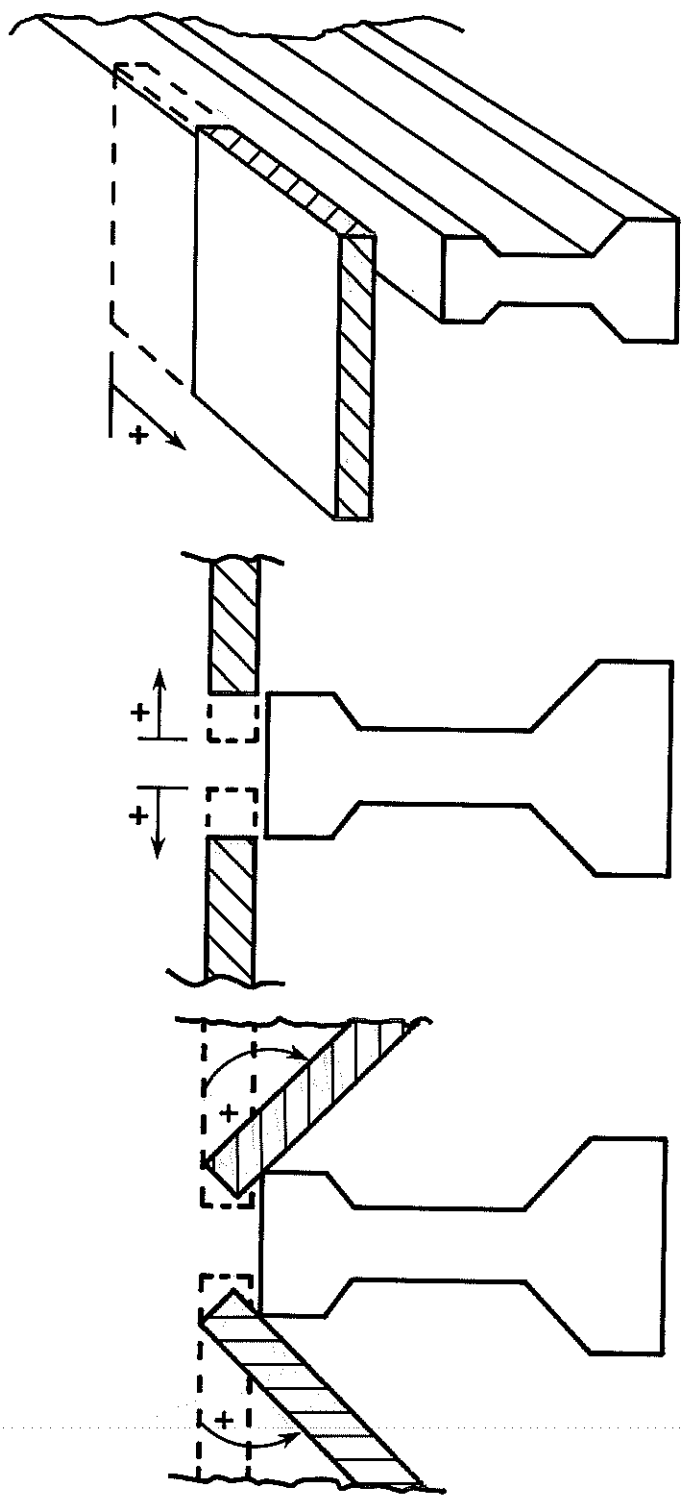

A. ANGLE CHANGES B. SEPARATION C. SLIP

FIGURE 6.1 - COMPOSITE ACTION MEASUREMENTS

The post-cracking performance of the center girder under fatigue loading will be compared with results obtained in a previous investigation [6].

Actual capacity under concentrated loads will be compared to predicted capacities calculated using yield-line theory and AASHTO punching shear provisions. The physical cracking pattern of the bridge deck under concentrated loads will also be discussed.

All results for the fatigue and static loadings are expressed in terms of the applied axle loads. As noted previously, those loadings were applied symmetrically at approximate third points of the bridge. For consistency, all such axle loads will be described in terms of the magnitude of one of the axle loads "P", as shown in Fig. 6.2. For example, if a certain bridge deflection occurred when the bridge had a total load of 100 kips, the corresponding axle load, P, would be one-half this, or 50 kips. That deflection would be referred to as occurring under an axle load of 50 kips. Results for the concentrated load tests will be discussed in terms of the load actually applied at the single point.

Periodically, the results will be compared to design loads. For the purposes of this report, the design live loadings referred to will be those based on AASHTO HS 20-44 truck loading with an AASHTO applied impact factor [7]. Thus, design axle loads will be:

$$32 \text{ kips} \times 1.29 = \underline{41 \text{ kips}}$$

6.2 Flexural Tests

6.2.1 Overall Behavior. The actual load-deflection behavior of the bridge is shown in Fig. 6.3, in terms of the centerline deflection of the center girder. The plotted deflections are total measured

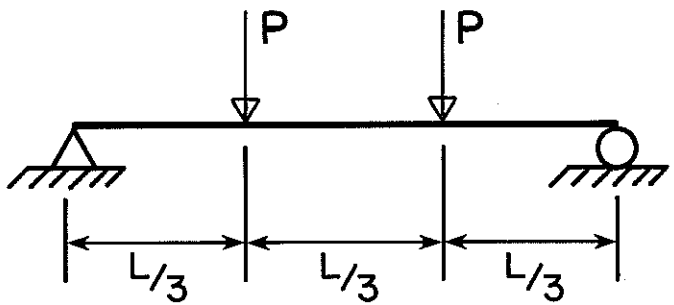

FIGURE 6.2 - APPLIED AXLE LOADS "P"

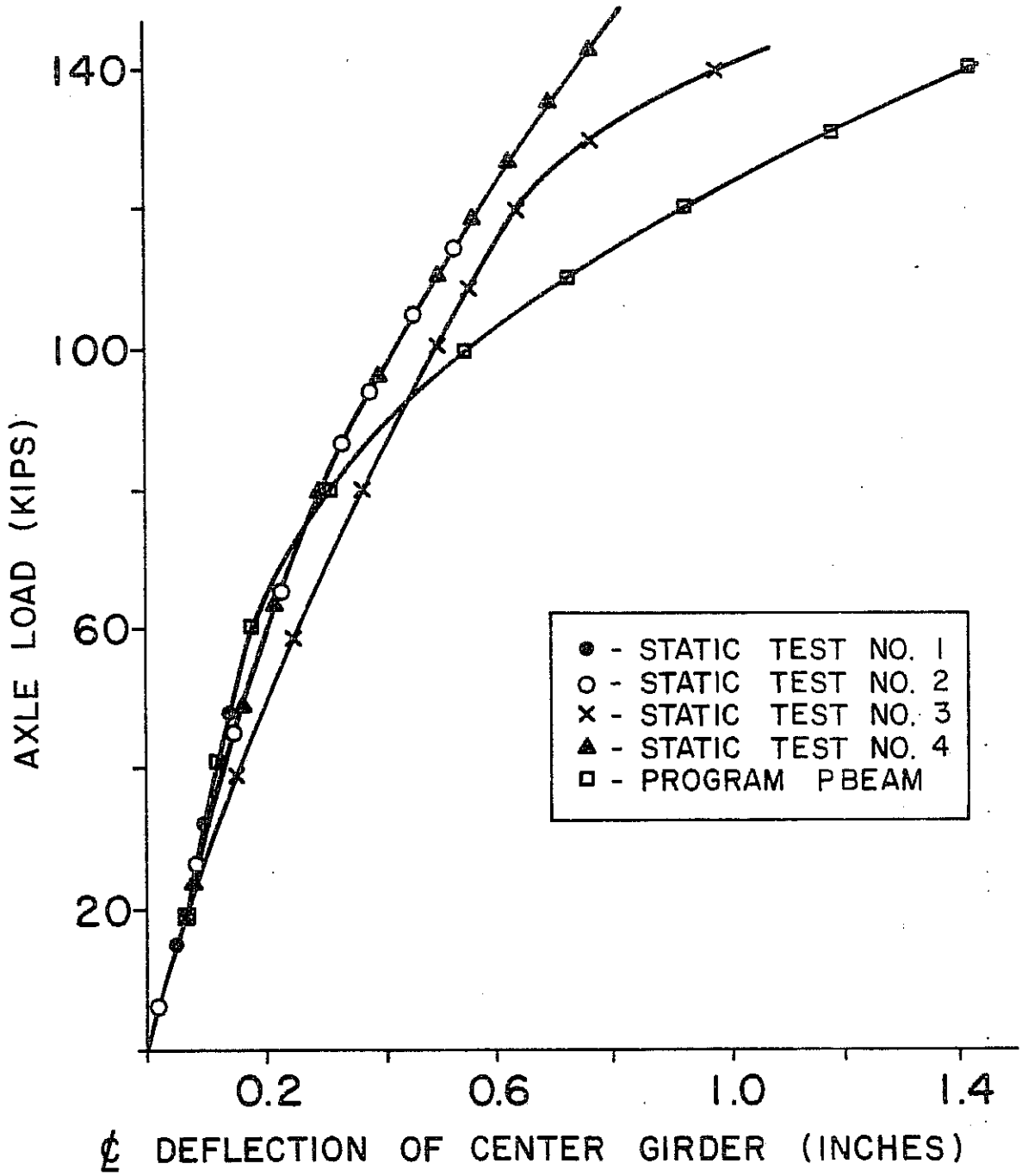

FIGURE 6.3 - LOAD-DEFLECTION CURVES

deflections, minus the average of the support deflections at each end of the center girder. The results from Static Tests No. 1, 2, and 4 are very similar. At any given axle load, the results from Static Test No. 3 show slightly more deflection than do those of the other static tests. However, it is important to note that the curves remain fairly consistent in spite of the fact that they were obtained at different times during the bridge's load history. In particular, the bridge was subjected to 6.5 million fatigue cycles between Tests No. 1 and 2, cracked at the end of Test No. 2, and 5 million more fatigue cycles were applied between Tests No. 3 and 4.

These deflection results were compared with analytical results obtained in the following manner: The computer program SLAB 49 [13], a structural analysis program for bridge decks, was used to determine how loads on the bridge deck were transferred to the center girder, assuming uncracked, linear elastic behavior. The results showed that each of the three girders took almost exactly one-third of the slab deck self-weight. Under the four concentrated loads only, the program calculated the moment diagram for the center girder, as shown in Fig. 6.4a. The moment diagram is statically consistent with the loadings shown in Fig. 6.4b. To simplify the problem, this moment diagram was replaced by the close approximation shown by dashed lines in Fig. 6.4a. This simple approximation is statically consistent with the loadings shown in Fig. 6.4c. Although the program SLAB 49 was developed for use with continuous bridge decks rather than the panel-type construction studied here, the results are believed to be reasonable. While the distribution of load to the center girder would be affected by cracking in the deck, the minor cracking observed is believed to have no significant effect on the load distribution.

These simplified equivalent loads, shown in Fig. 6.4c, were then applied to the center girder, and its centerline deflections were calculated and compared with the experimentally observed deflections. The beam deflections were computed using the computer program

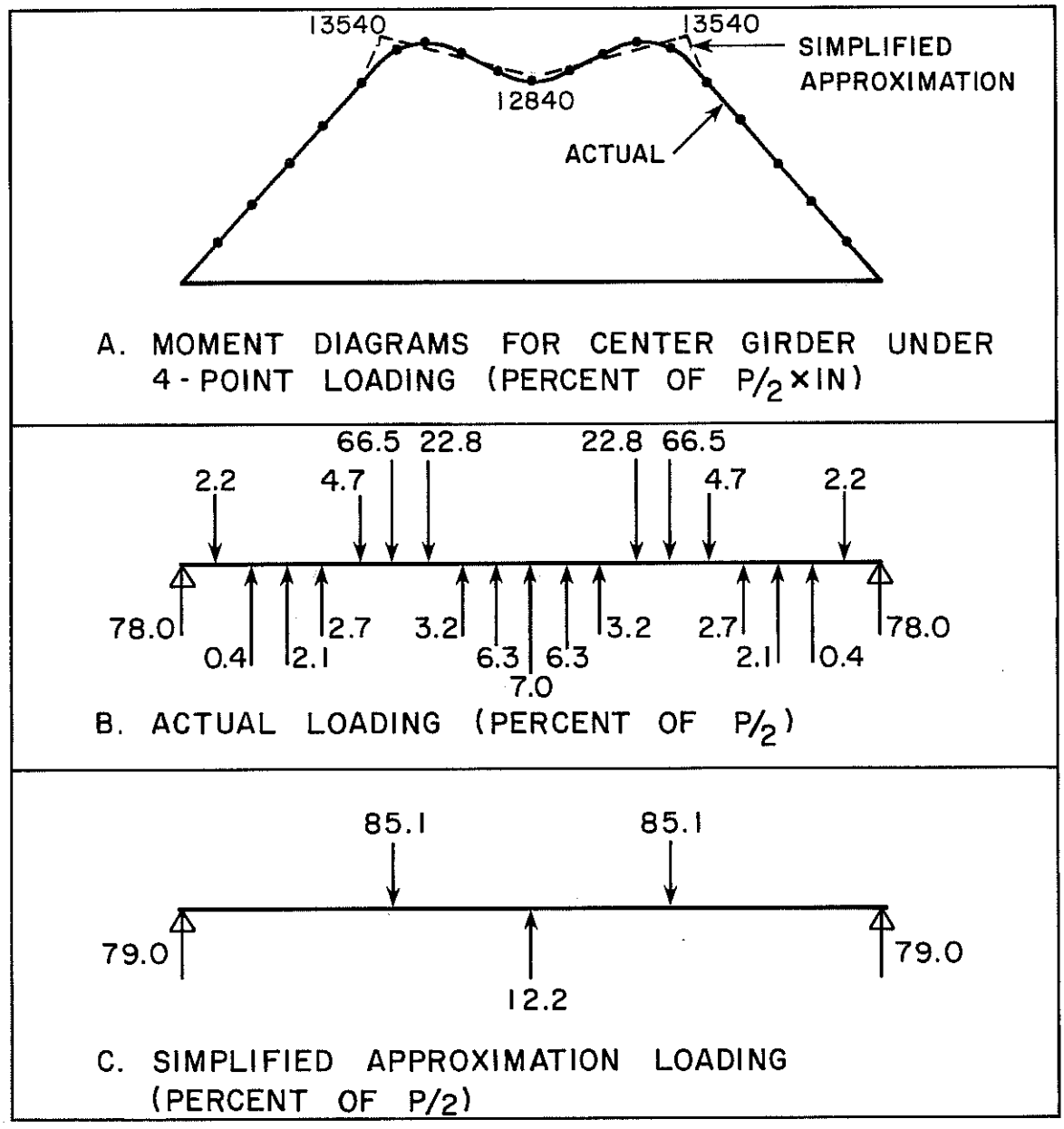

FIGURE 6.4 - LOADING FOR PROGRAM PBEAM

PBEAM [14], which takes into account factors such as creep, shrinkage, relaxation, and tensile cracking. The idealized center girder cross section used is shown in Fig. 3.1, and the material characteristics are summarized in Table 3.1. The tensile cracking resistance of the girder was taken as $6\sqrt{f'_c}$ (psi units). Centerline deflections of the center girder were computed under a load history which included all four static loadings, and which considered the different times in the life of the bridge at which these loads were applied. The center girder was considered to be loaded by its own self-weight, plus the tributary dead load due to slab self-weight, plus the simplified equivalent girder loads determined as discussed above. Fig. 6.3 shows the calculated load-deflection results due to application of these equivalent girder loads in addition to the dead loads, and also shows the experimentally obtained load-deflection behavior. Comparison of the observed and calculated behavior shows that the calculated behavior very closely models the actual initial stiffness. The calculated results indicate a probable ultimate capacity of about 160 kips. While the static tests were not continued to failure, and while there is some variation between bridge behavior in Static Tests No. 3 and 4, both sets of results are reasonably consistent with that calculated capacity. At axle loads "P" in excess of 100 kips, the calculated load-deflection behavior is more flexible than that actually observed. This tendency has been observed in previous uses of the program PBEAM [14], and is probably due to an overestimate of the effect of tensile cracking. The program PBEAM assumes that once a tensile crack has propagated up to a given level, the entire width of the girder is completely cracked up to that level. This approach is conservative, since it neglects the local effects of longitudinal and transverse reinforcement in delaying the propagation of tensile cracks across the width of the cross section. In general, however, the analytical load-deflection results agree closely with those observed experimentally.

6.2.2 Local Behavior

6.2.2.1 Concentrated Angle Changes Across Panel Joints. The concentrated angle changes between the panels and the center girder are shown for Static Tests Nos. 1 through 4 in Figs. 6.5 through 6.8, respectively. Refer to Appendix B for sample calculations.

As noted previously, at any given load level the magnitude of these angle changes increases as the continuity across the longitudinal panel/girder joint decreases. Because the center girder deflects vertically more than the two outside girders deflect, the panels rotate upward with respect to the center girder. The results from Static Test No. 1 show small angle changes (maximum value: -7×10^{-3} degrees), with most movement occurring at the southwest quadrant of the bridge. However, because the maximum static axle load used in this test (48 kips) was too small to produce significant relative movements, these angle changes are not clear indications of the extent of continuous action. For Static Tests No. 2 and No. 3, the results clearly show more angle change occurring at the southwest and southeast than at the northwest and northeast quadrants of the bridge. Here the maximum angle change is -35×10^{-3} degrees, and most of it does not occur until a static load of 60 kips is exceeded. Angle change results from Static Test No. 4 again show most of the movement occurring at the southwest quadrant, with substantial movements at the southeast and northwest quadrants. However, most of the major movements occur in the form of large jumps between data points. This was probably due to the effect of local cracking. Prior to Fatigue Test Series No. 2, this cracking was minimal, and relative rotations increased reasonably smoothly with applied load. The cracks that formed during Fatigue Test Series No. 2 (Fig. 6.19), however, caused subsequently observed rotations to occur in jumps, as the cracks opened and closed. Thus, when Static Test No. 4 was run, excessive jumps in gage readings occurred due to the larger crack openings in the bridge deck at gage locations. Also, for this test, note that large rotations did not occur until after the 50-kip static axle load was exceeded.

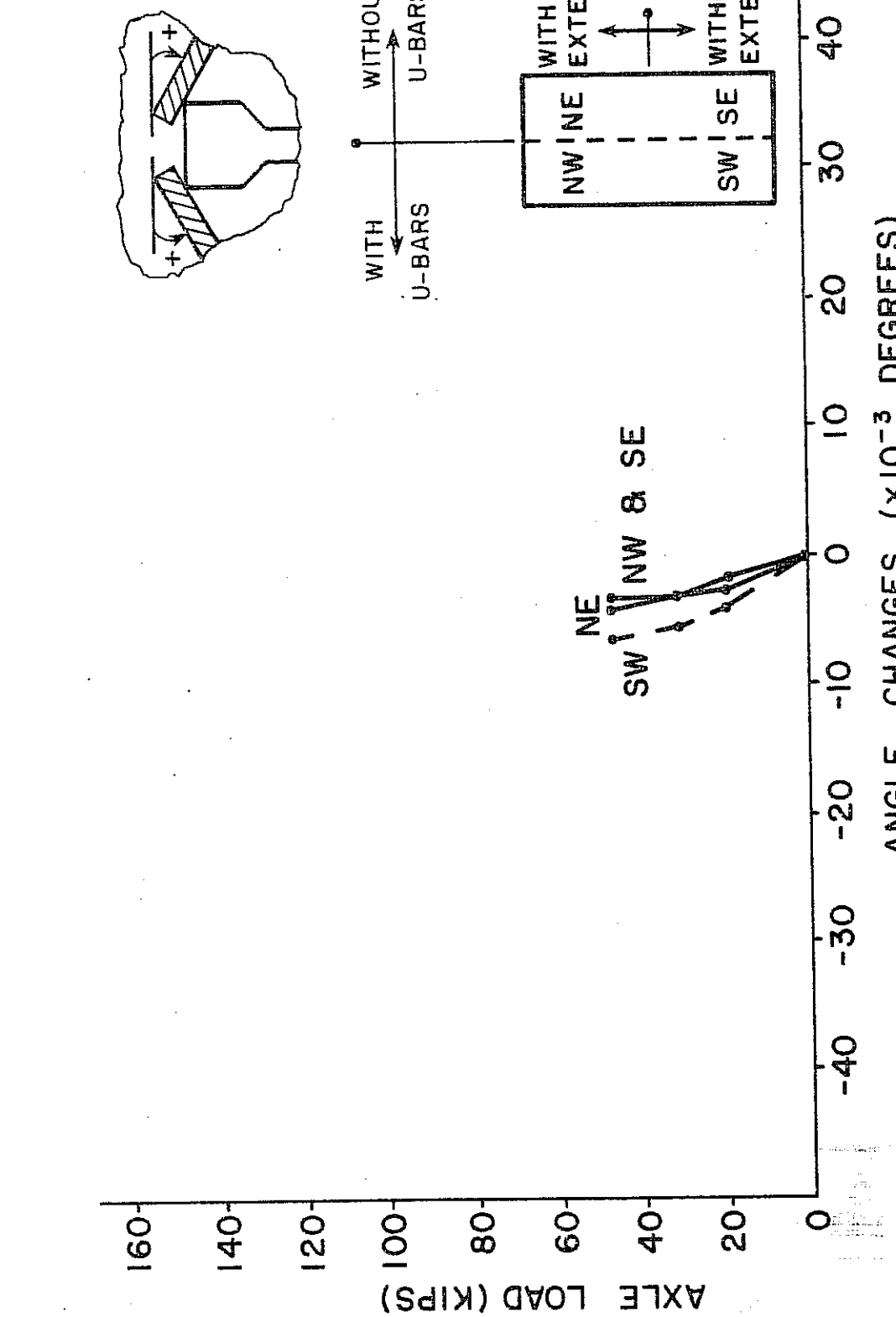

FIGURE 6.5 - ANGLE CHANGES FOR STATIC TEST NO. 1

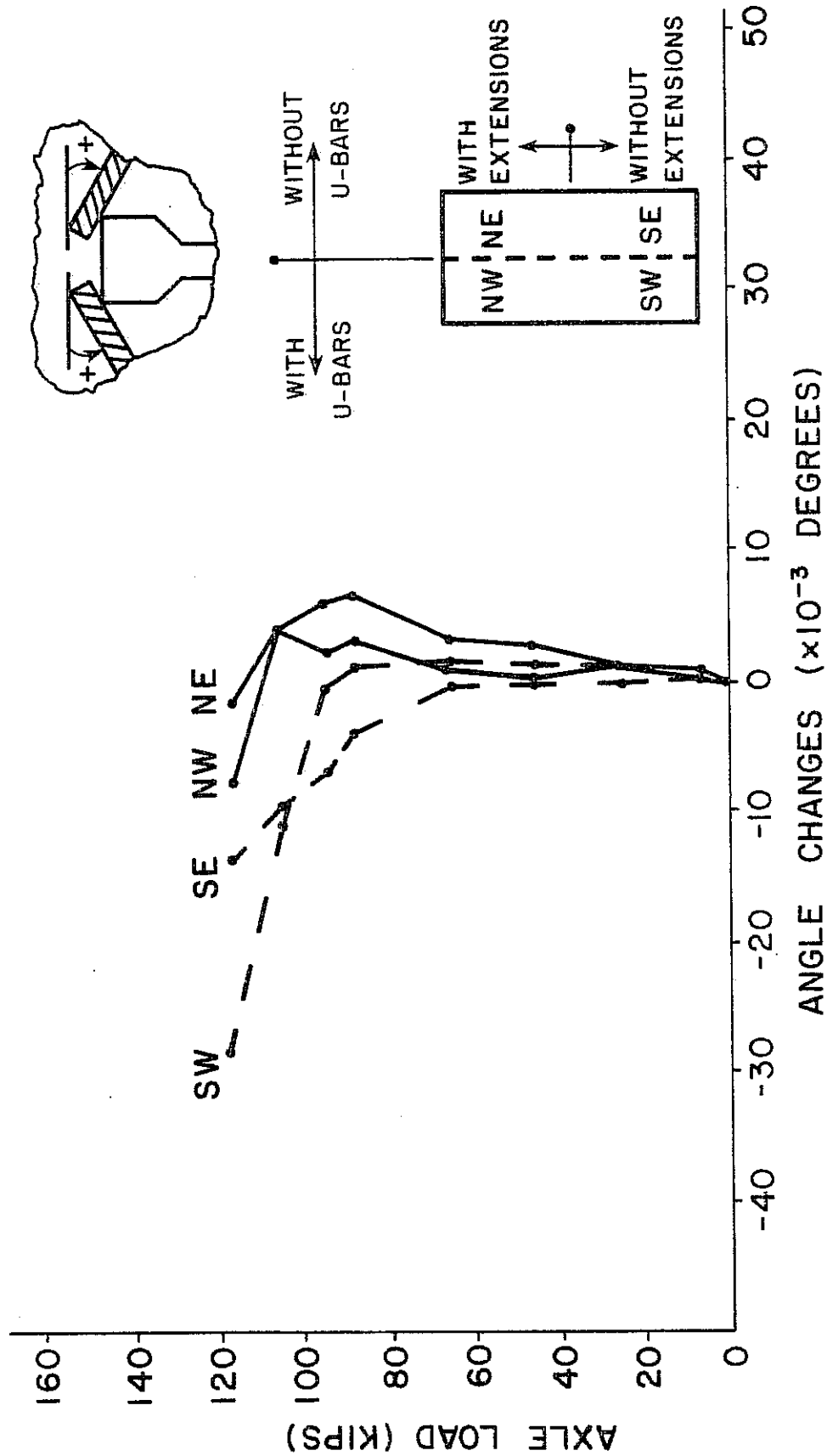

FIGURE 6.6 - ANGLE CHANGES FOR STATIC TEST NO. 2

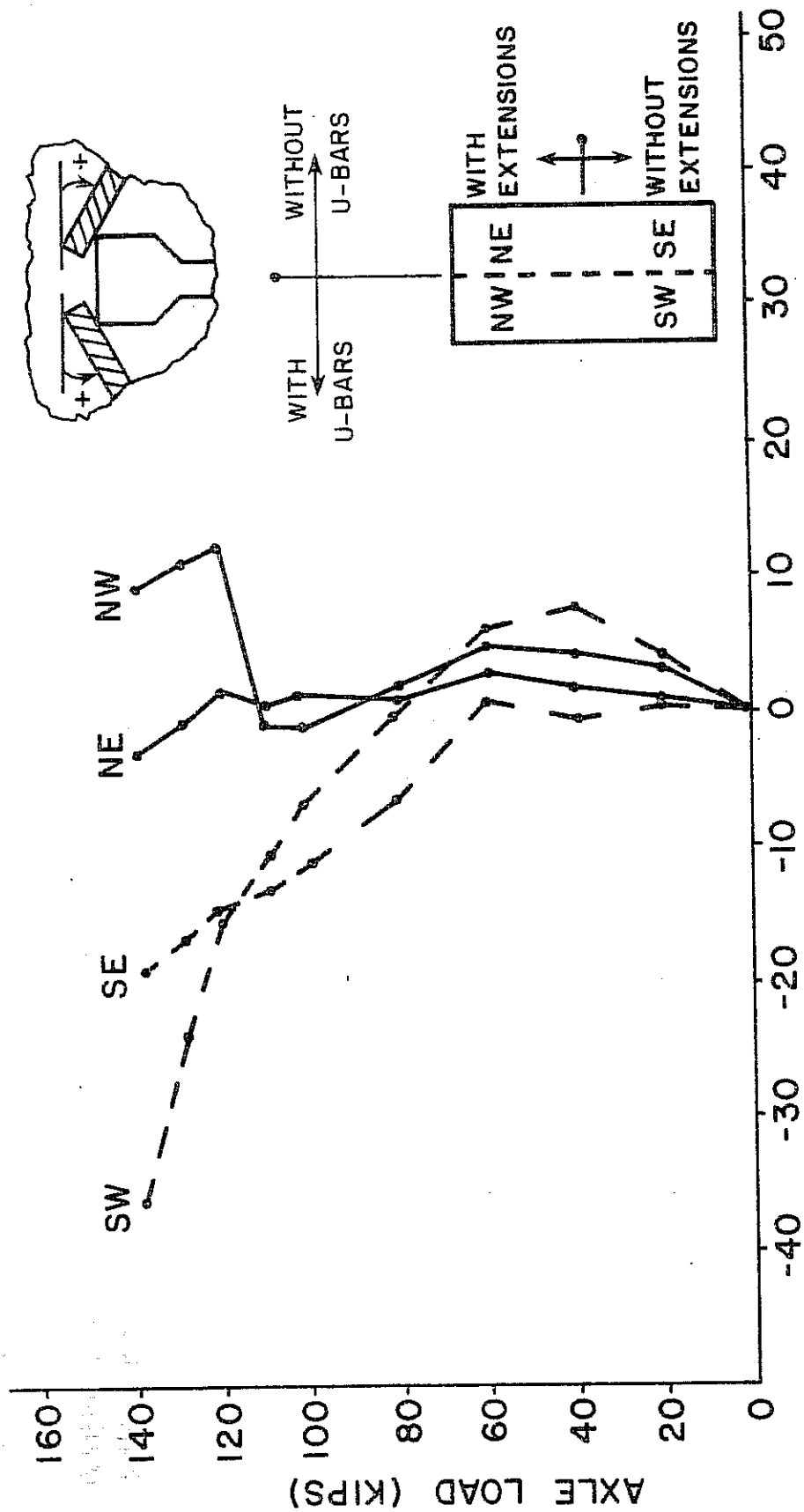

FIGURE 6.7 - ANGLE CHANGES FOR STATIC TEST NO. 3

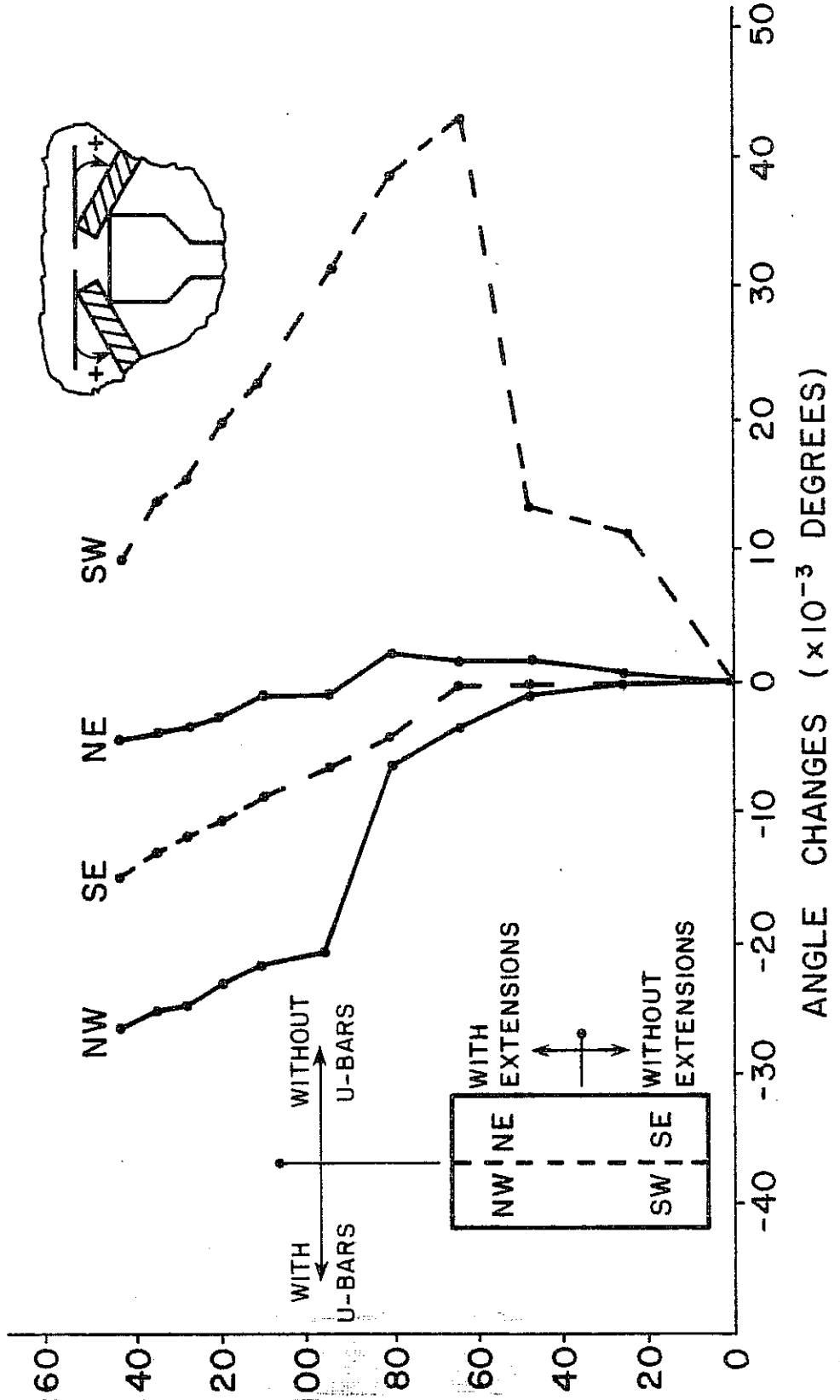

FIGURE 6.8.- ANGLE CHANGES FOR STATIC TEST NO. 4

In summary, larger relative rotations occurred at longitudinal panel joints on the south half of the bridge, where the panels without strand extensions were placed, than on the north half of the bridge. However, the maximum magnitude of these angle changes was quite small, less than 45×10^{-3} degrees. As shown in Fig. 6.9, if this angle change were conservatively considered to occur at one point, it would be consistent with a local slab crack less than 0.006 in. in width, well below the maximum acceptable flexural crack width implied by ACI 318-77 [15]. Also, most of the angle change occurred after the bridge had been subjected to axle loads of 50 kips, clearly in excess of the design axle loads. It should be noted that the second fatigue series tests led to more jumps in angle change data with increasing load, but did not greatly increase the magnitudes of those angle changes. Examination of Figs. 6.5 - 6.8 also shows a slight tendency toward decreased local continuity on the west side of the deck as opposed to the east. This tendency is believed not conclusive enough to indicate a significant difference in behavior, and no explanations for it were readily apparent.

6.2.2.2 Separations at Panel Joints. The separation of the panels across their longitudinal joint with the center girder is shown for Static Test Nos. 1 through 4 in Figs. 6.10 through 6.13, respectively. Refer to Appendix B for sample separation calculations.

As with angle changes, the magnitude of these separations at any given load increases as the continuity across the longitudinal panel/girder joint decreases. The results from Static Test Nos. 1, 2, and 3 all show that more panel separation occurs at the southwest and southeast quadrants of the bridge than at the northwest and northeast quadrants. However, the results from Static Test No. 1 are not conclusive for evaluation purposes, due to their small magnitudes (-2×10^{-4} in.). The maximum separations for Static Test Nos. 2 and 3 were 23×10^{-4} in. Again, most of the separation in these tests occurred under static axle loads in excess of 60 kips.

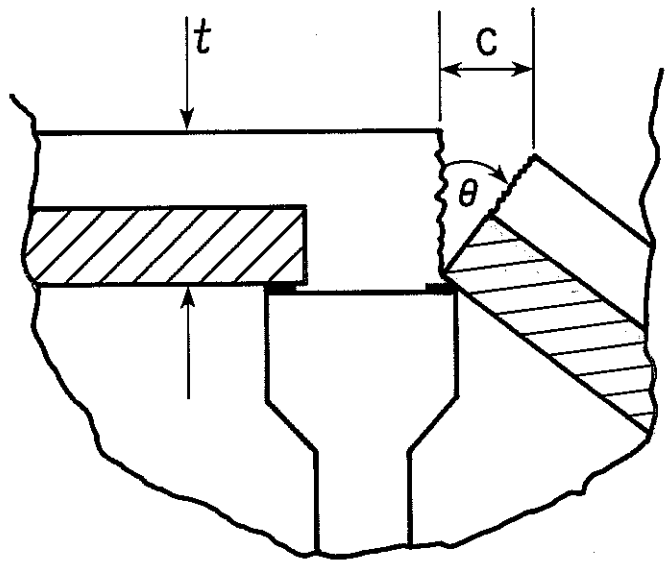

$\theta = 45 \times 10^{-3}$

$t = 7\ 1/2$ in.

$\text{SIN}\ \theta = C/t$

$C = t\ \text{SIN}\ \theta$

$C = 0.0059$ in.

FIGURE 6.9 - CRACK WIDTH ASSOCIATED WITH MAXIMUM ROTATION

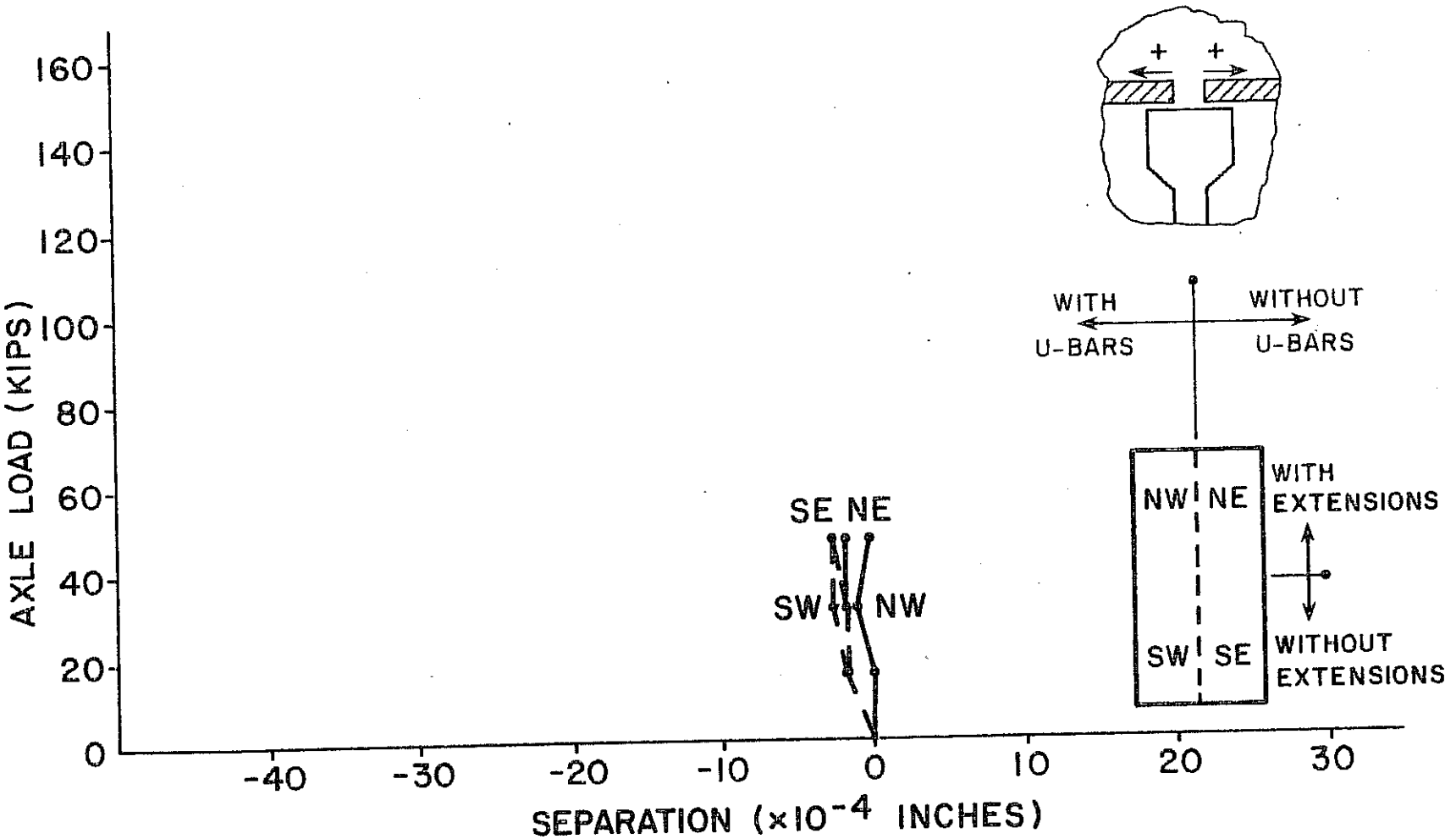

FIGURE 6.10 - SEPARATION - STATIC TEST NO. 1

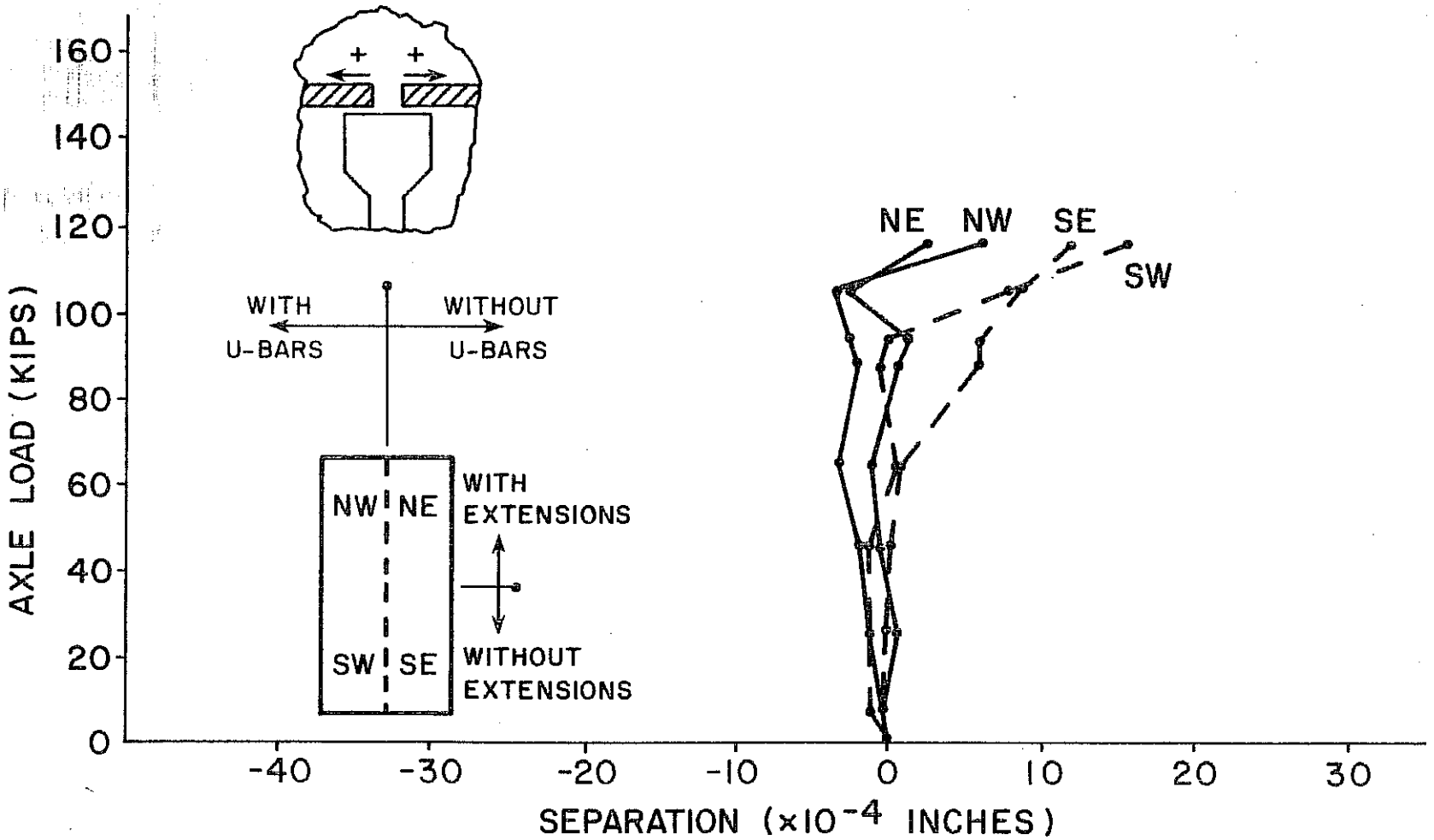

FIGURE 6.11 - SEPARATION - STATIC TEST NO. 2

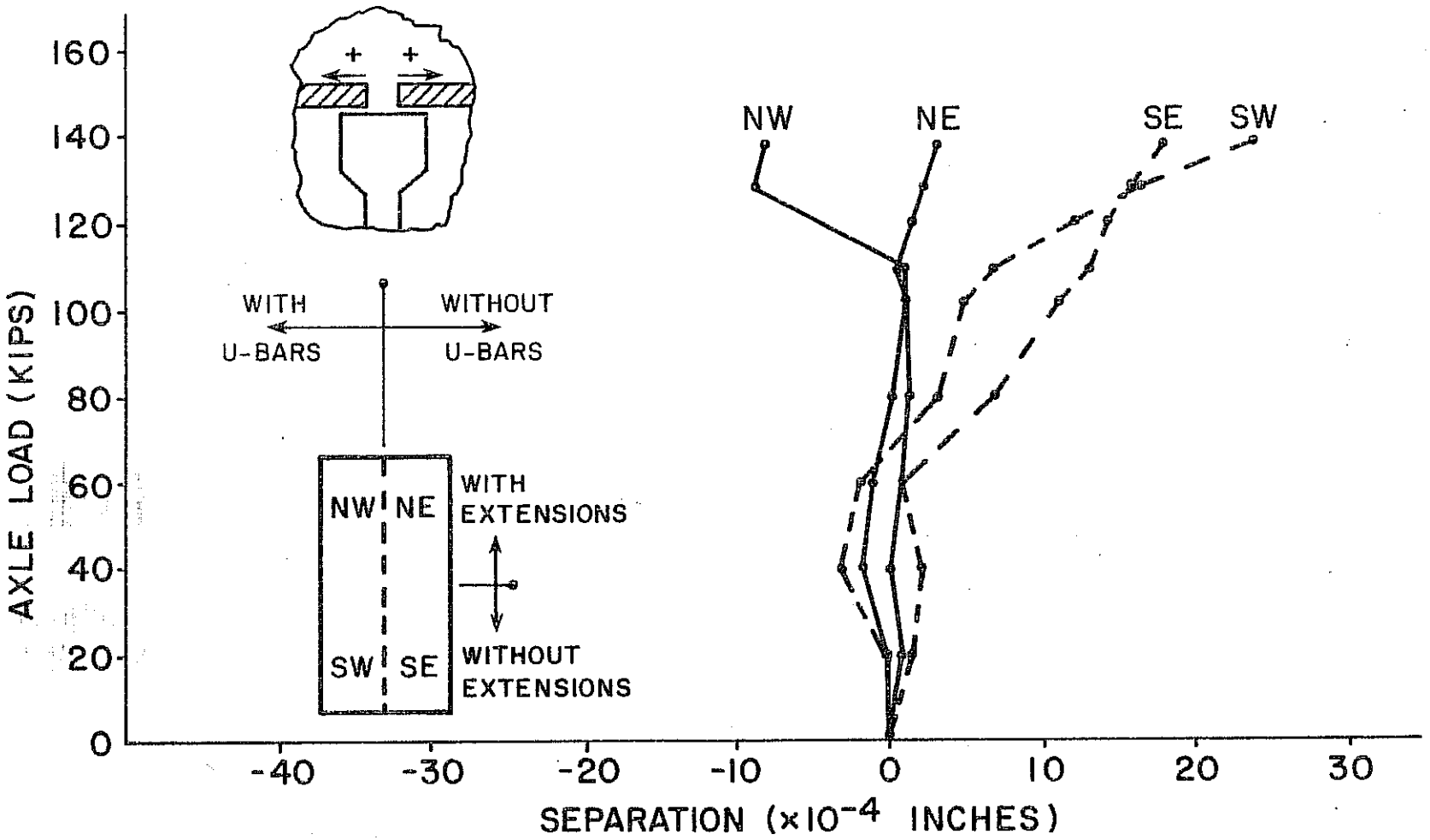

FIGURE 6.12 - SEPARATION - STATIC TEST NO. 3

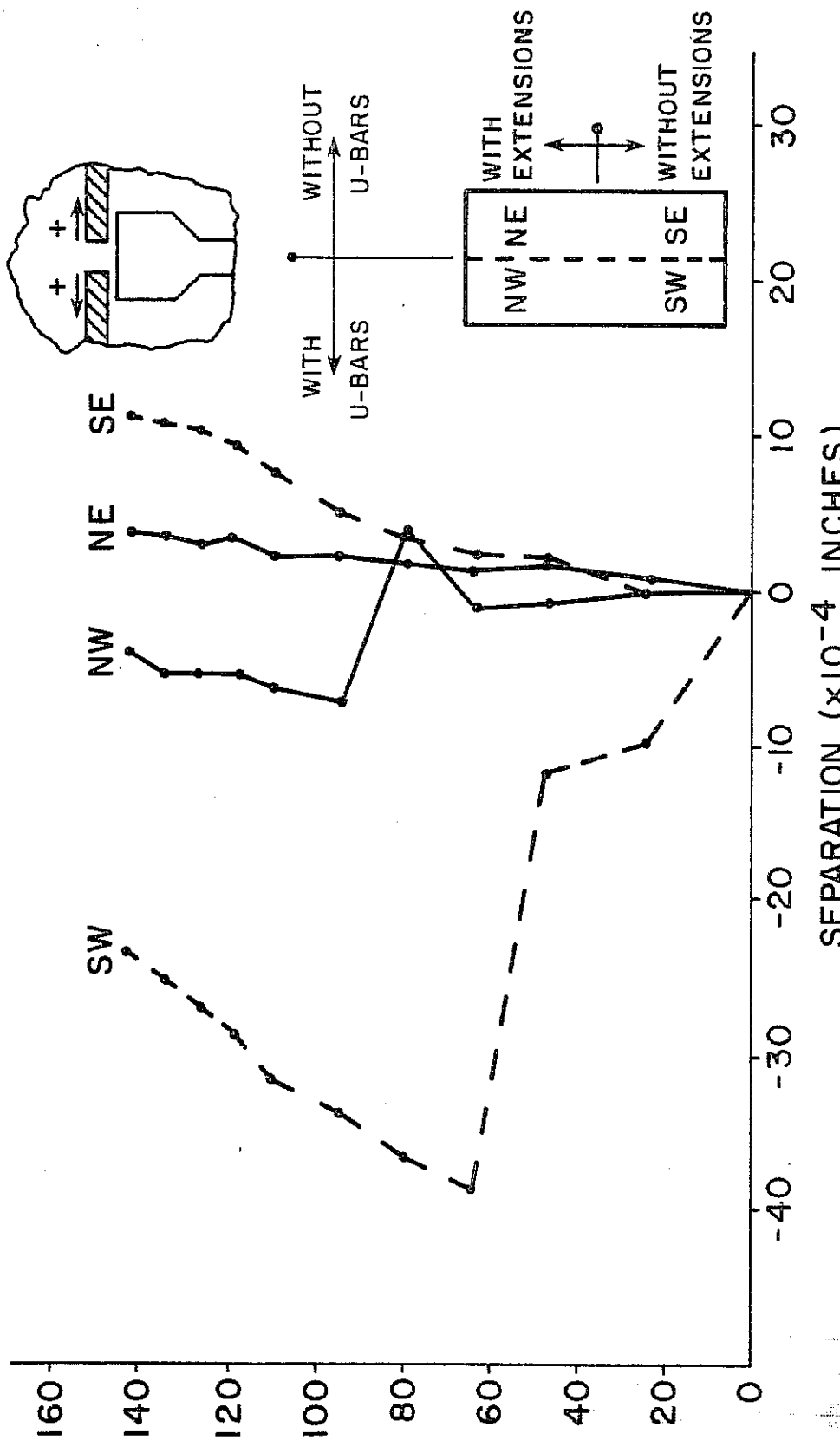

FIGURE 6.13 - SEPARATION - STATIC TEST NO. 4

Separation results from Static Test No. 4 show that most of the movement occurs at the southwest quadrant, with some movement also occurring at the southeast and northwest quadrants. Most of the movement occurs in the form of large jumps between data points, similar to those observed in the angle change results for Static Test No. 4. As before, it is felt that this erratic movement was due to the extra fatigue cracking that occurred between Static Test Nos. 3 and 4. Again, note that most of the movement does not occur until the static axle load exceeds 50 kips.

In summary, more panel separation occurred on the south half of the bridge, where panels without strand extensions were placed, than on the north half of the bridge. However, as in the case of panel rotations, the maximum magnitude of panel separations was small, only 40×10^{-4} in. This separation, if considered to occur at one single location, would be conservatively consistent with a slab crack having a width of about 0.004 in., considerably less than the acceptable maximum width for flexural cracks. Again, most movement occurred at axle loads clearly in excess of design axle loads. While the second fatigue series tests led to more erratic results, they did not increase separation magnitudes. Examination of Figs. 6.10 through 6.13 also shows a slight tendency toward decreased local continuity on the west side of the deck as opposed to the east. This tendency is believed not conclusive enough to indicate a significant difference in behavior, and no explanation for it was readily apparent.

6.2.2.3 Longitudinal Slip Between Panels and Girders. The longitudinal slip between panels and the center girder is shown for Static Test Nos. 1 through 4 in Figs. 6.14 through 6.17, respectively. Refer to Appendix B for sample slip calculations.

These results show that at any given load level the magnitude of the slip increases as the extent of composite action of the bridge decreases. As before, the results from Static Test No. 1 show movements too small to be useful for evaluation purposes. However, the slip results from Static Test Nos. 2, 3, and 4 all show

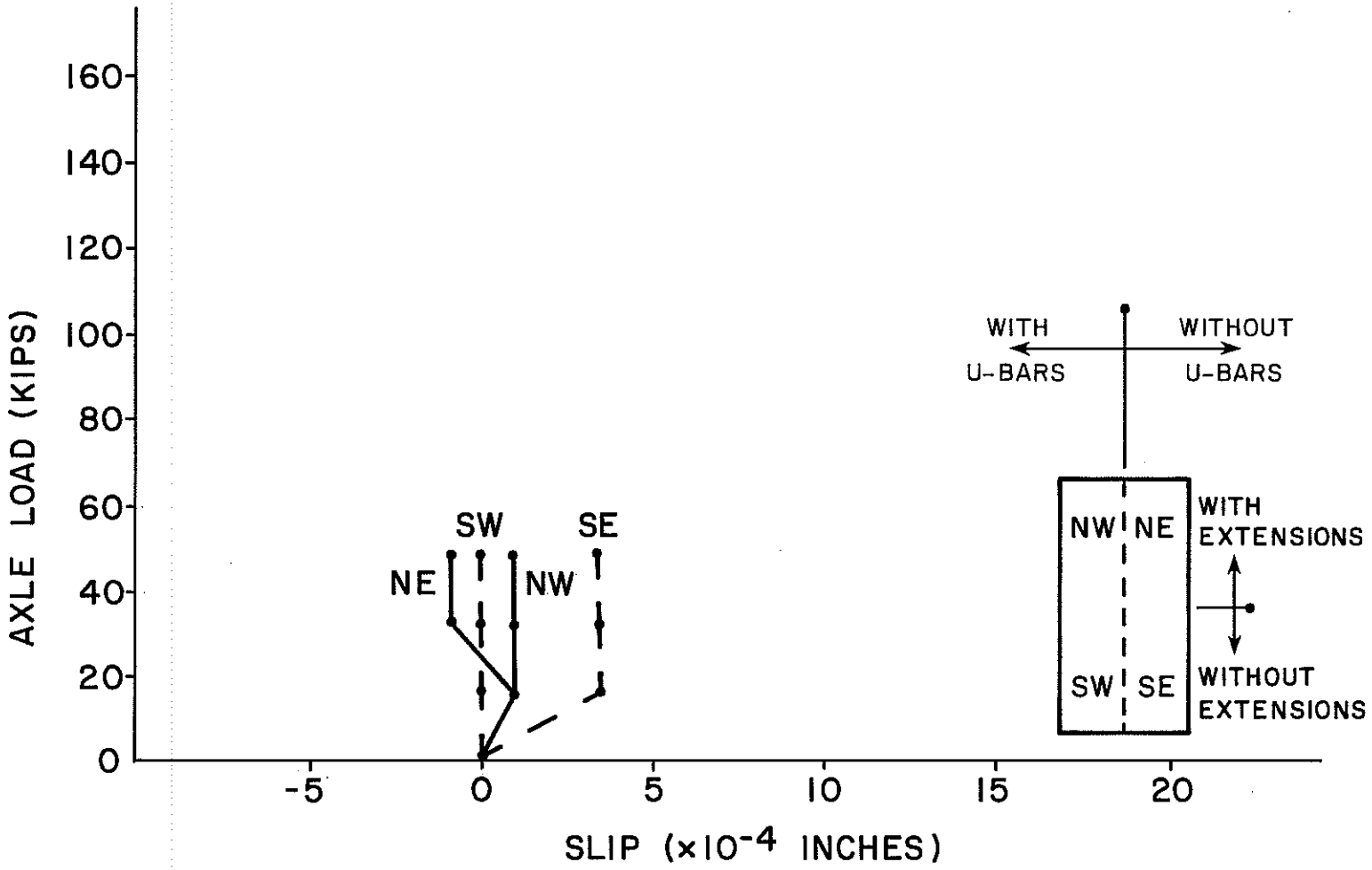

FIGURE 6.14 - LONGITUDINAL SLIP FOR STATIC TEST NO. 1

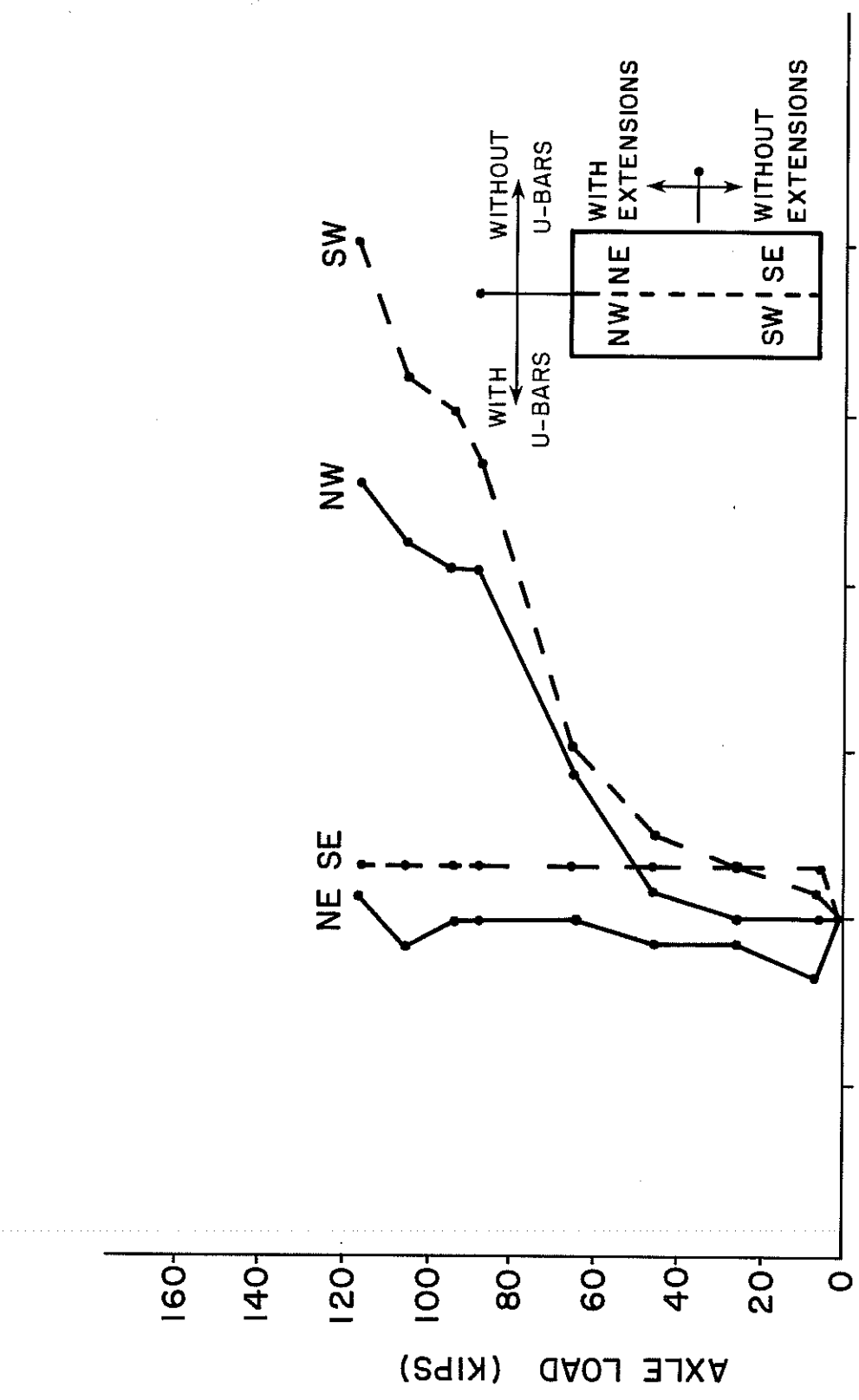

FIGURE 6.15 - LONGITUDINAL SLIP FOR STATIC TEST NO. 2

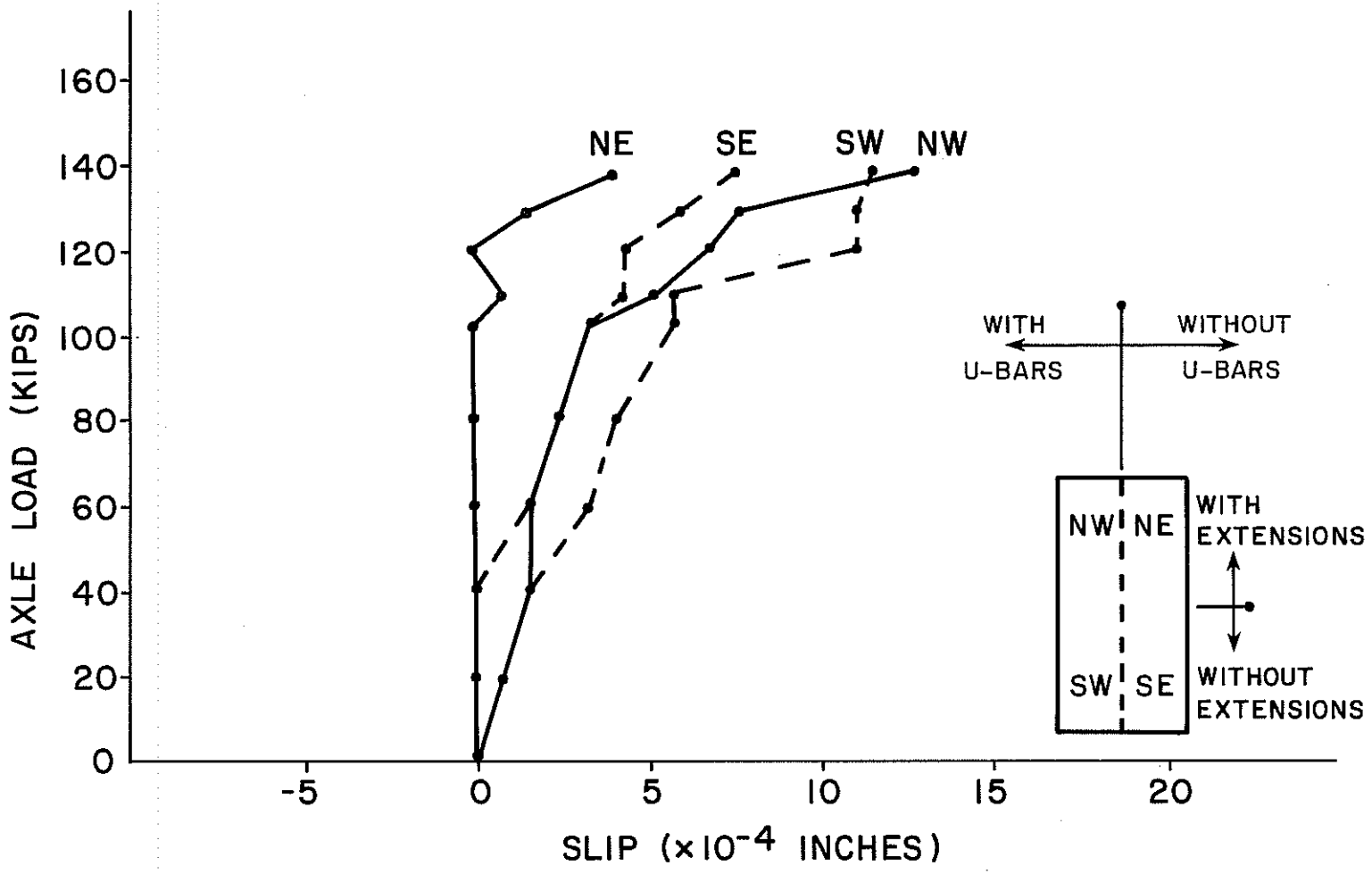

FIGURE 6.16 - LONGITUDINAL SLIP FOR STATIC TEST NO. 3

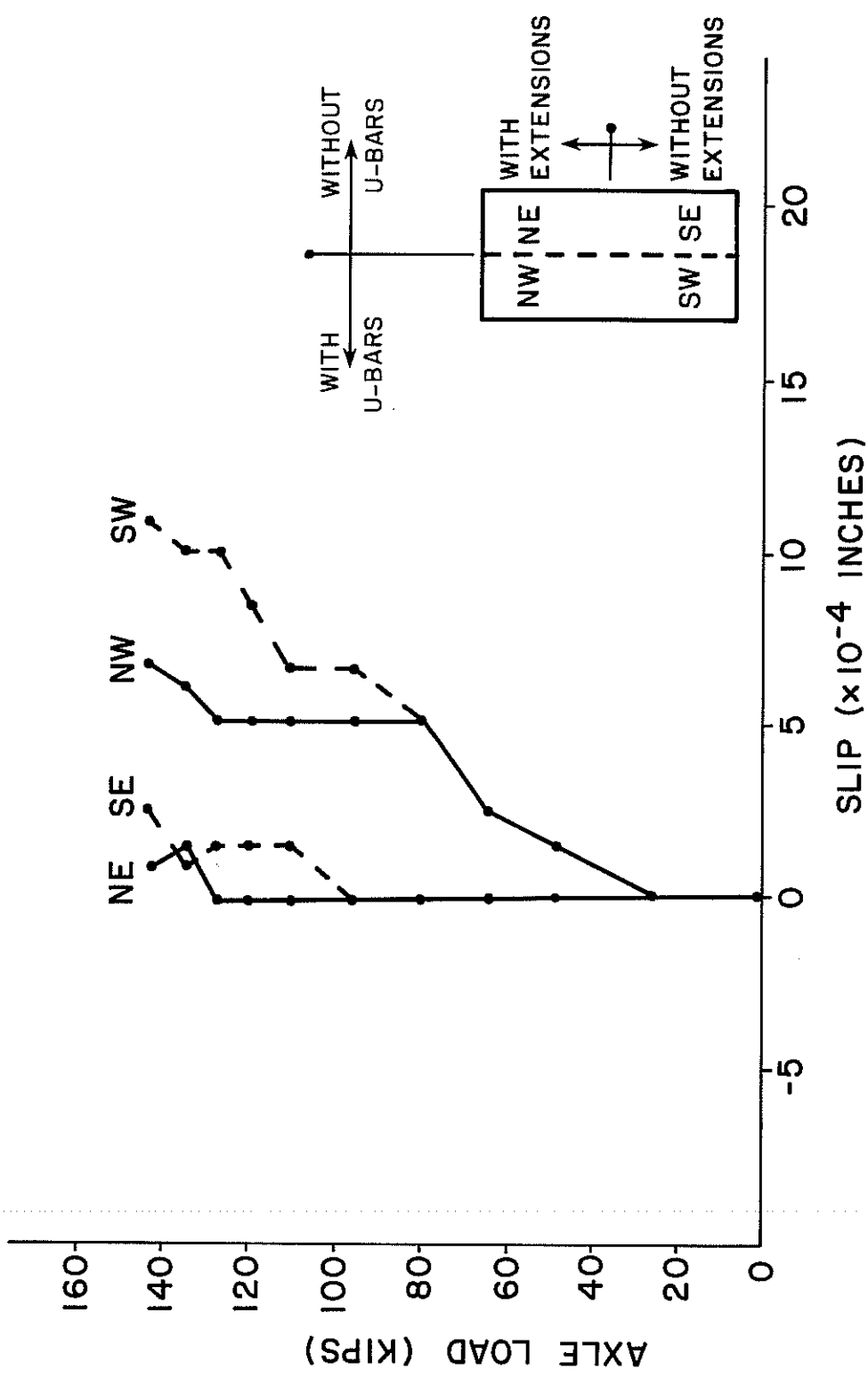

FIGURE 6.17 - LONGITUDINAL SLIP FOR STATIC TEST NO. 4

more slip occurring on the northwest and southwest quadrants of the bridge than on the northeast and southeast quadrants. The maximum recorded slip was 20×10^{-4} in., and most of this slip did not start until after an axle load of 60 kips had been reached.

The reasons for these differences in longitudinal slip behavior between the east and west sides of the bridge are not completely clear. As mentioned previously, there is also a similar but less conclusive tendency with respect to angle changes and panel separations across longitudinal joints. The most obvious physical difference between the two sides of the bridge is that the U-bars were left on the panels on the west side, but cut off the panels on the east side. While this could possibly produce some decrease in continuity between the cast-in-place slab and the panels on the east side, this decrease could not be very significant, considering the miniscule cross-sectional area of the U-bars compared with that of the roughened top surfaces of the panels. In addition, the data on local movements indicate more flexibility on the west side of the bridge, opposite to what might logically be expected were this difference due to the presence or absence of the U-bars.

It was also hypothesized that east-west differences in longitudinal slip could be due to decreased penetration of sound concrete under the panel overhangs on the west side of the center girder. However, when the bridge was dismantled, both sides of the girder seemed similar in this respect. As will be discussed in Section 6.2.2.5, the east-west differences in slip behavior are more probably due to variations in the gaps between panels at transverse joints.

In summary, more longitudinal slip occurred on the west half of the bridge than on the east. However, the maximum slip was small in any event (20×10^{-4} in.), and most slip did not occur until an axle load in excess of design axle loads had been applied to the bridge. The similarity of results for the north and south halves of the bridge shows that longitudinal slip was not significantly affected by the presence or absence of transverse strand extensions on the panels.

6.2.2.4 Bridge Deck Cracking Results. Figure 6.18 shows the cracking pattern on the bridge deck top surface after Fatigue Test Series No. 1. Cracking occurred mainly at transverse panel joints, and maximum crack widths measured about 0.008 in. No significant differences were observed among the four quadrants of the bridge.

Figure 6.19 shows the additional cracking observed on the bridge deck after Fatigue Test Series No. 2 was completed. Cracks widened to a maximum width of about 0.020 in. Cracking was now no longer limited to transverse panel joints, and extended completely across the bridge. In some locations on the cast-in-place overhangs, cracks propagated completely through the slab. The north end of the deck showed slightly more longitudinal cracking over the center girder, possibly due to the relatively poor fit between the panels at that end. It should again be noted that these cracks occurred under loads more than three times as large as design axle loads.

6.2.2.5 Transverse Panel Joint Behavior. Observations of the behavior of the bridge at transverse panel joints was not originally included within the scope of this investigation, because it was felt that this behavior would be unaffected by the presence or absence of strand extensions on the panels. However, some data were obtained and will be presented below.

Figure 6.20 shows the angle changes measured across transverse panel joints during Static Test No. 3. Because of excessive slab cracking, some points jumped irregularly off the scaled axis range. These data are not graphed but are included in Table B.5 of Appendix B. The maximum recorded angle change, neglecting the irregular, large-jump data, was -26×10^{-3} degrees. Figure 6.21 shows the separations measured at transverse panel joints during Static Test No. 3. Again, some scattered results occurred due to excessive cracking. Here the maximum separation, neglecting the irregular, large-jump data, was -54×10^{-4} in. These maximum angle changes and separations are conservatively consistent with maximum bridge deck crack widths of

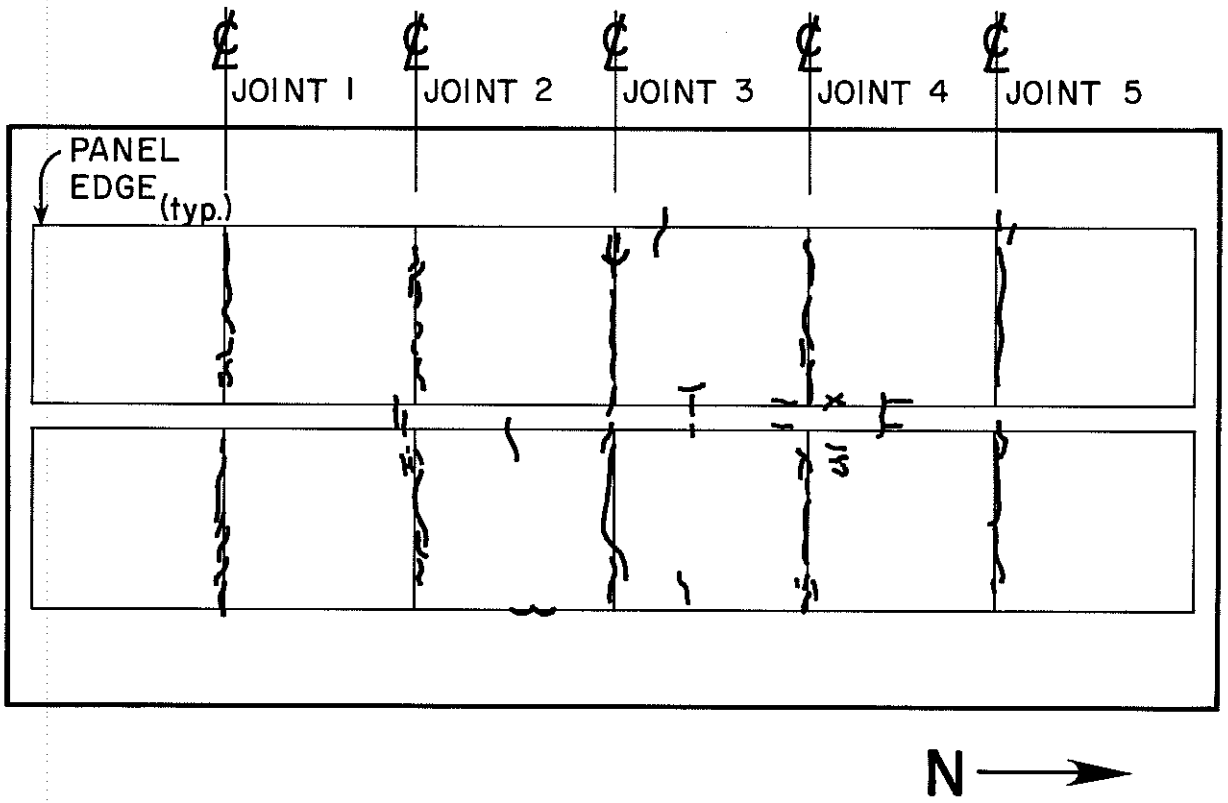

FIGURE 6.18 - CRACKING PATTERN AFTER FATIGUE TEST SERIES NO. 1

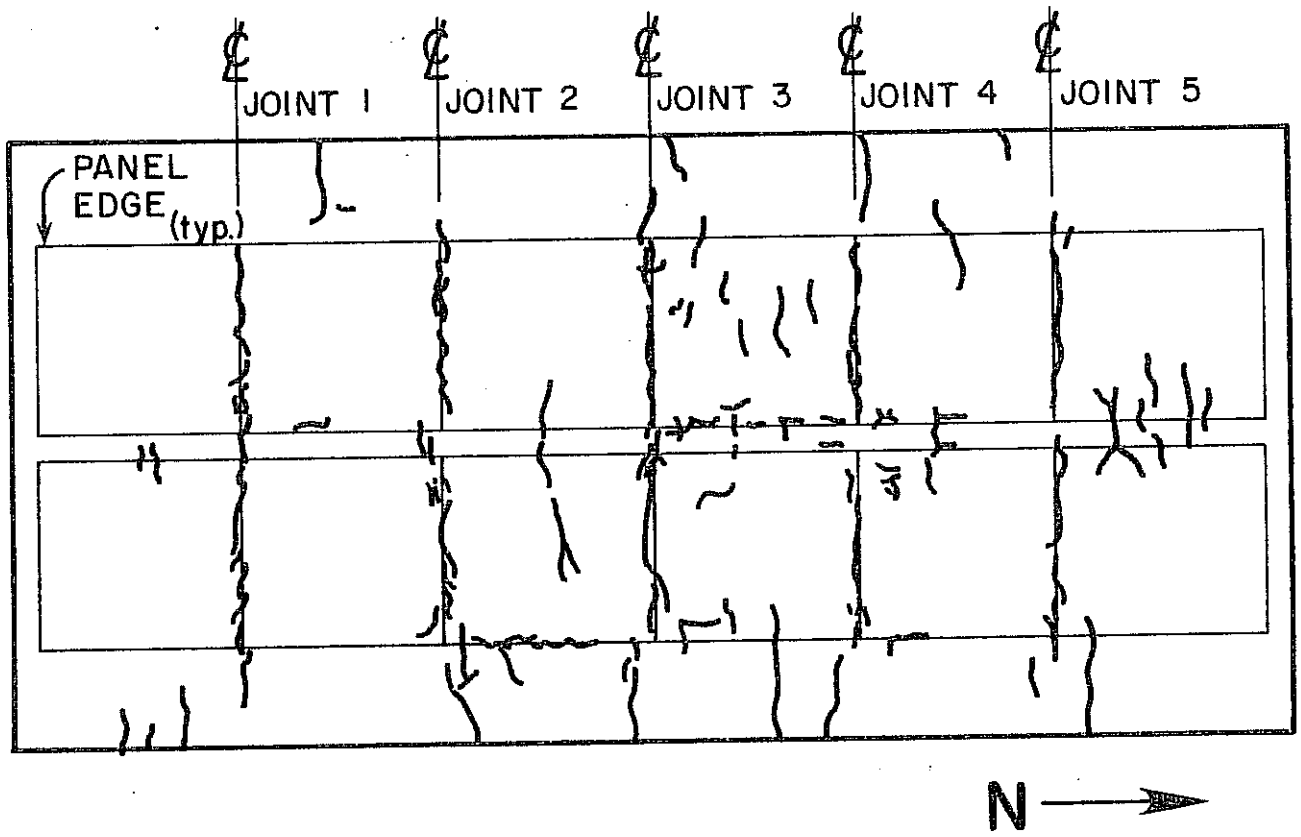

FIGURE 6.19 - CRACKING PATTERN AFTER FATIGUE TEST SERIES NO. 2

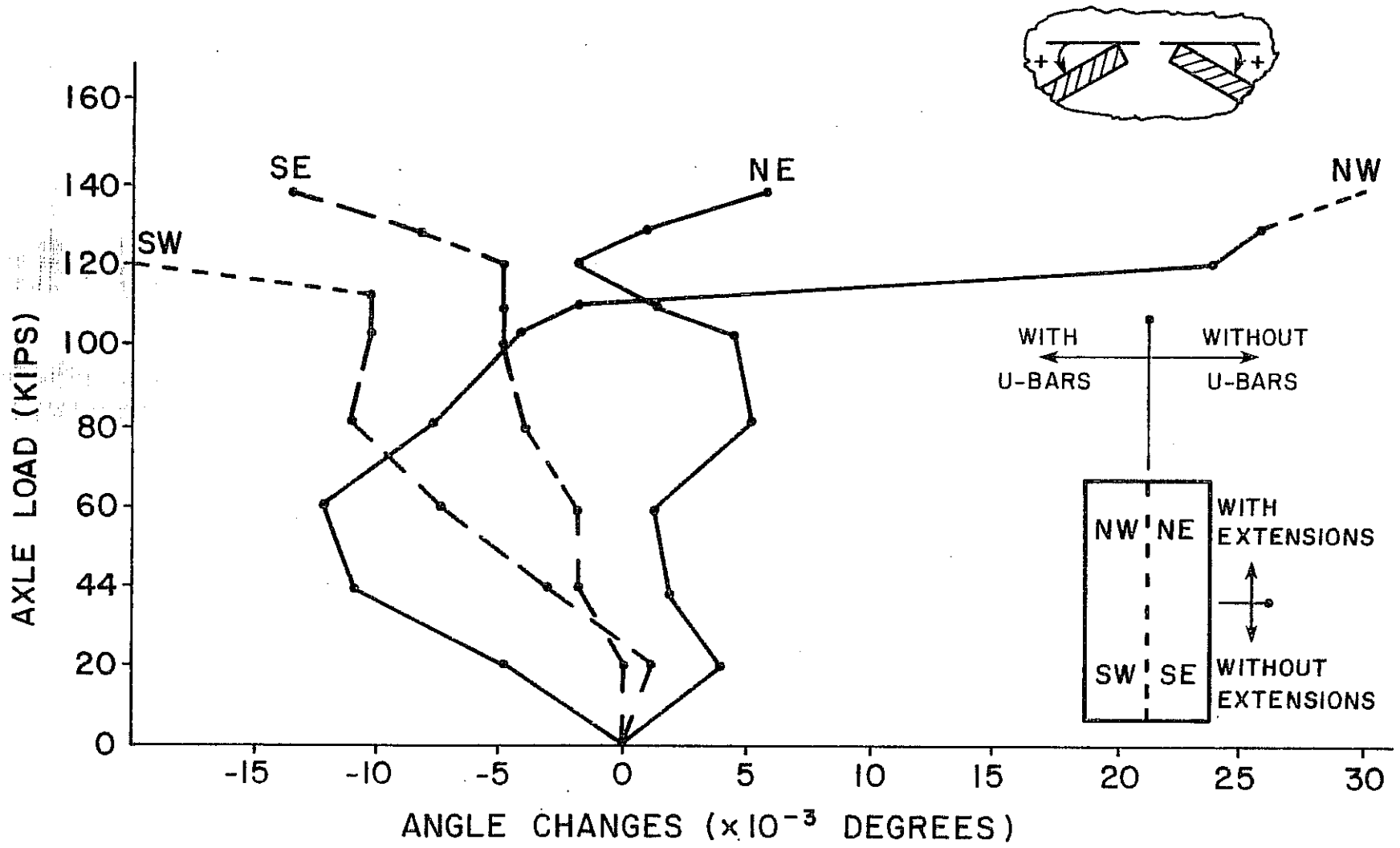

FIGURE 6.20 - ANGLE CHANGES FOR TRANSVERSE JOINTS

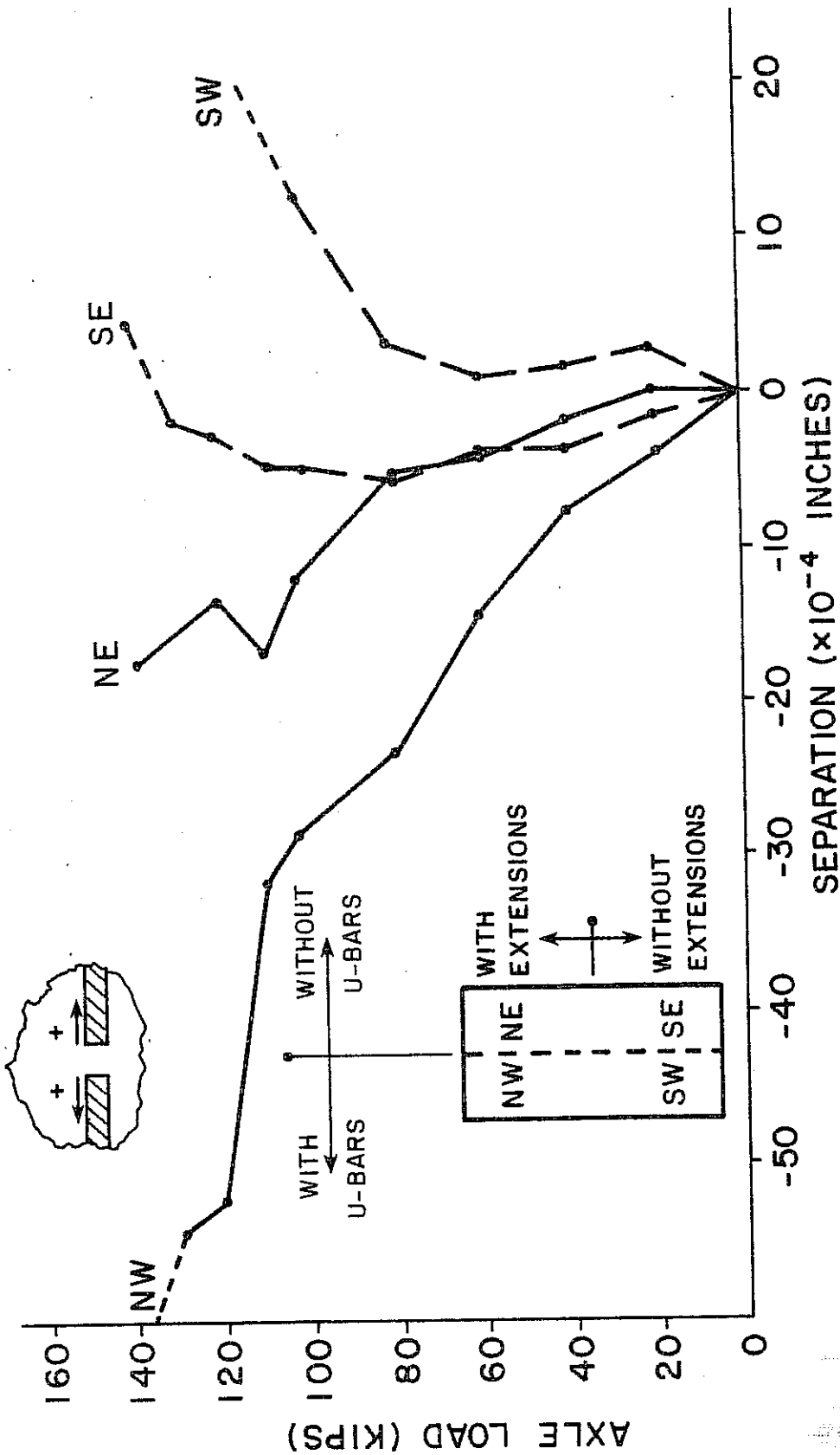

FIGURE 6.21 - SEPARATION FOR TRANSVERSE JOINTS

0.003 in. and 0.006 in., respectively, well within allowable limits. The data from Static Test Nos. 1, 2, and 4, though not reduced completely, gave maximum angle change and separation values similar to and not significantly greater than those cited above. In summary, as previously stated and as evidenced by the physical cracking results, these results show that the behavior of the transverse panel joints was not affected by the presence or absence of panel strand extensions, and that the local cracking at those joints was not a significant problem.

The transverse panel joint data presented in Figs. 6.20 and 6.21 show more flexibility across transverse panel joints in the west side of the bridge than in the east side. As discussed previously, this pattern was also observed with respect to longitudinal joint movements and longitudinal slip. In addition, note that Figs. 6.20 and 6.21 show significantly greater separations in the north half than the south, and angle changes of opposite signs in the two halves.

These differences are believed to be due to variations in the widths of the transverse joints between the panels. First, consider the north-south differences. As noted previously, the nonrectangular shapes of the panels in the north half of the bridge resulted in large gaps at the transverse panel joints at that end. Figure 6.22a is a schematic representation of a wide transverse joint. Exaggerated deformation at that joint due to the bridge's own self-weight is shown in Fig. 6.22b. A small negative angle change is created. As shown in Fig. 6.22c, when a concentrated load is applied to the panel near the joints, as in this case, it will produce a large positive angle change across the joint due to the panel gap. This large positive angle change, combined with the previous small negative one, results in a net positive angle change across the joint. This hypothesis seems consistent with the data present in Fig. 6.20, in which positive angle changes occur on the north end of the bridge.

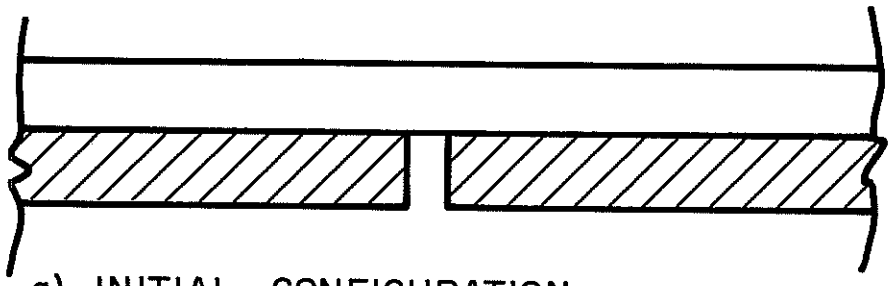

a) INITIAL CONFIGURATION

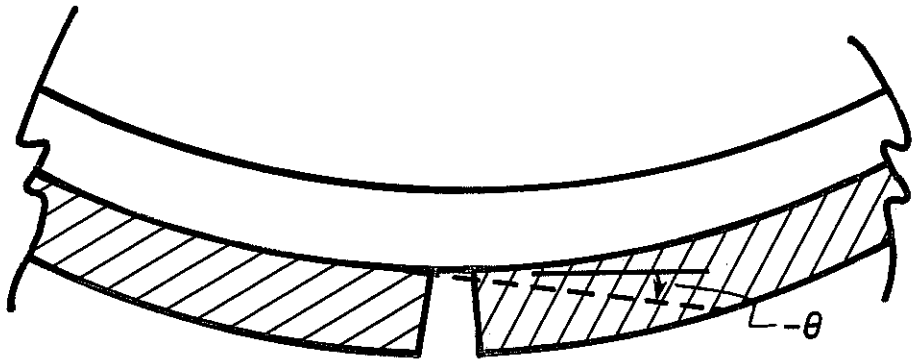

b) DEFORMED CONFIGURATION DUE TO SELF-WEIGHT

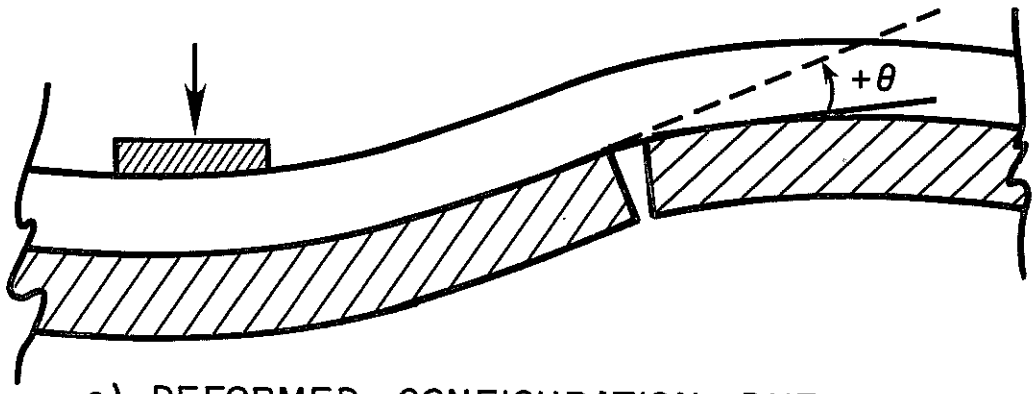

c) DEFORMED CONFIGURATION DUE TO APPLIED LOAD

FIGURE 6.22 - TRANSVERSE PANEL JOINTS ON NORTH HALF OF BRIDGE

Now consider the closely spaced panels on the south half of the bridge, shown in Fig. 6.23a. As shown in an exaggerated form in Fig. 6.23b, the deformations from self-weight produce a slight negative angle change across the joint. When a concentrated load is applied near the joint, as shown in Fig. 6.23c, the panel edges will butt against each other, resulting in only a very small positive angle change. Using this hypothesis, the net angle change across the joint is still slightly negative, consistent with the data in Fig. 6.20, in which small negative angle changes occur across the transverse joints on the south end of the bridge.

Though harder to visualize, this hypothesis also predicts slight positive separations between the tightly butted panels on the south end, and larger negative separations between the widely spaced panels on the north end, consistent with the separation data presented in Fig. 6.21.

It is believed that similar hypotheses, based on differences in the widths of the transverse joints between the panels, are the most probable explanation for the increased longitudinal slip on the west side of the bridge as compared to the east, which is evident in Figs. 6.14 through 6.17. Larger gaps between panels would decrease the longitudinal in-plane stiffness of the bridge deck on the side with the gaps, resulting in differences in local shearing stress between the panels and the east and west sides of the center girder. Exact analysis of this question was considered beyond the scope of this report, and data on transverse panel joint widths were, unfortunately, not taken in this study. However, the authors believe that all local deformation data for transverse joints indicate that tight-fitting transverse panel joints result in better local continuity.

6.2.2.6 Girder Cracking and Fatigue Response. The center girder began to crack near the end of Static Test No. 2, under axle loads "P" of approximately 120 kips. The outside girders began to

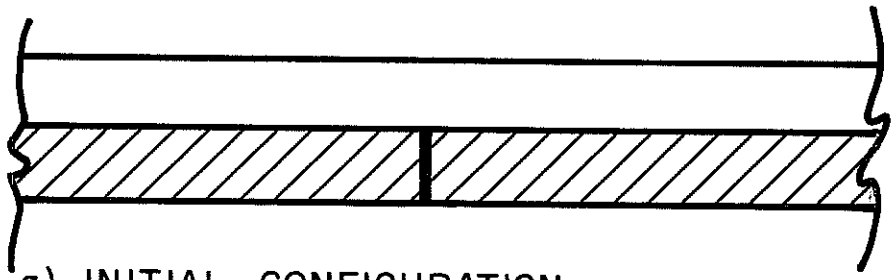

a) INITIAL CONFIGURATION

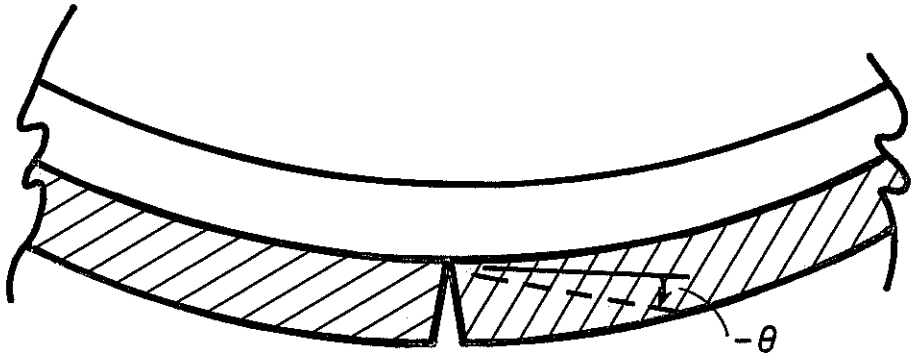

b) DEFORMED CONFIGURATION DUE TO SELF-WEIGHT

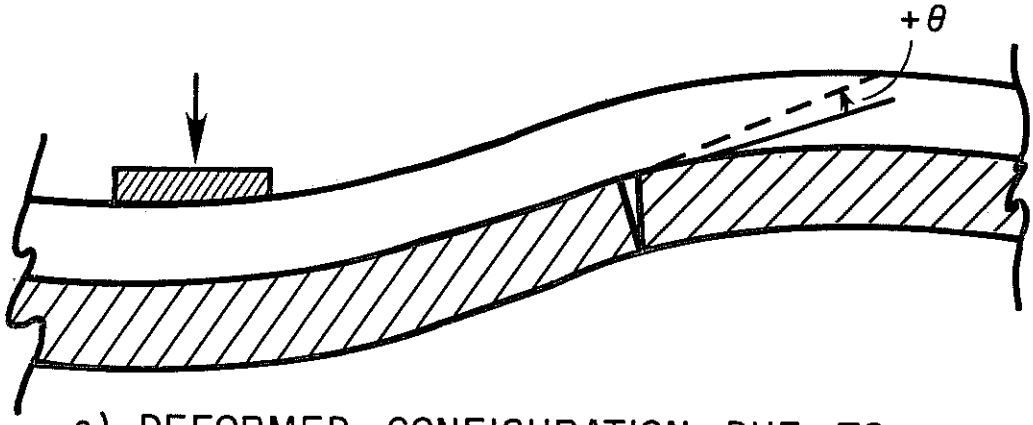

c) DEFORMED CONFIGURATION DUE TO APPLIED LOAD

FIGURE 6.23 - TRANSVERSE PANEL JOINTS ON SOUTH HALF OF BRIDGE

crack, and additional cracks occurred in the center girder during Static Test No. 3. Figure 6.24 shows typical girder cracking conditions after Static Test Nos. 2 and 3. Cracks extended from the bottom fiber up through the web, in some cases reaching the top girder flange. The cracks were spaced along the girders at approximately 12 to 20 in. During the test, the widest crack measured was 0.016 in. in width. All cracks closed completely after the load was removed from the bridge.

In Fatigue Test Series No. 2, these cracked bridge girders were tested under loads corresponding to bottom fiber tensile stresses of $6\sqrt{f'_c}$ in the uncracked transformed section. After 5 million additional fatigue cycles at this stress level, no prestressing strands failed in any of the girders, in spite of the significant flexural cracking discussed above. These results differ from those obtained by Rabbat, et al. [6], in which strand failure was observed in a girder-deck specimen in which simulated flexural cracks had been introduced using crack formers. The reasons for this difference in results are not clear, and are the subject of a current investigation sponsored by the Texas SDHPT.

6.3 Concentrated Load Tests

6.3.1 Local Behavior. Typical local bridge cracking due to the concentrated loads is shown in Figs. 6.25 and 6.26.

Figure 6.25 shows a cut-away view of a typical interior slab failure due to an applied concentrated load. The top surface was cracked around a rectangular cut-out coinciding with the perimeter of the loading plate. From that cut-out, the slab crack propagaged downward at approximately a 35° angle to the horizontal, until it reached the level of the prestressing strands. At this point the angle of inclination of the failure surface decreased sharply and the crack flattened out over the entire precast panel, propagating at the level of the panel steel to the panel edges. The portion of the panel below the crack then failed at its supporting edges and dropped

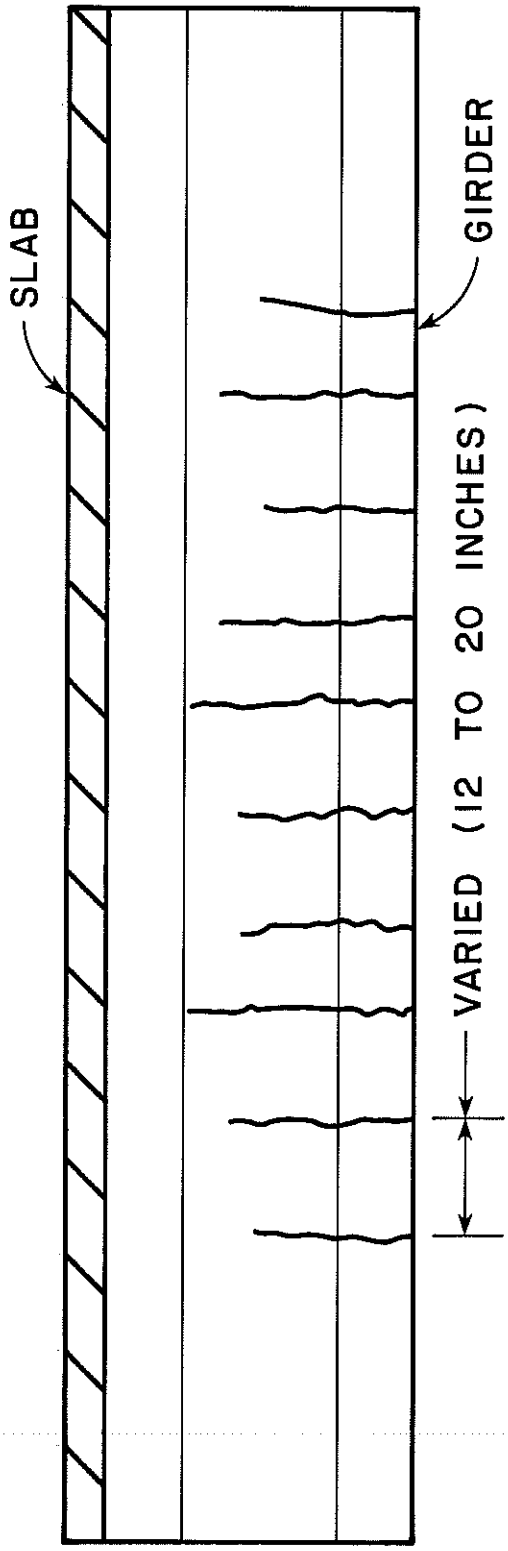

FIGURE 6.24 - FLEXURALLY CRACKED GIRDER

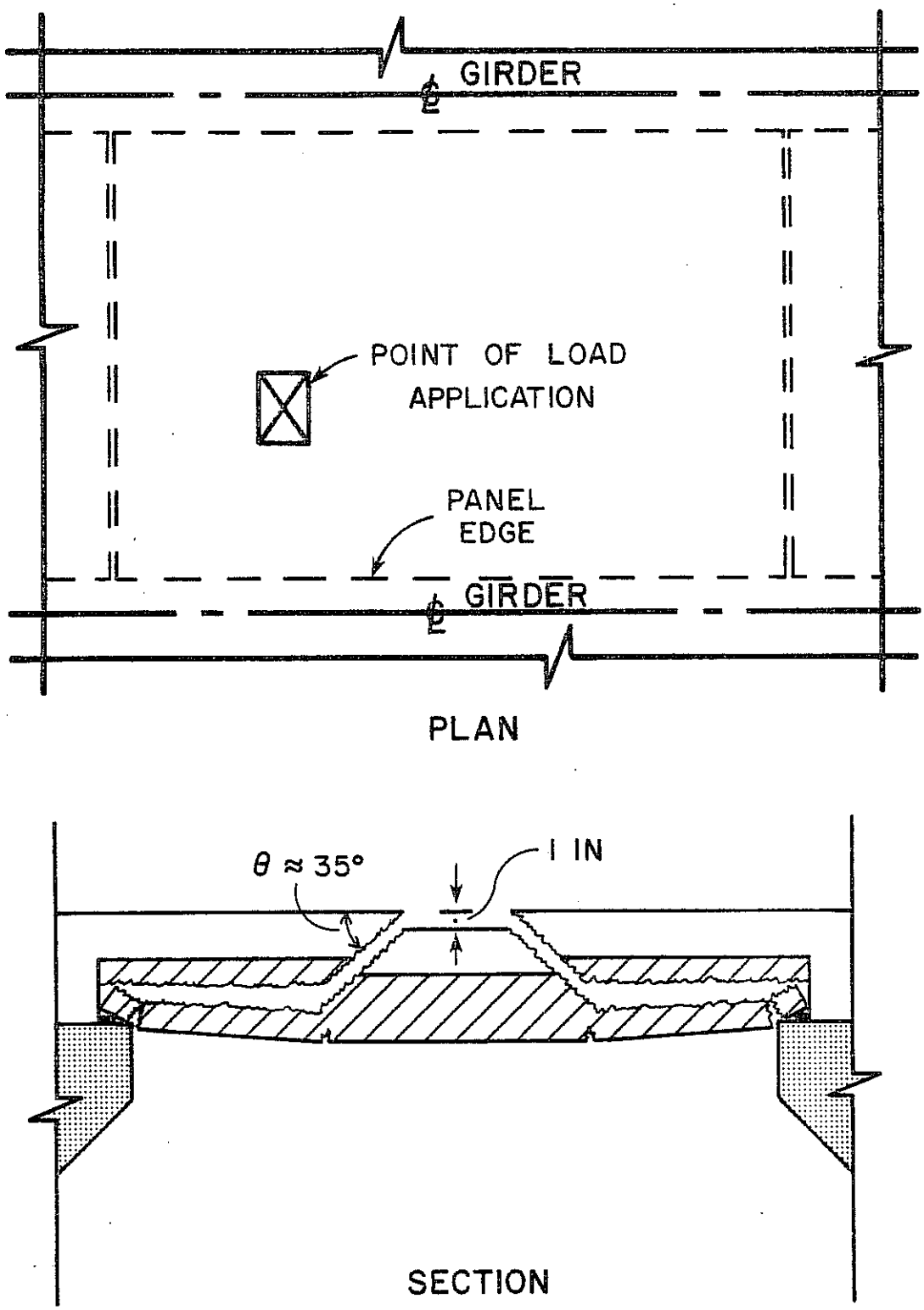

FIGURE 6.25 - INTERIOR CONCENTRATED LOAD FAILURE

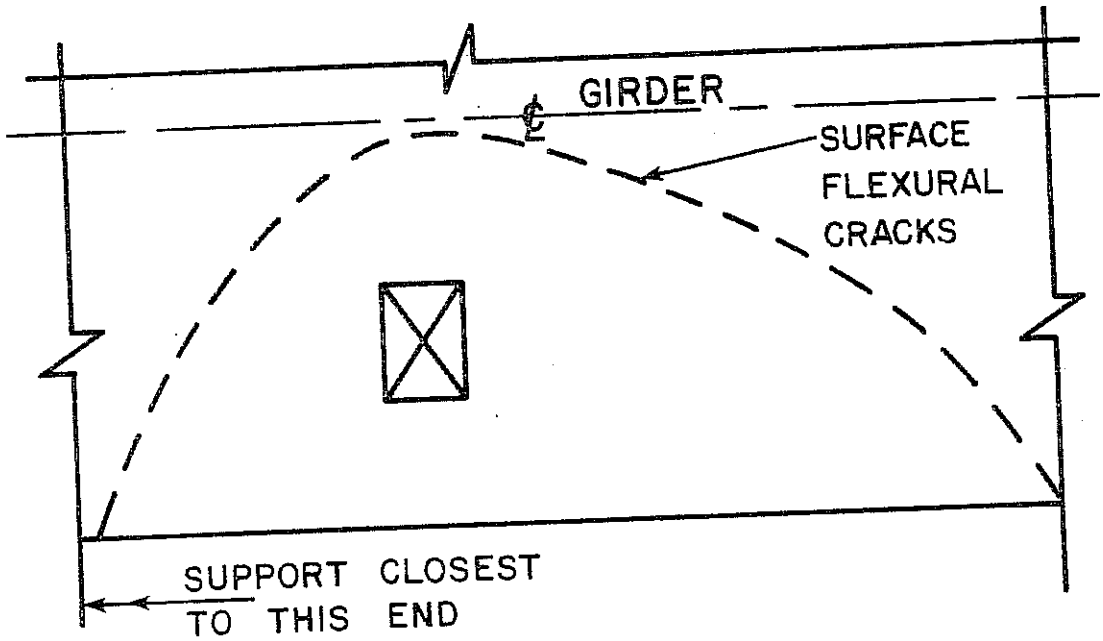

PLAN

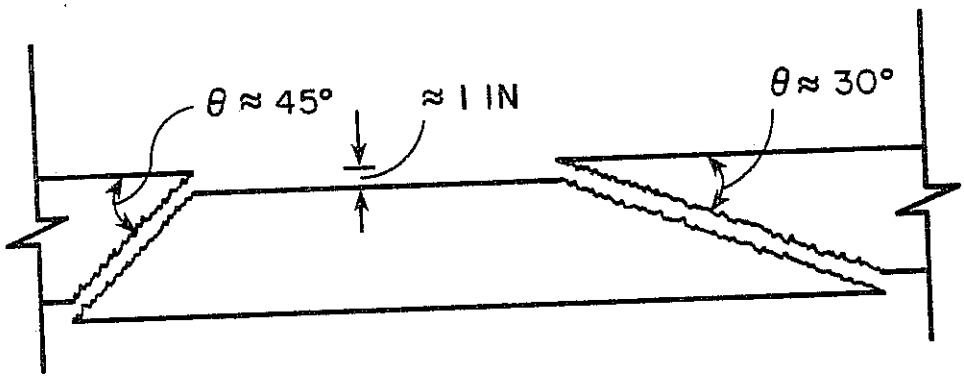

SECTION

FIGURE 6.26 - OVERHANG CONCENTRATED LOAD FAILURE

about 1 in. The lower surface of the panel was also cracked along diagonal lines connecting the panel corners, suggesting a yield-line failure mechanism in the lower part of the panel combined with a punching shear failure in the upper part of the panel and the overlying cast-in-place slab.

Figure 6.26 shows a typical cut-away view of the slab failure at a middle exterior overhang location due to an applied concentrated load. These failures all began with significant flexural cracking, suggesting a yield-line failure mechanism. These cracks propagated through the slab depth at about a 45° slope on the side closest to the bridge support and at about a 30° slope on the other side, suggesting the possibility of a punching shear mechanism as well. Failures at other exterior overhang locations, including corners, were very similar to this type of failure.

6.3.2 Overall Behavior. Results from the concentrated load tests are given in Table 6.1. These loads have been compared with predicted failure loads using the punching shear provisions of the AASHTO Standard Specificstions [7], and also using yield-line theory.

6.3.2.1 Punching Shear Theory. Punching shear capacity was evaluated using the provisions of Section 1.5.35(F) of AASHTO Standard Specifications for Highway Bridges. No capacity reduction factor ϕ was applied, since bridge deck dimensions and material characteristics were known. For the interior concentrated load tests (Nos. 1, 3, 5, and 7), the average f'_c for the composite deck slab was assumed to be 6000 psi, considered to be a reasonable compromise between the higher-strength panels and the lower-strength cast-in-place topping. The effective depth d was taken as 5.50 in., based on the distance from the top of the slab to the centroid of the prestressing steel in the panels. For the interior tests with the rectangular plate, the nominal capacities calculated using AASHTO punching shear theory ranged from 11 to 19 percent less than the experimentally observed

TABLE 6.1 CONCENTRATED LOAD TEST RESULTS

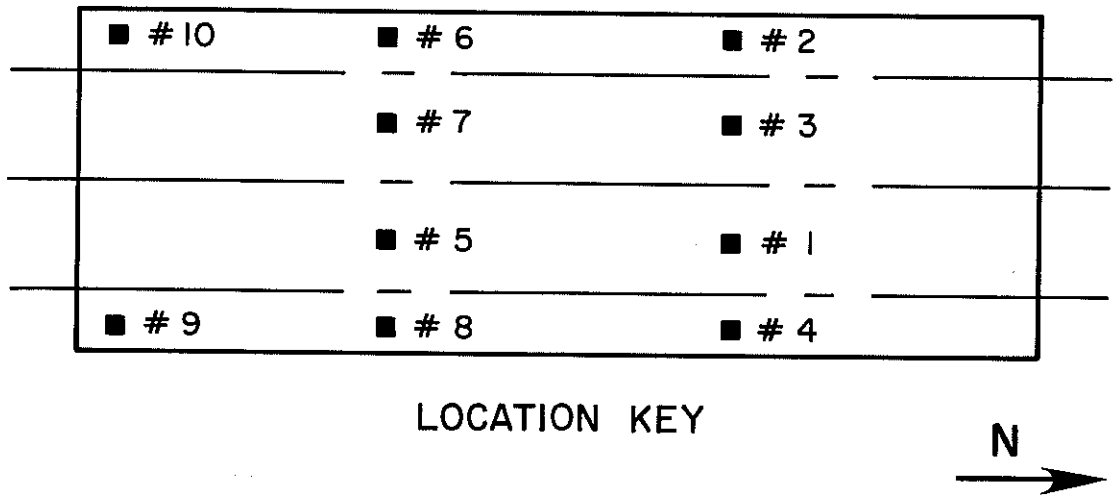

Location No.	Test Date	Actual Capacity (kips)	Predicted Capacity (kips)				Loading Plate
			Punching Shear (AASHTO)		Yield Line		
			P_{calc}	P_{calc}/P_{test}	P_{calc}	P_{calc}/P_{test}	
1	8-24-81	185	119	0.64	130	0.70	12"×12" pl.
2	8-25-81	116	100	0.86	131	1.13	8"×20" pl. on neoprene pad
3	8-25-81	156	133	0.85	130	0.83	" " "
4	8-25-81	111	100	0.90	131	1.18	" " "
5	8-28-81	149	133	0.89	130	0.87	" " "
6	8-28-81	121	100	0.83	131	1.08	" " "
7	8-28-81	165	133	0.81	130	0.79	" " "
8	8-28-81	114	100	0.88	131	1.15	" " "
9	9-10-81	97	60	0.62	98	1.01	" " "
10	9-10-81	93	60	0.65	98	1.05	" " "

capacity values. For the square plate, which was also smaller in cross-sectional area than the rectangular plate, the calculated capacity was 36 percent less than the experimentally observed capacity.

In applying the AASHTO punching shear theory to load locations along the overhang, other than at the corners (Concentrated Load Test Nos. 2, 4, 6, and 8), the side of the hypothetical failure surface parallel with and closest to the free edge was considered ineffective, and the perimeter b_o of the hypothetical failure surface was decreased accordingly. The value of f'_c used was 4400 psi, corresponding to the average measured strength of the cast-in-place deck. The effective depth d was taken as 5.75 in., based on the distance from the top of the slab to the centroid of the bottom longitudinal steel in the cast-in-place deck. The calculated capacities ranged from 10 to 17 percent less than the experimentally observed capacities.

In calculating the theoretical capacity, governed by punching shear, under concentrated loads located at the overhang corners (Concentrated Load Test Nos. 9 and 10), both of the open sides were considered ineffective, and the effective perimeter b_o was reduced accordingly. The same values of f'_c and d were used for the corners as for the rest of the overhang. The calculated capacities were almost 40 percent less than the experimentally observed ones, assuming failure governed by punching shear.

In summary, the nominal capacities calculated using the AASHTO punching shear theory were lower than the capacities actually obtained experimentally. The calculated values were closest to the actual values for the interior and overhang tests, while the calculated values for the overhang corners were consistently very conservative (low). In spite of the fact that b_o was smaller for the square loading plate than for the rectangular loading plate, the slab actually withstood more load with the square plate than the rectangular one. The concentrated loads required to cause failure were in all cases far in excess of design loads for the bridge deck. Also, no significant difference in results was noted between the north and south halves

of the bridge, indicating, as might be expected, that the presence or absence of transverse panel strand extensions did not affect the deck's concentrated load capacity.

6.3.2.2 Yield-line Theory. As noted above, punching shear theory did not accurately predict the concentrated load capacity of the overhang. Yield-line theory was examined as an alternative failure model.

Figure 6.27 shows the idealized yield-line patterns for the three types of concentrated load tests, considering the effects of both positive and negative moment resistances of the deck in each direction. Small displacements were assumed, and internal work due to in-plane stresses (arching action) was neglected. The flexural resistances per unit width of the slab were calculated using nominal material characteristics, and are listed in Table 6.2. No capacity reduction factor ϕ was applied. Each yield-line pattern corresponds to an equilibrium relationship between external concentrated load (considered to be applied at a single point) and the internal resisting moments. The capacities predicted using yield-line theory, for each of the patterns in Fig. 6.27, are given below those patterns, using units of kips and ft. Substituting the values in Table 6.2 into these formulas, yields the predicted capacities shown in Table 6.1.

The calculated capacities for the interior load locations were comparable to those predicted using AASHTO punching shear theory, and hence were still conservative when compared to actual values. For locations in the middle of the overhangs (Concentrated Load Test Nos. 2, 4, 6, and 8), the capacity predicted by yield-line theory is from 8 to 18 percent greater than the actual failure loads. Coupled with the previously discussed failure observations, this suggests that the failure in the overhang, under concentrated loads, occurs due to a combination of flexural mechanisms (associated with overestimates of capacity), and punching shear mechanisms (associated

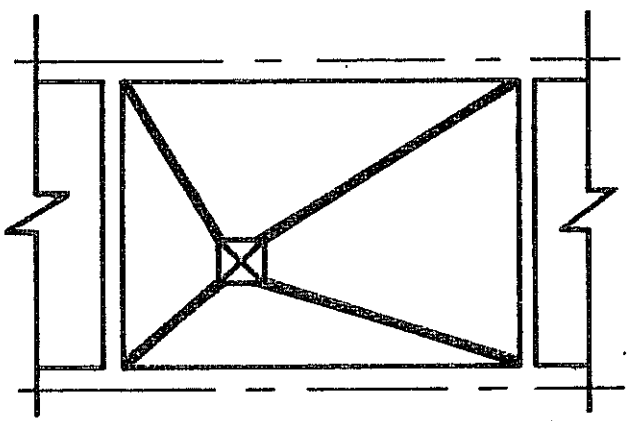

$P_u = 5.23\ M^+_{TRANS} + 4.17\ M^+_{LONG}$

A. INTERIOR

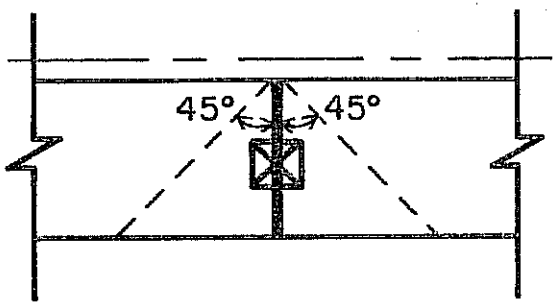

$P_u = 4(M^-_{LONG} + M^+_{LONG} + M^-_{TRANS})$

B. OVERHANG MIDDLE

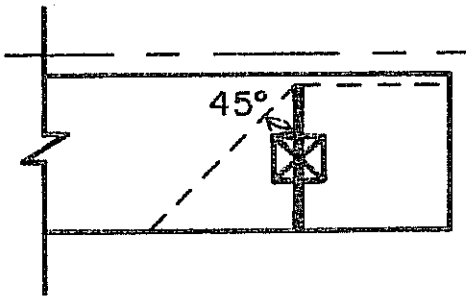

$P_u = 4.30\ M^-_{TRANS} + 2(M^-_{LONG} + M^+_{LONG})$

C. OVERHANG CORNER

NEGATIVE MOMENT YIELD-LINE

POSITIVE MOMENT YIELD-LINE

GIRDER CENTERLINES

FIGURE 6.27 - IDEALIZED YIELD-LINE FAILURE PATTERNS

TABLE 6.2 SLAB MOMENT CAPACITIES

	Interior (kip-ft/ft)	Overhang (kip-ft/ft)
Longitudinal		
M+	9.33	10.64
M-	---	7.70
Transverse		
M+	19.50	11.18
M-	---	14.32

with underestimates of capacity). In the exterior overhang corner areas, concentrated load capacity, as predicted by yield-line theory, is within a few percent of the actual failure loads, indicating that failure in those areas is well modeled by yield-line mechanisms.

In addition to its value in predicting capacity under concentrated loads, yield-line theory also provides a valuable indication of the effectiveness of various types of overhang reinforcement in increasing this capacity. The capacity formulas for the overhang yield-line patterns of Fig. 6.27 show the importance of the overhang moment resistance in the longitudinal direction, particularly in the middle of the overhang. This shows the beneficial effect on overhang capacity of longitudinal steel placed at the top and bottom of the overhang.

Table 6.1 shows that the concentrated load capacity of the interior areas is underestimated by both the AASHTO punching shear theory and yield-line theory. The concentrated load capacity in the middle of the overhang area of the slab will probably lie between the capacity predicted by AASHTO punching shear theory and that predicted by yield-line theory. The concentrated load capacity of the overhang corner area can best be estimated using the yield-line theory.

CHAPTER 7

SUMMARY AND CONCLUSIONS

A series of static and dynamic loading tests was conducted on a full-scale bridge specimen, constructed using prestressed precast panels placed on top of prestressed precast girders, and covered with a cast-in-place bridge deck. The north half of the bridge specimen was made with panels having transverse prestressing strands extending beyond the panel edges, and the south half with smooth-sided panels.

The major objective of this study was to determine if the absence of strand extensions would cause significant deterioration in the bridge's performance under fatigue and static loading. Other objectives were to evaluate the static and fatigue response of the bridge and girders, the capacity of the deck under concentrated loads, and the effects of some practical construction details on bridge response. The bridge was subjected to four static tests (three of these at levels high enough to cause girder cracking), and two fatigue tests (to a total of 11.5 million cycles).

Additionally, ten concentrated load tests were made on the bridge deck. All loadings were applied equally to each half of the bridge. All tests are described in Chapter 2.

Section 6.2.2 describes the local behavior observed during the static and fatigue tests. Overall bridge deck cracking showed no significant differences in pattern or crack width between the north and south halves of the bridge. Local angle changes and separations at the longitudinal joints between the panels and center girder indicated that more relative movement occurred at the panel edges without strands (on the south half of the bridge) than with

strands (on the north half). However, the magnitude of these relative movements was quite small, and most of the movement did not occur until the bridge was subjected to loads clearly in excess of design axle loads.

The load-deflection behavior of the bridge, discussed in Section 6.2.1, changed very little throughout all four static tests. The extensive fatigue cycles and the flexural cracking in all three girders did not result in significant deterioration, over time, of overall load-deflection behavior. Experimentally observed load-deflection results were compared with those obtained using nonlinear computer models of the bridge, and the calculated load-deflection results were in reasonable agreement with those actually observed.

No girder prestressing strands fractured under the initial 6.5 million fatigue cycles, nor under the additional 5 million fatigue cycles which were applied after the girders had been cracked during a static load test. The last 10 million (of the 11.5 million total) fatigue cycles were applied at a level sufficient to produce a calculated tensile stress of $6\sqrt{f'_c}$ at the bottom of the center girder, assuming uncracked conditions. All girder cracks closed completely when load was removed from the bridge.

The results of the concentrated load tests, discussed in Section 6.3, indicated that both the AASHTO punching shear theory and the yield-line theory give conservative estimates of the failure load at interior bridge deck locations. For the middle areas of the overhang, the AASHTO punching shear theory underestimates the failure load, while the flexural yield-line theory overestimates it, indicating that under concentrated loads, failure in those areas occurs due to a combination of flexural and punching shear mechanisms. At the corners of the overhang, the flexural yield-line theory predicts the failure load very accurately, while the AASHTO punching shear theory greatly underestimates it. Yield-line theory indicates the

importance of longitudinal slab steel in increasing the concentrated load capacity of the overhangs.

As far as local construction details are concerned, the evidence gathered in the course of this investigation related to three details in particular:

First, local continuity between panels and girders is enhanced by ensuring good contact between the cast-in-place deck and the underside of the panels overhanging the fiberboard strip. If the strip is too thin, concrete cannot penetrate the gap between the top of the girder and the underside of the panel. If the overhang distance is insufficient, the panel bears primarily on the relatively flexible fiberboard strips, resulting in panel settlement and longitudinal cracking along the panel edges at the girders. Clearly, there is a trade-off involved here: thick fiberboard strips will facilitate the placement of concrete, but, due to their flexibility, can lead to longitudinal cracking unless sufficient panel overhang is provided.

Second, while some means of lifting and placing the panels is necessary, U-bars do not seem to have any significant effect on the structural performance of the bridge. Although such a case was not investigated in this study, the U-bars could conceivably provide shear transfer if the top surface of the panel were so contaminated as to eliminate normal concrete bond behavior.

Third, results for local deformations at transverse joints indicate that increased transverse joint width is associated with decreased local continuity. Gaps at transverse joints can be minimized by controlling the shape of the panels and by carefully supervising their placement in the field.

Four major conclusions are apparent from this study:

(1) The overall and local behavior of bridges without transverse prestressing strand extensions is just as satisfactory as that of bridges with the extensions;

(2) In some cases, prestressed girders can be cracked flexurally and subjected to extensive fatigue cycling without strand fracture;

(3) Bridge deck capacity under concentrated loads should be investigated using yield-line models as well as punching shear models, particularly in overhang areas; and

(4) Construction details were not observed to affect the overall performance of the bridge investigated in this study. However, as discussed above, they can sometimes have significant effects on local behavior.

A P P E N D I X A

EFFECT OF DYNAMIC RESPONSE ON EVALUATION OF FATIGUE PERFORMANCE

Introduction

Any structure can vibrate freely at a large number of frequencies, each of which corresponds to a unique displacement pattern. These are termed the natural frequencies and corresponding mode shapes of the structure. If the structure is loaded slowly, its response will be essentially static. But when the structure is subjected to loads which vary, over time, at frequencies close to those natural frequencies, its response will be dynamic rather than simply static. In other words, the inertial forces developed within the structure, and opposing the accelerations of the structure, will constitute a significant part of its response. The internal stresses and external displacements of the structure will depend on these inertial forces as well as on the applied loads.

In order to carry out, within a reasonable period of time, the fatigue tests described herein, it was necessary to apply cyclic loads to the bridge at a rate which could not be considered slow compared to the lowest, or fundamental, period of vibration of the bridge. Under fatigue loads, the bridge would therefore respond dynamically. The fatigue loading was designed to apply a cyclic maximum tensile stress of $6\sqrt{f'_c}$ to the bottom of the center girder. According to prior computations carried out by the Texas SDHPT, the center girder would carry 3/8 of this loading, applied as shown in Fig. A1. It was calculated that the required center girder moment could be produced if a static axle load of 80 kips were applied to each half of the bridge. The change in vertical deflection at the centerline of the center girder under this 80-kip static

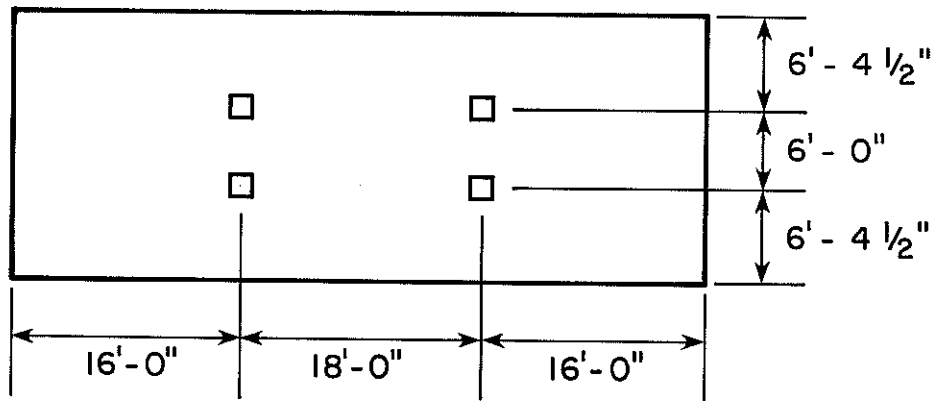

FIGURE A.1 - LOCATION OF POINTS OF LOAD APPLICATION

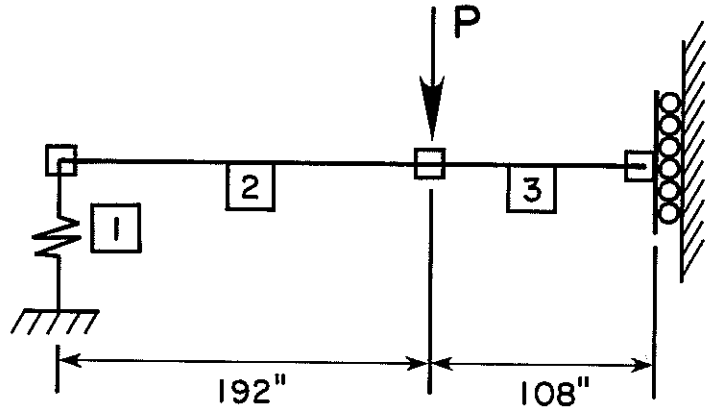

FIGURE A.2 - MATHEMATICAL IDEALIZATION OF BRIDGE

load was measured to be 0.271 in., about 10 percent of this being rigid-body motion due to support deflections. This deflection was associated with an increase in centerline moment of 1283 kip-ft, across the entire width of the bridge.

For a given frequency of cyclic load application, it was therefore necessary to calculate the maximum value of the load which would produce that same 1283 kip-ft moment increment. A commonly used technique would be to adjust the maximum value of the load so that the maximum deflection of the bridge was 0.271 in. Provided that the dynamic displaced shape of the bridge did not differ significantly from the displaced shape under static loads, that procedure would produce bridge moments and corresponding stresses very close to the target values. Such a procedure is extremely easy to apply in practice: the 80-kip axle loads are applied statically, and a dial gage is adjusted so that the bridge is just touching it. The load is then applied cyclically, and its magnitude adjusted so that at maximum deflection, the moving bridge barely touches the preset dial gage.

Objectives and Scope

Because that procedure is so simple, it was desired to apply it in this study. Before doing so, it was necessary to determine whether or not that technique would actually produce the desired result, i.e. whether the static and dynamic displaced shapes would essentially coincide. This was checked analytically, using the following steps:

(1) The bridge was idealized as a multi-degree-of-freedom, linear elastic system. That idealization was checked by comparing its fundamental frequency with that actually observed experimentally for the bridge.

(2) Using a set frequency of load application, maximum and minimum cyclic load values were determined experimentally as outlined above. A cyclic load having that same frequency

and those same maximum and minimum load values was then applied to the mathematical model, and its maximum moment response was computed and compared to the target value of 1283 kip-ft.

The maximum calculated moment, including dynamic as well as static effects, was less than 5% over the target value, and the experimental procedure described above could therefore be used to set the load magnitudes for the fatigue tests described in this report. In the rest of this Appendix, the steps outlined above will be described in more detail.

Description of Mathematical Model

Taking advantage of structural symmetry about its centerline, the bridge was idealized as shown in Fig. A2, using the member properties described in Table A1. The moment of inertia of Members 2 and 3 was the gross moment of inertia of the entire bridge cross section, and the area was the gross area of the cross section. Shear deformations were included, and the effective shear area was taken as 5/6 the gross area of the girders alone. The modulus of elasticity was taken as 57000 $\sqrt{f'_c}$ in psi units, using f'_c = 6000 psi, judged to be a reasonable average value for the compressive strengths of the girders, panels, and topping. The bridge's weight was assumed to be distributed uniformly along its length, and was computed using the gross cross-sectional area and a unit concrete weight of 145 pcf. Member 1 is a fictitious member having an axial stiffness equal to that of the neoprene pads actually used. This stiffness was determined by applying a symmetrically located load to the bridge, producing an increase in reaction equal to one-half that load at each end of the bridge. The vertical deflections of each end of the bridge girders were measured, and the neoprene pad stiffness was computed as the change in end reaction divided by the average change in girder end deflection. As noted in

TABLE A.1 MEMBER PROPERTIES

Member 1	K = 2395 kips/in. (support stiffness)
Members 2 and 3	E = 4415 ksi (modulus of elasticity)
	I = 482568 $in.^4$ (moment of inertia)
	$\mu = 6.04 \times 10^{-4}$ $kip\text{-}sec^2/in.^2$ (mass/unit length)
	A = 2780 $in.^2$ (area)
	A_v = 929 $in.^2$ (effective shear area)

Table A1, that spring stiffness is large but not infinite. The flexibility of these end supports was found to have a significant effect on the dynamic response of the bridge.

Calculation of Frequencies and Mode Shapes

The general purpose matrix manipulation program SMIS74 [16] was used to assemble the stiffness matrix and consistent mass matrix for the structure, and the resulting eigenvalue problem was solved for the frequencies and corresponding mode shapes. The fundamental frequency was calculated as 7.58 Hz (cycles per second), very close to the measured value of 7.8 Hz as determined by experimental measurements of actual bridge response to transient impact loads. The calculated circular frequencies of the bridge are designated as ω_i, and the corresponding mode shapes as $\underset{\sim}{\phi}_i$.

Calculated Response to Cyclic Load

Based on the results of trials with the actual experimental apparatus, it was decided that a loading frequency of about 4.5 Hz would be sufficiently fast to permit the application of the desired number of cycles within a reasonable time, yet be far enough away from the bridge's fundamental frequency so that the bridge's dynamic response could easily be controlled. For the final 5 million cycles of Fatigue Test Series No. 1, for example, the axle load applied by the fatigue pulsator varied sinusoidally at 28.2 rad/sec (4.5 Hz), from an average of 26.4 kips to an average maximum of 69.2 kips. That particular maximum load level was selected because it was slightly less than the static load producing comparable effects. The difference between the maximum and minimum load levels was determined by the mechanical limitations of the pulsator and the stability of the reaction frame. As shown in Fig. A3, this is equivalent to the superposition of a constant static load

$$P_{static} = 47.8 \text{ kips}$$

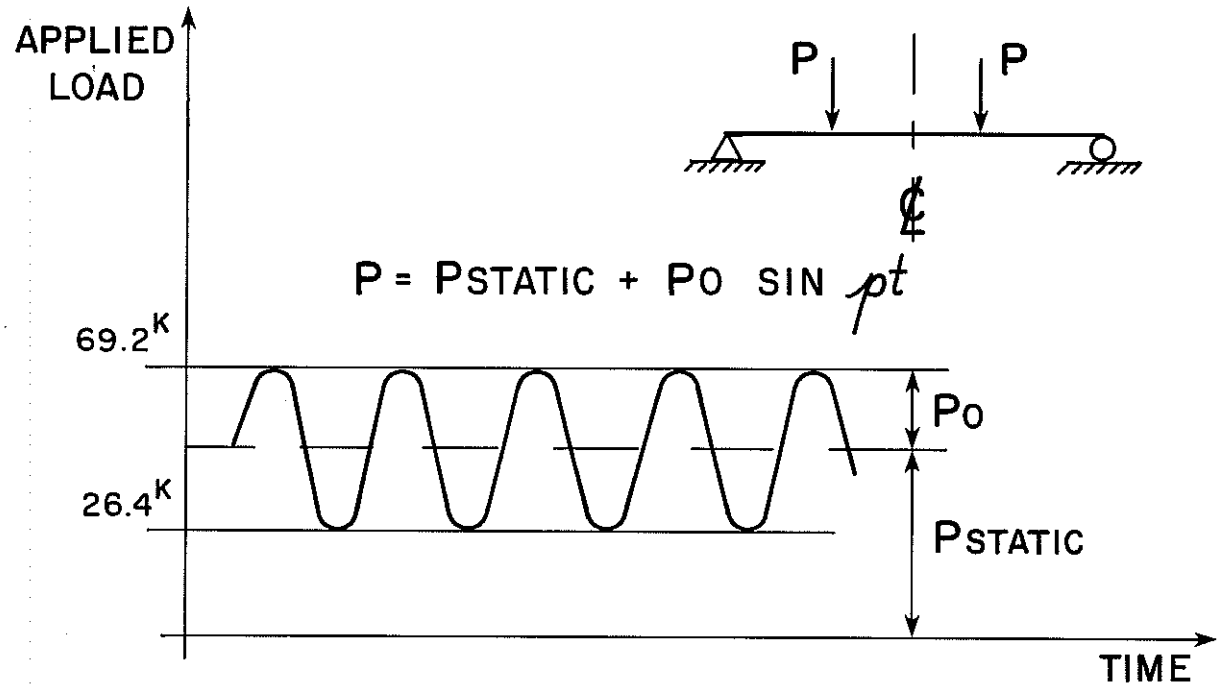

FIGURE A.3 - APPLIED LOAD AS THE SUPERPOSITION OF STATIC LOAD AND SINUSOIDAL LOAD

and a sinusoidally varying load

$$P_o \sin pt = 21.4 \sin pt \text{ kips}$$

so that

$$P(t) = P_{static} + P_o \sin pt$$

The maximum bridge moment produced by the static portion of this load is simply the static moment due to axle loads P_{static}, applied 16 ft from each end of the bridge:

$$\underset{\text{static}}{\text{Moment}_{\text{max}}} = 16\ P_{static} \qquad \text{(units of kip-ft)}$$

The undamped dynamic response of the bridge, in any mode, to the sinusoidal portion of the load is given by

$$Y_{i\ \text{max}} = \frac{P^*_{oi}}{K^*_i \left(1 - p^2/\omega_i^2\right)}$$

This assumes that negligible energy is dissipated as the bridge vibrates. For a clean structure vibrating elastically, such as this bridge, that assumption is physically reasonable as well as computationally convenient. In that expression,

$Y_{i\ \text{max}}$ = generalized sinusoidal displacement response in the $i^{\underline{th}}$ mode

P^*_{oi} = sinusoidal portion of the generalized axle load in the $i^{\underline{th}}$ mode, calculated as

$$P^*_{oi\ \text{sinusoidal}} = \underset{\sim}{\phi}_i^T \underset{\sim}{P}_o$$

K^*_i = generalized stiffness in the $i^{\underline{th}}$ mode, equal to $\omega_i^2 M^*_i$, where M^*_i is the generalized mass in the $i^{\underline{th}}$ mode, set to unity by the SMIS program

p = circular frequency of the applied sinusoidal load, radians/sec

ω_i = $i^{\underline{th}}$ circular frequency of the structure, rad/sec

$\underset{\sim}{\phi}_i$ = $i^{\underline{th}}$ mode shape of the structure

The actual maximum deflection response of the structure in the $i^{\underline{th}}$ mode is then calculated by

$$\underset{\sim}{u}_i = \underset{\sim}{\phi}_i \, Y_{i_{max}}$$

which also gives the displaced configuration of each member of the structure. Using this displaced configuration, the maximum moments in each member can be calculated. In our case, the maximum probable centerline moment due to the bridge's dynamic response in its first four modes was obtained as the RMS combination of the maximum moments produced by each modal response:

$$\text{Moment}_{max} = 26.51 \, P_o \qquad \text{(units of kip-ft)}$$

The maximum centerline moment, combining static and dynamic response, was then

$$\text{Moment}_{max} = 16 \, P_{static} + 26.51 \, P_o \quad \text{(units of kip-ft)}$$

Substituting the known values of P_{static} and P_o

$$\text{Moment}_{max} = 764.8 + 567.3 = 1332 \text{ kip-ft}$$

This is less than 4% above the desired target value of 1283 kip-ft for midspan moment.

As shown in Fig. 2.1, the maximum and minimum cyclic load values were reduced slightly from the end of Fatigue Test Series No. 1 to the beginning of Fatigue Test Series No. 2. The reason for this is that the bridge's natural frequencies of vibration were decreased as a result of the tensile cracking produced during the intervening Static Test Nos. 2 and 3. Using a frequency of 4.5 Hz as before, this would have caused an increase in the effective dynamic load applied to the bridge, had the same loads been applied as before. So that the effect on the bridge would remain constant, the applied axle load magnitudes were reduced slightly.

A P P E N D I X B

CLIP GAGE MEASUREMENTS

Reduction of Clip Gage Data

Consider the clip gage movement shown in Fig. B.1, in which the bases separate but do not rotate. In that case the curvature of the top strip is related to the base separation Δ by

$$\phi = \frac{\Delta h_1}{L} \tag{B.1}$$

where h_1 is the upper leg length, and L is the length of the flexible strip. Including the gage factor, the separation is

$$\Delta = C(\mu\varepsilon) \tag{B.2}$$

in which $(\mu\varepsilon)$ is the microstrain reading from the bridge, and C is an overall constant involving the geometry of the clip gage and the gage factors of the strain gages. This calculation was used to reduce the microstrain readings from the clip gages measuring longitudinal slip.

Now consider the clip gage movement shown in Fig. B.2, in which the curvature of the top strip depends on the base rotation as well as separation. Given just the curvature of a single clip gage, it would be impossible to calculate a unique corresponding combination of base separation and rotation. However, this can be done when two clip gages are used at each point, as was done in this study (Fig. B.3).

As shown in Fig. B.3, the relative movement can be considered as a separation of the panels Δ_{top} at the top surface and Δ_{bottom} at the bottom surface, corresponding to a concentrated angle change $\Delta\theta$.

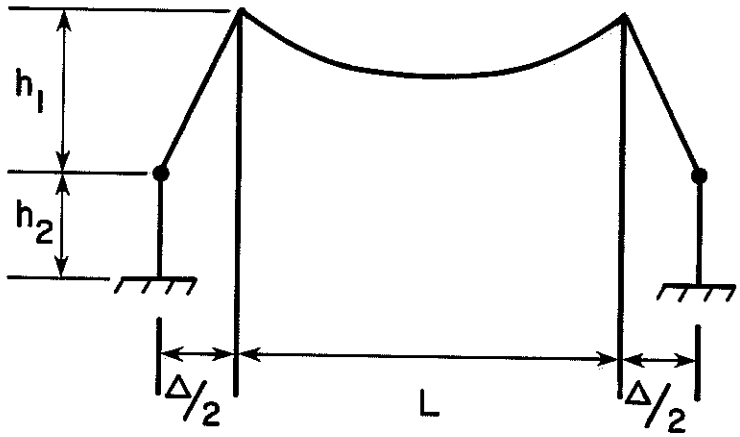

FIG. B.1

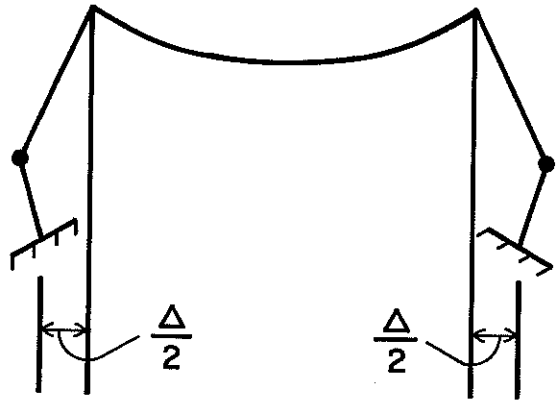

FIG. B.2

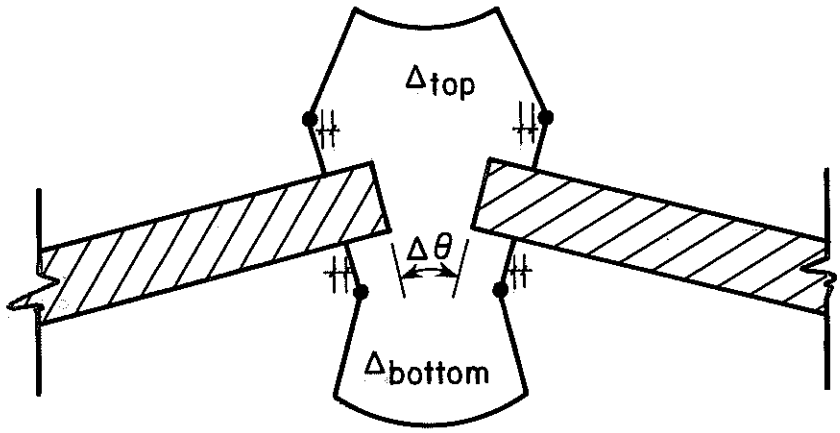
Δtop
Δθ
Δbottom

FIG. B.3

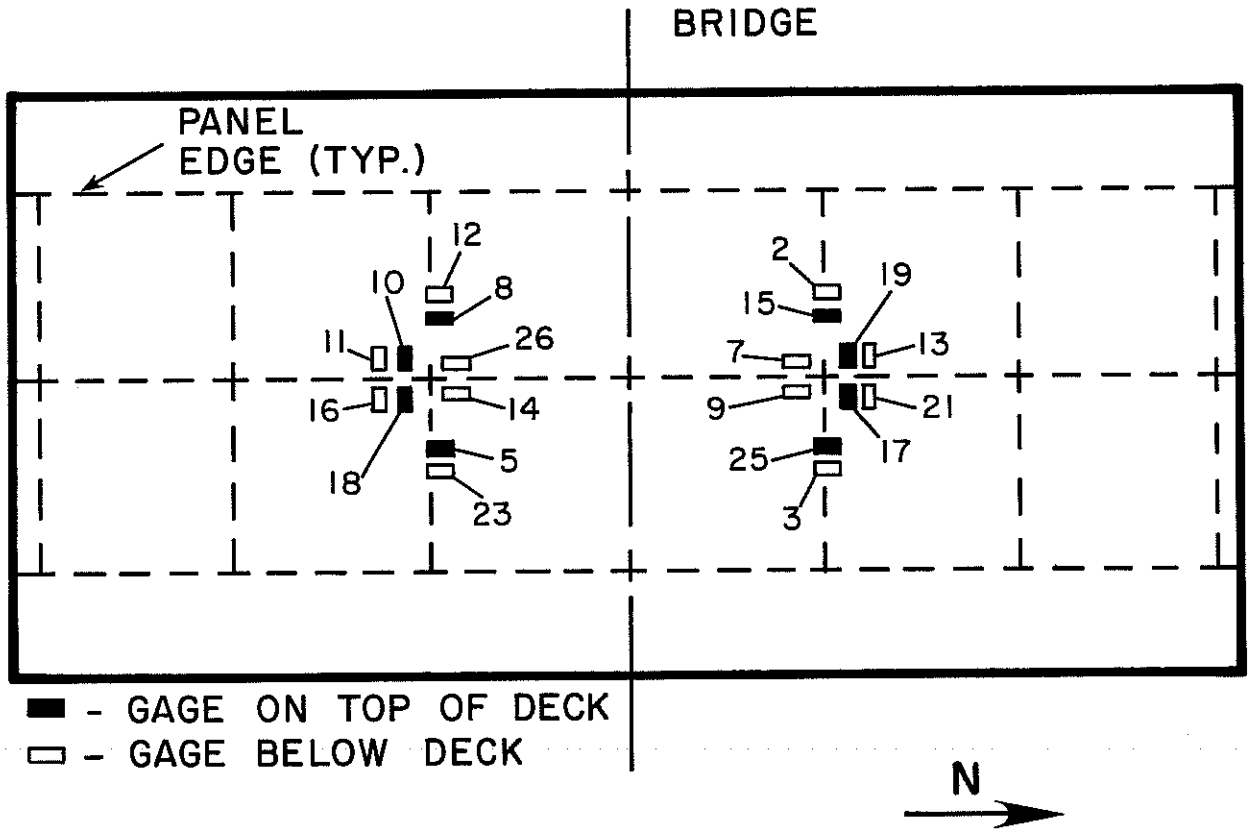
BRIDGE
PANEL
EDGE (TYP.)
12
10
8
11
26
16
14
18
5
23
2
19
15
7
13
9
21
25
17
3
■ - GAGE ON TOP OF DECK
▭ - GAGE BELOW DECK
N

FIG. B.4

As a result of that movement, the hinges of the top clip gage will separate a distance $(\Delta_{top} + \Delta\theta h_2)$, and those at the bottom by $(\Delta_{bottom} - \Delta\theta h_2)$, where h_2 is the lower leg length of the clip gage as shown in Fig. B.1. The microstrain readings of each clip gage will then be

$$(\mu\varepsilon)_{top} = \frac{1}{C_{top}} (\Delta_{top} + \Delta\theta h_2) \tag{B.3}$$

$$(\mu\varepsilon)_{bottom} = \frac{1}{C_{bottom}} (\Delta_{bottom} - \Delta\theta h_2) \tag{B.4}$$

Using the additional relationship

$$\Delta\theta = \left(\frac{\Delta_{top} - \Delta_{bottom}}{t} \right) \tag{B.5}$$

where t is the deck thickness, the resulting three equations in three unknowns can be solved for Δ_{top} and Δ_{bottom} in terms of $(\mu\varepsilon)_{top}$ and $(\mu\varepsilon)_{bottom}$:

$$\text{Let } \alpha \equiv \left[(1 + h_2/t) - \frac{(h_2/t)^2}{(1 + h_2/t)} \right] \tag{B.6}$$

and

$$\beta \equiv \frac{(h_2/t)}{(1 + h_2/t)} \tag{B.7}$$

Then

$$\Delta_{top} = \frac{C_{top}}{(1 + h_2/t)} \left\{ (\mu\varepsilon)_{top} + \frac{(h_2/t) \left[\frac{C_{bottom}}{C_{top}} (\mu\varepsilon)_{bottom} + \beta(\mu\varepsilon)_{top} \right]}{\alpha} \right\} \tag{B.8}$$

and

$$\Delta_{bottom} = \frac{C_{bottom}}{\alpha} \left[(\mu\varepsilon)_{bottom} + \frac{C_{top}}{C_{bottom}} \beta(\mu\varepsilon)_{top} \right] \tag{B.9}$$

The average separation and angle change are then given by

$$\Delta = \frac{\Delta_{top} + \Delta_{bottom}}{2} \qquad (B.10)$$

$$\Delta\theta = \frac{\Delta_{top} - \Delta_{bottom}}{t} \qquad (B.11)$$

In this case, $h_2/t = 0.175$, and the two equations B.8 and B.9 for Δ_{top} and Δ_{bottom} simplify to

$$\Delta_{top} = 0.8704\ C_{top}(\mu\varepsilon)_{top} + 0.1296\ C_{bottom}(\mu\varepsilon)_{bottom} \qquad (B.12)$$

$$\Delta_{bottom} = 0.1296\ C_{top}(\mu\varepsilon)_{top} + 0.8704\ C_{bottom}(\mu\varepsilon)_{bottom} \qquad (B.13)$$

Clip Gage Data

Figure B.4 identifies all clip gages by number and location. Longitudinal slip was measured using single gages on the underside of the deck, while angle changes and separations were measured using information from pairs of gages as explained above. To reduce complexity and space, clip gage data have been partially reduced, as explained above, and are presented in Tables B.1 - B.5. Data for movement at longitudinal joints between the panels and center girder are presented in Tables B.1 through B.4 for Static Tests No. 1 through No. 4, respectively. Table B.5 shows the data for movement at transverse joints between panels. Complete transverse joint data are given for Static Test No. 3, and data corresponding to maximum load levels only are given for Static Tests 2 and 4. Transverse joint data for Static Test No. 1 were not included, due to the low load levels used in that test.

Sample Calculations for Table B.1

(Northwest quadrant, Static Test No. 1, load = 48 kips)

a) Δ_{slip} is calculated directly using the gage constant

b) For the longitudinal panel joints,

$$\Delta_{top} = -1.8 \times 10^{-4} \text{ in.}$$

$$\Delta_{bottom} = 2.0 \times 10^{-4} \text{ in.}$$

separation:

$$\Delta = \frac{\Delta_{top} + \Delta_{bottom}}{2} = \frac{(-1.8 \times 10^{-4}) + (2.0 \times 10^{-4})}{2}$$

$$= \underline{0.1 \times 10^{-4} \text{ in.}}$$

angle change:

$$\Delta\theta = \frac{\Delta_{top} - \Delta_{bottom}}{t} \quad \text{(in radians, for small } \Delta\theta\text{)}$$

$$\Delta\theta = \frac{\Delta_{top} - \Delta_{bottom}}{t}\left(\frac{180^\circ}{\pi}\right) = \frac{(-1.8 \times 10^{-4}) - (2.0 \times 10^{-4})}{7.5}\left(\frac{180^\circ}{\pi}\right)$$

$$= \underline{-2.9 \times 10^{-3^\circ}}$$

TABLE B.1 DATA FROM STATIC TEST NO.1

Load (kips)	Δ_{slip} ($\times 10^{-4}$ in.)	Δ_{top} ($\times 10^{-4}$ in.)	Δ_{bottom} ($\times 10^{-4}$ in.)	$\Delta\theta$ ($\times 10^{-3}$ Degrees)	Separation Δ ($\times 10^{-4}$ in.)
Northwest - Slip Gage #7, Top Gage #19, Bottom Gage #13					
0	0.0	0.0	0.0	0.0	0.0
16	0.9	-1.2	1.4	-2.0	0.1
32	0.9	-2.7	1.1	-2.9	-0.8
48	0.9	-1.8	2.0	-2.9	0.1
Northeast - Slip Gage #9, Top Gage #17, Bottom Gage #21					
0	0.0	0.0	0.0	0.0	0.0
16	0.9	-3.7	0.2	-3.0	-1.8
32	-0.9	-3.7	0.2	-3.0	-1.8
48	-0.9	-4.4	0.8	-4.0	-1.8
Southwest - Slip Gage #26, Top Gage #10, Bottom Gage #11					
0	0.0	0.0	0.0	0.0	0.0
16	0.0	-4.5	0.9	-4.1	-1.8
32	0.0	-6.0	1.4	-5.7	-2.3
48	0.0	-6.7	2.0	-6.6	-2.4
Southeast - Slip Gage #14, Top Gage #18, Bottom Gage #16					
0	0.0	0.0	0.0	0.0	0.0
16	3.5	-3.1	-0.5	-2.0	-1.8
32	3.5	-3.7	0.2	-3.0	-1.8
48	3.5	-4.5	0.0	-3.4	-2.3

TABLE B.2 DATA FROM STATIC TEST NO. 2

Load (kips)	Δ_{slip} ($\times 10^{-4}$ in.)	Δ_{top} ($\times 10^{-4}$ in.)	Δ_{bottom} ($\times 10^{-4}$ in.)	$\Delta\theta$ ($\times 10^{-3}$ Degrees)	Separation Δ ($\times 10^{-4}$ in.)
Northwest - Slip Gage #7, Top Gage #19, Bottom Gage #13					
0	0.0	0.0	0.0	0.0	0.0
6	0.0	-0.2	-1.6	1.0	-0.9
26	0.0	-0.4	-2.4	1.5	-1.4
46	0.9	0.1	-3.8	3.0	-1.8
65	4.3	-0.8	-5.5	3.6	-3.2
87	10.4	2.6	-6.5	6.9	-2.0
94	10.4	1.8	-6.6	6.5	-2.4
105	11.2	-0.2	-6.2	4.6	3.2
116	13.0	1.6	11.0	-7.2	6.3
Northeast - Slip Gage #9, Top Gage #17, Bottom Gage #21					
0	0.0	0.0	0.0	0.0	0.0
6	-1.7	-0.1	-0.8	0.5	-0.4
26	-0.8	1.4	-0.5	1.5	0.5
46	-0.8	-0.1	-0.8	-0.5	-0.4
65	0.0	-0.2	-1.5	1.0	-0.9
87	0.0	2.7	-1.8	3.5	0.5
94	0.0	3.0	-0.3	2.5	1.3
105	-0.8	0.6	-5.8	4.9	-2.6
116	0.8	2.0	3.2	-1.0	2.6
Southwest - Slip Gage #26, Top Gage #10, Bottom Gage #11					
0	0.0	0.0	0.0	0.0	0.0
6	0.8	-0.1	-0.8	0.5	-0.4
26	1.7	-0.4	-2.3	1.5	-1.3
46	2.5	-0.4	-2.3	1.5	-1.3
65	5.1	1.5	-0.5	1.5	0.5
87	13.6	0.6	-1.4	1.5	-0.4
94	15.2	0.0	0.0	0.0	0.0
105	16.1	0.6	14.6	-10.7	7.6
116	20.3	-2.7	33.9	-28.0	15.6
Southeast - Slip Gage #14, Top Gage #18, Bottom Gage #16					
0	0.0	0.0	0.0	0.0	0.0
6	1.7	-0.1	-0.7	0.5	-0.4
26	1.7	0.0	0.0	0.0	0.0
46	1.7	0.0	0.0	0.0	0.0
65	1.7	0.7	1.0	-0.2	0.8
87	1.7	3.5	8.4	-3.8	6.0
94	1.7	1.5	10.3	-6.7	5.9
105	1.7	2.2	14.7	-9.6	8.4
116	1.7	3.1	20.6	-13.4	11.8

TABLE B.3 DATA FROM STATIC TEST NO. 3

Load (kips)	Δ_{slip} ($\times 10^{-4}$ in.)	Δ_{top} ($\times 10^{-4}$ in.)	Δ_{bottom} ($\times 10^{-4}$ in.)	$\Delta\theta$ ($\times 10^{-3}$ Degrees)	Separation Δ ($\times 10^{-4}$ in.)
Northwest - Slip Gage #7, Top Gage #19, Bottom Gage #13					
0	0.0	0.0	0.0	0.0	0.0
20	0.0	1.8	-2.0	2.9	-0.1
40	0.0	1.5	-4.4	4.5	-1.5
59	1.7	2.2	-4.3	4.9	-1.0
81	2.6	1.9	-1.3	2.4	0.3
102	3.5	1.0	1.7	-0.6	1.3
109	5.2	1.0	1.7	-0.6	1.3
120	6.9	-0.4	-17.0	12.6	-8.7
130	7.8	-1.0	-16.3	11.7	-8.6
139	13.0	-1.4	-14.0	9.7	-7.7
Northeast - Slip Gage #9, Top Gage #17, Bottom Gage #21					
0	0.0	0.0	0.0	0.0	0.0
20	0.0	1.5	0.2	1.0	0.9
40	0.0	1.3	-1.3	2.0	0.0
59	0.0	2.9	-1.0	3.0	0.9
81	0.0	2.3	0.3	1.5	1.3
102	0.0	2.3	0.3	1.5	1.3
109	0.8	1.5	0.2	1.0	0.9
120	0.0	3.1	0.5	2.0	1.8
130	1.7	2.8	3.4	-0.5	3.1
139	4.2	2.3	5.5	-2.4	3.9
Southwest - Slip Gage #26, Top Gage #10, Bottom Gage #11					
0	0.0	0.0	0.0	0.0	0.0
20	0.8	2.7	-2.6	4.1	0.0
40	1.7	1.9	-8.1	7.6	-3.1
59	3.4	2.3	-5.8	6.1	-1.8
81	4.2	3.7	3.6	0.1	3.6
102	5.9	1.4	9.4	-6.1	5.4
109	5.9	0.5	13.8	-10.2	7.1
120	11.0	2.5	21.7	-14.7	12.1
130	11.0	1.7	32.2	-23.3	17.0
139	11.9	0.8	47.4	-35.6	24.1
Southeast - Slip Gage #14, Top Gage #18, Bottom Gage #16					
0	0.0	0.0	0.0	0.0	0.0
20	0.9	1.7	1.0	0.5	1.3
40	1.7	1.9	2.4	-0.4	2.1
59	1.7	1.5	0.2	1.0	0.9
81	2.5	3.2	11.3	-6.2	7.2
102	3.4	4.3	18.6	-11.0	11.4
109	4.3	4.7	21.6	-12.9	13.1
120	4.3	5.0	23.8	-14.3	14.4
130	6.0	5.5	26.7	-16.2	16.1
139	7.7	6.0	30.4	-18.6	18.2

TABLE B.4 DATA FROM STATIC TEST NO. 4

Load (kips)	Δ_{slip} ($\times 10^{-4}$ in.)	Δ_{top} ($\times 10^{-4}$ in.)	Δ_{bottom} ($\times 10^{-4}$ in.)	$\Delta\theta$ ($\times 10^{-3}$ Degrees)	Separation Δ ($\times 10^{-4}$ in.)
Northwest - Slip Gage #7, Top Gage #24, Bottom Gage #13					
0	0.0	0.0	0.0	0.0	0.0
24	0.0	0.0	0.0	0.0	0.0
48	1.7	-1.4	-0.2	-0.9	-0.8
64	2.6	-1.0	2.9	-3.0	-0.9
80	5.2	0.4	7.7	-5.6	4.1
96	5.2	-20.4	6.2	-20.3	-7.1
111	5.2	-20.1	7.7	-21.2	-6.2
119	5.2	-19.9	9.3	-22.3	-5.3
127	5.2	-21.1	10.7	-24.3	-5.2
135	6.1	-21.1	10.7	-24.3	-5.2
143	6.9	-20.7	13.0	-25.7	-3.9
Northeast - Slip Gage #9, Top Gage #17, Bottom Gage #21					
0	0.0	0.0	0.0	0.0	0.0
24	0.0	1.5	0.2	1.0	0.9
48	0.0	2.3	0.3	1.5	1.3
64	0.0	2.3	0.3	1.5	1.3
80	0.0	3.1	0.5	2.0	1.8
96	0.0	1.9	2.5	-0.5	2.2
111	0.0	1.9	2.5	-0.5	2.2
119	0.0	2.2	4.7	-1.9	3.5
127	0.0	1.4	4.6	-2.4	3.0
135	1.7	1.6	5.4	-2.9	3.5
143	0.9	1.7	6.1	-3.4	3.9
Southwest - Slip Gage #26, Top Gage #10, Bottom Gage #11					
0	0.0	0.0	0.0	0.0	0.0
24	0.0	-2.6	-17.1	11.1	-9.9
48	1.7	-3.0	-20.3	13.2	-11.7
64	2.5	-10.0	-67.0	43.5	-38.5
80	5.1	-10.8	-61.8	39.0	-36.3
96	6.8	-12.8	-54.5	31.9	-33.7
111	6.8	-16.3	-46.6	23.1	-31.5
119	8.5	-15.6	-41.9	20.1	-28.8
127	10.2	-16.5	-37.5	16.0	-27.0
135	10.2	-16.0	-34.4	14.1	-25.2
143	11.0	-16.9	-29.9	9.9	-23.4
Southeast - Slip Gage #14, Top Gage #18, Bottom Gage #16					
0	0.0	0.0	0.0	0.0	0.0
24	0.0	0.0	0.0	0.0	0.0
48	0.0	1.8	1.7	0.0	1.8
64	0.0	2.6	2.5	0.0	2.6
80	0.0	0.9	5.9	-3.8	3.4
96	0.0	1.3	8.8	-5.7	5.1
111	1.7	2.0	13.2	-8.6	7.6
119	1.7	2.4	16.2	-10.5	9.3
127	1.7	2.6	17.6	-11.5	10.1
135	0.9	2.1	19.0	-12.9	10.6
143	2.6	1.5	20.4	-14.4	11.0

TABLE B.5 TRANSVERSE JOINT DATA

Load (kips)	Static Test Number	Δ_{top} ($\times 10^{-4}$ in.)	Δ_{bottom} ($\times 10^{-4}$ in.)	$\Delta\theta$ ($\times 10^{-3}$ Degrees)	Separation Δ ($\times 10^{-4}$ in.)
Northwest - Top Gage #15, Bottom Gage #2					
0	3	0.0	0.0	0.0	0.0
20	3	-7.5	-1.1	-4.9	-4.3
40	3	-14.8	-0.8	-10.7	-7.7
59	3	-22.0	-6.1	-12.1	-14.1
81	3	-28.4	-18.5	-7.6	-23.5
102	3	-31.4	-26.1	-4.0	-28.7
109	3	-33.0	-30.6	-1.8	-31.8
120	3	-35.8	-68.2	24.8	-52.0
130	3	-37.2	-71.3	26.1	-54.2
139	3	-53.1	-172.3	91.0	-112.7
116	2	-27.9	-33.5	4.3	-30.7
143	4	-36.6	-31.9	-3.6	-34.3
Northeast - Top Gage #25, Bottom Gage #3					
0	3	0.0	0.0	0.0	0.0
20	3	2.9	-1.8	3.6	0.6
40	3	-0.5	-3.0	2.0	-1.7
59	3	-3.1	-4.9	1.4	-4.0
81	3	-1.2	-8.3	5.4	-4.8
102	3	-8.5	-14.6	4.6	-11.5
109	3	-15.2	-17.1	1.4	-16.1
120	3	-14.6	-12.5	-1.6	-13.5
130	3	-14.2	-15.4	1.0	-14.8
139	3	-12.7	-21.1	6.5	-16.9
116	2	-20.4	-25.2	3.7	-22.8
143	4	-33.2	-25.7	-5.7	-29.5
Southwest - Top Gage #8, Bottom Gage #12					
0	3	0.0	0.0	0.0	0.0
20	3	3.4	1.9	1.1	2.7
40	3	-0.2	3.6	-2.9	1.7
59	3	-3.7	5.9	-7.4	1.1
81	3	-3.9	10.3	-10.8	3.2
102	3	9.3	15.8	-5.0	12.6
109	3	9.3	15.8	-5.0	12.6
120	3	93.9	666.5	-437.5	380.2
130	3	93.3	667.9	-438.9	380.6
139	3	90.3	663.1	-437.6	376.7
116	2	1.4	24.8	-17.9	13.1
143	4	-20.9	20.0	-31.2	-0.5
Southeast - Top Gage #5, Bottom Gage #23					
0	3	0.0	0.0	0.0	0.0
20	3	-1.7	-1.8	0.1	-1.8
40	3	-4.7	-2.3	-1.8	-3.5
59	3	-4.7	-2.3	-1.8	-3.5
81	3	-7.6	-2.7	-3.7	-5.2
102	3	-7.4	-1.1	-4.8	-4.2
109	3	-7.4	-1.1	-4.8	-4.2
120	3	-5.7	0.7	-4.9	-2.5
130	3	-6.7	3.8	-7.9	-1.5
139	3	-3.7	13.7	-13.3	5.0
116	2	-4.0	-7.7	2.8	-5.9
143	4	-15.6	6.4	-16.8	-4.6

REFERENCES

1. Kluge, R. W., and Sawyer, H. A., "Interacting Pretensioned Concrete Form Panels for Bridge Decks," PCI Journal, V. 20, No. 3, May-June 1975, pp. 34-61.

2. Barnoff, R. M., Orndorff, J. A., Jr., Harbaugh, R. B., Jr., and Rainey, D. E., "Full Scale Test of a Prestressed Bridge with Precast Deck Planks," PCI Journal, V. 22, No. 5, Sept-Oct 1977, pp. 66-83.

3. Texas Highway Department, "Summary Report on Investigation to Determine Feasibility of Using In-Place Precast Prestressed Form Panels for Highway Bridge Decks," PCI Journal, V. 20, No. 3, May-June 1975, pp. 62-67.

4. Buth, E., Furr, H. L., Jones, H. L., and Toprac, A. A., "Evaluation of a Prestressed Panel, Cast-in-Place Concrete Bridge," Research Report 145-3, Texas Transportation Institute, Texas A & M University, College Station, Texas, September 1972.

5. Barker, J. M., "Research, Application, and Experience with Precast Prestressed Bridge Deck Panels," PCI Journal, V. 20, No. 6, Nov-Dec 1975, pp. 66-85.

6. Rabbat, B. G., and Russell, H. G., "Fatigue Tests of Full-Size Prestressed Girders," Research Report No. 113, Portland Cement Association, Skokie, Illinois, December 1977.

7. AASHTO, Standard Specifications for Highway Bridges, Twelfth Edition, The American Association of State Highway and Transportation Officials, Washington, D.C., 1977.

8. Texas Concrete Company, "Type 'B' Beam Detail," DWG. No. D-1137, Sheet No. F-1, Job No. 627-1, Victoria, Texas, 1980.

9. Texas Highway Department, "Prestressed Concrete Beam Standards Index," Bridge Division, April 1971.

10. Texas State Department of Highways and Public Transportation, "Miscellaneous Standards Index," Bridge Division, January 1977.

11. Texas Highway Department, "Standard Specifications for Construction of Highways, Streets and Bridges," State Highway Department of Texas, January 3, 1972.

12. Texas State Department of Highways and Public Transportation, Bridge Division, Drawing File 1284, Research Project 3-5-80-303, June 3, 1980.

13. Panak, J. J., and Matlock, H., "A Discrete-Element Method of Analysis for Orthogonal Slab and Grid Bridge Floor Systems," Research Report 56-25, Center for Highway Research, The University of Texas at Austin, Austin, Texas, May 1972.

14. Suttikan, C., "A Generalized Solution for Time-Dependent Response and Strength of Noncomposite and Composite Prestressed Concrete Beams," unpublished Ph.D. dissertation, The University of Texas at Austin, Austin, Texas, 1978.

15. ACI Committee 318, "Building Code Requirements for Reinforced Concrete," ACI Standard 318-77, American Concrete Institute, Detroit, Michigan, 5th Printing, August, 1979.

16. Becker, E. B., and Craig, R. R., Jr., "SMIS74--User's Manual with Programmer's Guide," TICOM Report 74-4, The Texas Institute for Computational Mechanics, The University of Texas at Austin, 1974, 72 pp.

E R R A T A S H E E T

"The Effect of Transverse Strand Extensions on the Behavior of Precast Prestressed Panel Bridges," by L. A. Bieschke and R. E. Klingner, Research Report No. 303-1F, Center for Transportation Research, June 1982.

1. page 38, line 19 - Figure 4.6a <u>should be</u> Fig. 6.4a.

2. page 47, Fig. 6.9 - $\theta = 45 \times 10^{3\ 0}$ <u>should be</u> $\theta = 45 \times 10^{-3}$

   SIN = c/t <u>should be</u> $SIN\theta = c/t$

3. p. 89, Fig. A.3 Number on applied load axis <u>should be</u> 26.4 rather than 29.4